AN EXPERIMENTAL INVESTIGATION INTO THE COMPONENTS OF SHIP RESISTANCE

by

Robert Cooke, B.Sc. (Civil) Engineering, Cape Town

A thesis submitted in partial fulfilment of the requirements for the degree Master of Science in Engineering

Department of Civil Engineering
University of Cape Town

September 1986

The University of Cape Town has been given the right to reproduce this thesis in whole or in part. Copyright is held by the author.

The copyright of this thesis vests in the author. No quotation from it or information derived from it is to be published without full acknowledgement of the source. The thesis is to be used for private study or non-commercial research purposes only.

Published by the University of Cape Town (UCT) in terms of the non-exclusive license granted to UCT by the author.

University of Cape Town

To my Dad

DECLARATION OF CANDIDATE

I, Robert Cooke, hereby declare that this thesis is my own work and that it has not been submitted for a degree at another university.

Signed by candidate

R COOKE

September 1986

University of Cape Town

SYNOPSIS

This thesis is an experimental investigation into the components of ship resistance. The traditional Froude method of scaling is investigated with reference to the measurement of skin friction and viscous pressure resistance. A literature review is given on the theoretical background and experimental measurement techniques.

Two models are used for the experimental work, which sizes are in the geometric ratio of 2,7 to 1. The model form is half a body of revolution with a vertical sided superstructure. The block coefficient of the model is 0,621 and the length to beam ratio is 7. Two surface models and one reflex model are tested. One of the models has 40 pressure tappings located on its hull which are used to measure the total pressure resistance of the model.

The components of resistance directly measured are total resistance, total viscous resistance and total pressure resistance. The resistance components inferred are skin friction resistance and wave-making resistance.

The deduced skin friction is found to deviate from the Prandtl-von Karman skin friction formulation. The wave-making resistance agrees favourably with the predicted values using Mitchell's integral. The total viscous resistance increases sharply at Reynolds numbers greater than 3×10^6.

ACKNOWLEDGEMENTS

The author wishes to thank the following:-

Professor F A Kilner, Department of Civil Engineering, U C T, thesis supervisor, for his insight, guidance and encouragement over the past two years.

The Council for Scientific and Industrial Research for the award of a post-graduate grant which made this research possible.

Mr K Balfour, undergraduate student, for his help with the glass flume experiments.

Messrs R F Beverton, G Bertuzzi, D J Botha, C Coetzee and R Edge of the Civil Engineering workshop, U C T, for their assistance with the fabrication of the experimental apparatus.

Mr J J Hesselink, Department of Electrical Engineering, U C T, for advice concerning electronic problems and the loan of equipment.

Mr J Mayer, Department of Mechanical Engineering, U C T, for the loan of equipment.

Mr A Sive, Department of Civil Engineering, U C T, for the many enlightening discussions.

Messrs J H George, N Hassan, J Petersen, A Siko, D S Swart and J J Williams of the Department of Civil Engineering, U C T, for the assistance and encouragement throughout the thesis.

Cheryl Wright for her efficient typing of this thesis.

TABLE OF CONTENTS

LIST OF FIGURES

LIST OF TABLES

LIST OF PHOTOGRAPHIC PLATES

NOMENCLATURE

Symbol		Units
A_F	frontal area	m^2
b	beam at midships	m
B	width of channel or flume	m
C	resistance coefficient = $\frac{R}{\frac{1}{2}\rho S_W V^2}$	
C_B	block coefficient = $\frac{\Delta}{Lbd}$	
c_o	speed of a deep water gravity wave = $\frac{gT}{2\pi}$	m/s
d	draught at midships	m
D	diameter of a body	m
D	water depth of channel or flume	m
F_r	Froude number = $\frac{V}{\sqrt{gL}}$	
g	acceleration due to gravity	9,81 m/s^2
k_{adm}	admissible roughness	m
L	length of ship at waterline	m
p	normal pressure	Pa
R	resistance	N
Re_D	Reynolds number based on diameter = $\frac{VD}{\nu}$	
Re_L	Reynolds number based on length = $\frac{VL}{\nu}$	
Re_x	Plate Reynolds number = $\frac{Vx}{\nu}$	

Symbol		Units
S	surface area	m^2
S_W	wetted surface area	m^2
T	period of a wave	s
V	velocity of body relative to fluid	m/s
X	dimensionless $x = 2x/L$	
Y	dimensionless $y = 2y/L$	
Z	dimensionless $z = z/d$	
Δ	ship displacement	m^3
λ	ratio of prototype length to model length $= L_p/L_m$	
λ_o	wave length of a deep water gravity wave $= \frac{gT^2}{2\pi}$	m
μ	coefficient of dynamic viscosity	kg/m.s
ν	coefficient of kinematic viscosity	m^2/s
ρ	density of fluid	kg/m^3
τ	tangential shear stress within fluid	Pa
τ_o	tangential shear stress at body surface	Pa
ϕ	angle between normal on body surface and direction of motion	degrees

Subscripts

F	denotes flat plate skin friction forces
m	denotes model
p	denotes prototype
P	denotes total pressure forces
R	denotes residual forces
S	denotes skin friction forces
T	denotes total forces
U	denotes viscous pressure forces
V	denotes total viscous forces
W	denotes wave-making forces

CO-ORDINATE SYSTEM

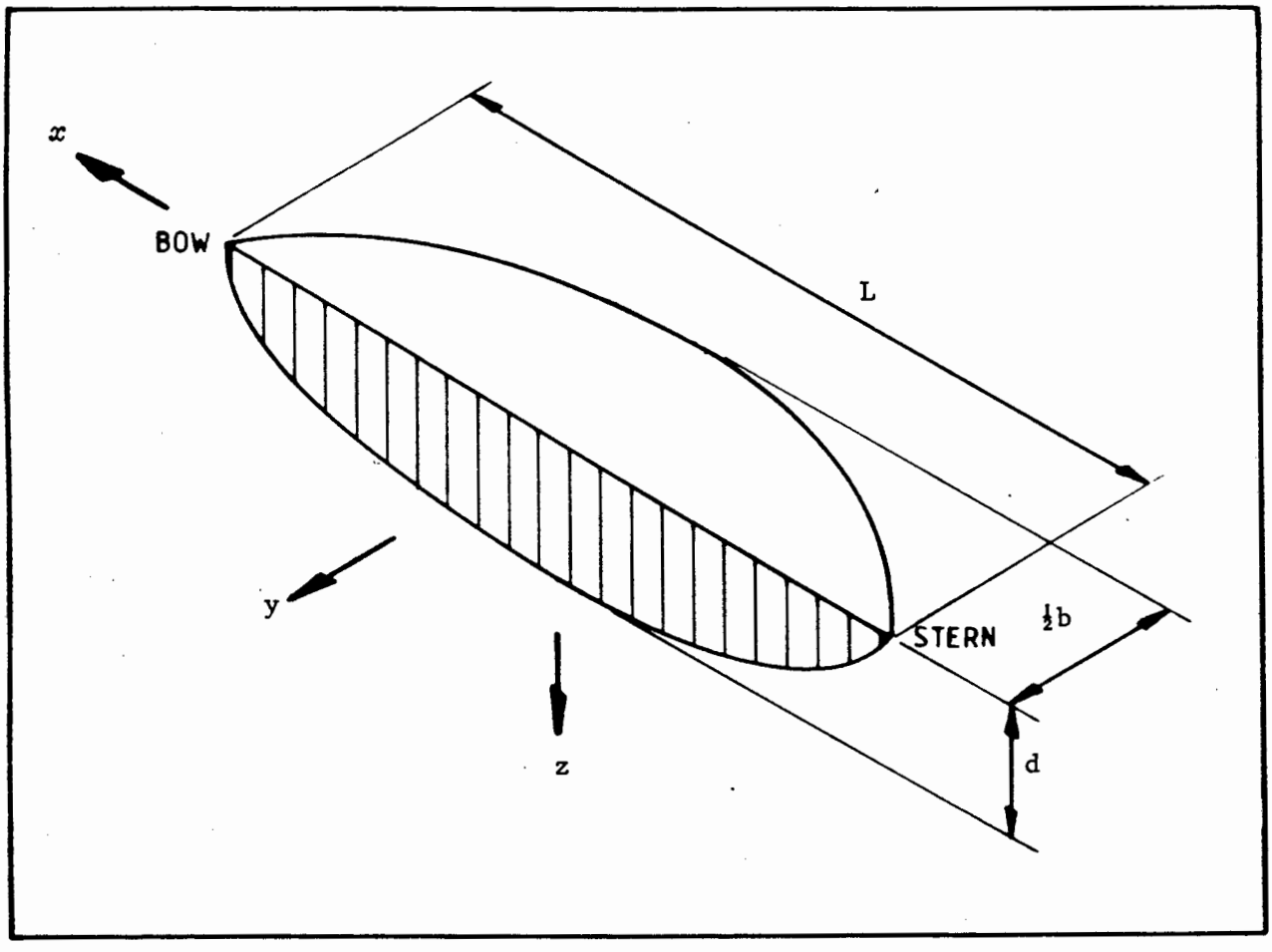

CHAPTER 1

INTRODUCTION

Knowledge of the forces resisting the motion of a ship moving through water is important in the design of ships. To optimise the ship's performance the ship should have the least possible resistance while meeting the requirements of its service. For more than a century now since William Froude's famous tests at Torquay in the 1870's, model ships have been used to predict the resistance of prototype ships.

Historically the method of determining prototype resistance from model tests has been to measure the total resistance of the model over a range of speeds. The skin friction of the model is then estimated by towing a flat plate of equivalent wetted area to the model. This estimated skin friction is then subtracted from the total resistance to determine the so called residuary resistance (i.e. all the resistance components that are not skin friction). The prototype skin friction is then estimated using an empirical skin friction formulation, while the residuary resistance is scaled using Froude number scaling.

The following points about this method justify further investigation:

a. How accurate is the assumption that the skin friction of a flat two-dimensional plate is equal to that of a curved three-dimensional body of the same wetted surface area?

b. The viscous pressure resistance as part of the residuary resistance is scaled up according to Froude number scaling while being dependent on Reynolds number. How great is the error in this approximation?

To answer these questions the resistance components of a body of revolution are experimentally investigated in both the surface and the deeply submerged conditions.

CHAPTER 2

THEORETICAL BACKGROUND

2.1 Definitions

2.1.1 Reynolds number

Reynolds number is defined as a velocity multiplied by a length dimension divided by the coefficient of kinematic viscosity of the fluid through which the body is travelling. Historically in the study of ship resistance the waterline length has been chosen as the length dimension although in certain areas of fluid mechanics the diameter of the body has been used. This leads to the definition of two Reynolds numbers:

$$Re_L = \frac{VL}{\nu} \tag{2.1}$$

$$Re_D = \frac{VD}{\nu} \tag{2.2}$$

where V = velocity of body relative to the fluid (m/s)
L = waterline length (m)
D = diameter (m)
ν = coefficient of kinematic viscosity (m^2/s)

Reynolds number is used for model scaling when pressure, inertial and viscous forces are dominant.

2.1.2 Froude number

Froude number is defined as velocity divided by the square root of the product of the acceleration due to gravity multiplied by a length dimension. The length dimension used historically has been the waterline length.

Thus $$F_r = \frac{V}{\sqrt{gL}} \qquad (2.3)$$

where g = acceleration due to gravity (m/s^2)

Froude number model scaling is used when pressure, inertial and gravity forces are dominant.

2.2 The nature of ship resistance

In fluid mechanics the term resistance is the retarding force experienced by a body when moving through a fluid. In aerodynamics this retarding force is generally called drag; however, naval architects have historically referred to it as resistance. Resistance is found in all situations where a real fluid moves relative to a body e.g. pipe flow, open channel flow and, of more specific interest, the resistance of the sea opposing the motion of a ship's hull.

Work must be done against the resistance to maintain the relative motion between the body and the fluid. The force exerted on the surface of the body can be considered to be the sum of the tangential shear stresses at the hull τ_o and the normal pressure p acting over each element dA of the surface of the body in contact with the fluid S_W (i.e. the wetted surface area), see Figure 2.1.

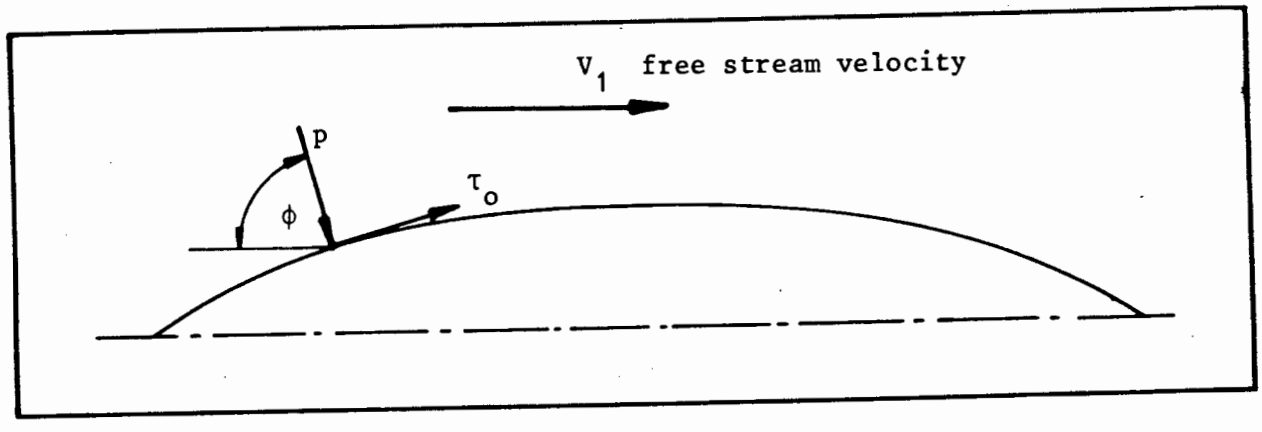

Figure 2.1 Shear stress and normal pressure on a ship hull

$$R_T = \int_{S_W} \tau_o \sin\phi \, dA + \int_{S_W} p \cos\phi \, dA \qquad (2.4)$$

where R_T = total resistance (N)

ϕ = angle between surface dA and direction of motion.

The first term on the righthand side of this equation is termed skin friction and is the longitudinal resultant of viscous shear forces of the fluid against the hull surface. The second term on the righthand side of the equation is called the total pressure resistance and is the longitudinal resultant of the normal pressures exerted at the surface.

To understand the nature of ship resistance it is useful to consider a fixed model placed in a moving fluid stream in two cases: firstly deeply submerged and secondly at the surface. Also consider that the fluid is initially an ideal frictionless fluid and is subsequently a real viscous fluid. The resistance of the model in these cases is illustrated in Figure 2.2, page 2.6, adapted from Lackenby (1965).

The following discussion leads to the division of the resistance of a ship into various components - these are depicted in Figure 2.3, page 2.7.

2.2.1 Resistance in an ideal fluid

2.2.1.1 Model submerged

The model would have normal pressures acting on it; however, if the normal forces acting on the bow are integrated longitudinally and compared to a similar integration for the stern, they will be found to be exactly equal and opposite. This is because no separation of the streamlines will occur in an ideal fluid. Therefore, the total pressure resistance of the model will be zero.

Similarly, there would be no tangential shear stresses acting on the model in this case. Thus the model would have zero resistance and this is represented as line OA in Figure 2.2.

2.2.1.2 Model at the surface

The model would generate a set of gravity waves in the fluid stream as it flowed past the model. The generation of the gravity waves would be seen at the hull of the model as normal pressures. The longitudinal integrated normal pressure forces would, therefore, be non-zero and equal to the theoretical wave-making resistance of the form. This is depicted as curve OB in Figure 2.2.

As the model is in an ideal fluid there would be no tangential shear stresses acting on the ship.

2.2.2 Resistance in a viscous fluid

2.2.2.1 Model submerged

Consider firstly the form of the model to be pressed out into a thin plate of the same length and wetted area as the model. Assume that the plate is infinitely thin so that when the fluid flows parallel to its plane there are no frontal pressures acting on the plate; however, tangential shear stresses will act on the plate due to the viscosity of the fluid. If these tangential shear stress forces are integrated longitudinally they would represent the flat plate skin friction shown as curve OC in Figure 2.2.

Consider again the three-dimensional body placed in a moving stream of viscous fluid. If the tangential shear stresses acting on the model are integrated longitudinally the answer will be the real skin

friction resistance of the model, shown as curve OD in Figure 2.2. This skin friction is slightly greater than the flat plate friction because the local fluid speeds are increased as the fluid is forced to move around the model.

Due to the build-up of the boundary layer around the model, separation occurs with the result that the longitudinally integrated normal pressure forces at the bow are greater than at the stern, i.e. the model experiences a resistance associated with normal pressures. This is known as viscous pressure resistance as it is due to the viscosity of the fluid.

The sum of the viscous pressure resistance and skin friction resistance is known as total viscous resistance which is depicted as curve OE in Figure 2.2.

2.2.2.2 Model at the surface

At the surface the model generates waves which are another source of resistance. This is again "seen" by the hull as changes in normal pressures, the longitudinally integrated component of which is wave-making pressure resistance. Therefore, the normal pressures acting on the model in this case are due to wave-making and to the viscosity of the fluid.

The sum of the total viscous resistance and wave-making resistance is the total resistance of the surface model, shown as curve OF in Figure 2.2.

SHIP RESISTANCE COMPONENTS

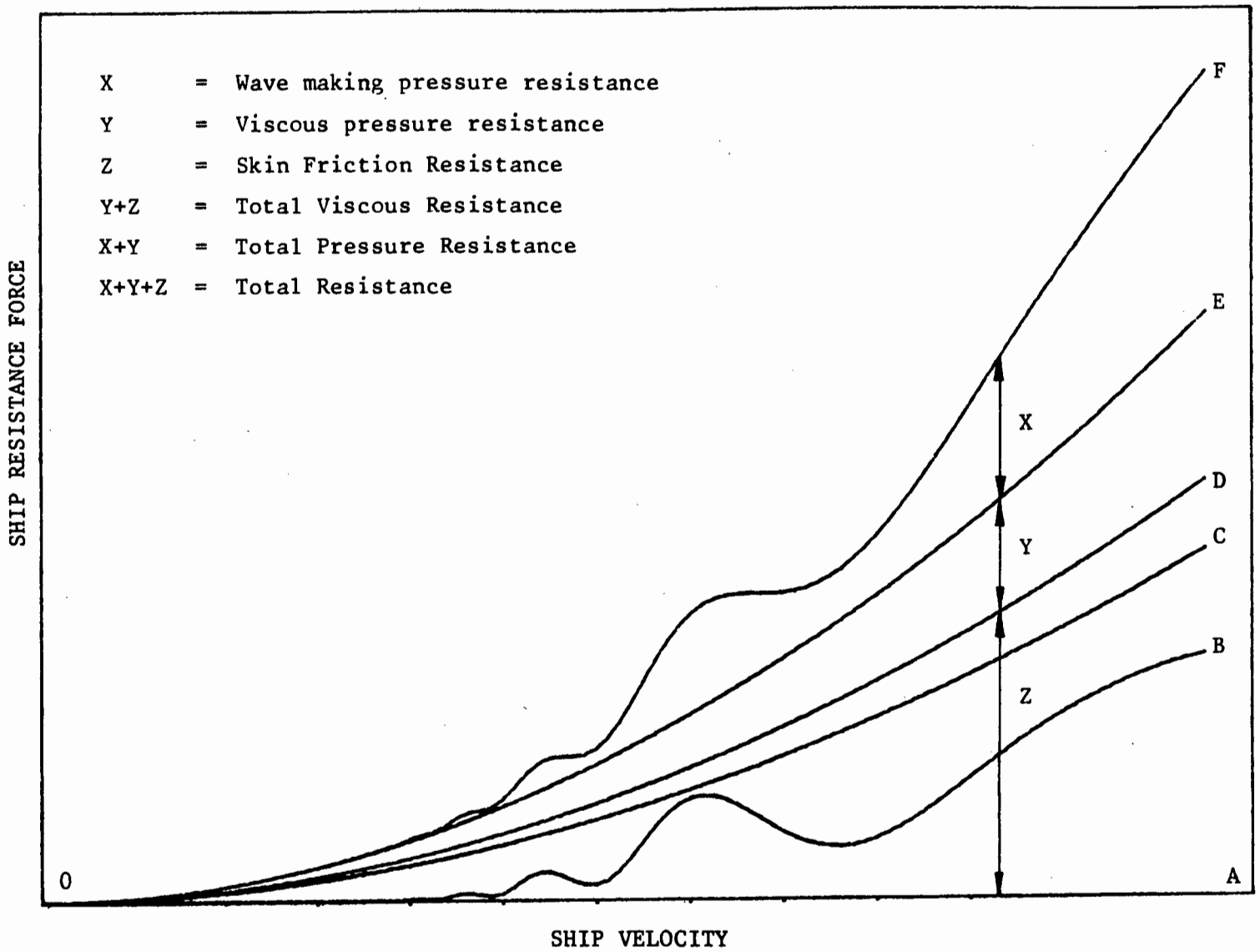

Figure 2.2 Components of Ship Resistance (adapted from Lackenby 1965)

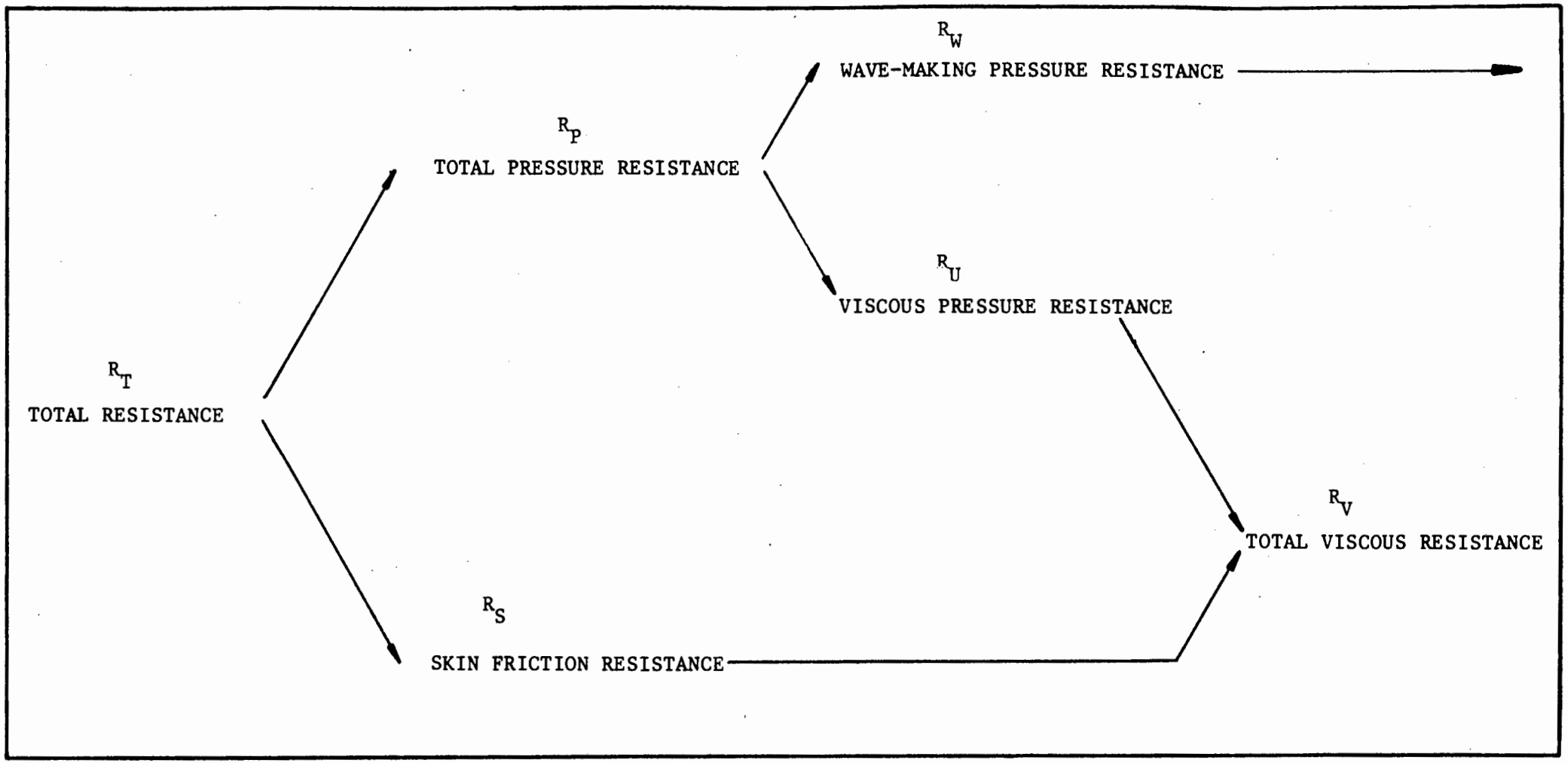

Figure 2.3 Schematic Diagram of the Components of Ship Resistance

2.3 Modelling ship resistance

2.3.1 Dimensional analysis for a surface body

Ship resistance is dependent on many variables and due to the complexity of the problems no exact solution that provides numerical answers to ship resistance has been found. Dimensional analysis may be used to find relationships between variables on which an empirical solution may be based. Dimensional analysis is a powerful tool since the correctness of the answer does not depend on detailed analysis but only on the right choice of variables.

Considering a ship moving through deep, still water its resistance may be taken to be a function of:

a.	The ship's speed relative to the water	V (m/s)
b.	Size of the ship - taken to be the water line length,	L (m)
c.	Dimensionless ratios expressing the form of the ship,	r_1 , r_2 , r_3 ...
d.	Density of the fluid,	ρ (kg/m^3)
e.	Dynamic viscosity of the fluid,	μ (kg/m.s)
f.	Acceleration due to gravity,	g (m/s^2)

R_T = ship's resistance at speed V

$$= f\ (V, L, r_1, r_2, r_3, \ldots, \rho, \mu, g) \qquad (2.5)$$

Since we are primarily concerned with the resistance of geometrically similar ships, the dimensionless ratios expressing the ships form may be ignored.

$$\therefore\ R_T = f\ (V, L, \rho, \mu, g) \qquad (2.6)$$

Raising each term to a power and rewriting in fundamental dimensions mass M , length L , time T

$$R_T = f\ (V^a,\ L^b,\ \rho^c,\ \mu^d,\ g^c) \tag{2.7}$$

$$\frac{ML}{T^2} = f\left[\ \left(\frac{L}{T}\right)^a,\ L^b,\ \left(\frac{M}{L^3}\right)^c,\ \left(\frac{M}{LT}\right)^d,\ \left(\frac{L}{T^2}\right)^e\ \right] \tag{2.8}$$

$\therefore$ $1 = c + d$

$1 = a + b - 3c - d + e$

$2 = a + d + 2e$

writing a, b and c in terms of d and e

$a = 2 - d - 2e$

$b = 2 - d + e$

$c = 1 - d$

Substituting into (2.7)

$$R_T = f\ (V^{2-d-2e}\ L^{2-d+e}\ \rho^{1-d}\ \mu^d\ g^e)$$

$$R_T = \rho\ V^2\ L^2\ f\left[\ \left(\frac{VL\rho}{\mu}\right)^{-d}\ \left(\frac{V}{\sqrt{gL}}\right)^{-2e}\ \right]$$

Coefficient of kinematic viscosity $= \nu = \frac{\mu}{\rho}$ (m^2/s)

Therefore

$$R_T = \rho\ V^2\ L^2\left[\ f_1\left(\frac{VL}{\nu}\right),\ f_2\left(\frac{V}{\sqrt{gL}}\right)\ \right]$$

where $\rho V^2 L^2$ has dimensions of force

$\frac{VL}{\nu}$, $\frac{V}{\sqrt{gL}}$ are dimensionless as are any functions containing them

$\frac{VL}{\nu}$ = Reynolds number = Re_L

$\frac{V}{\sqrt{gL}}$ = Froude number = F_r

Rewriting

$$R_T = \rho V^2 L^2 \left[f_1 (Re_L) , f_2 (F_r) \right] \qquad (2.9)$$

Dimensional analysis does not give any further information in determining the functions f_1 and f_2, nor does it indicate whether they are independent of each other.

2.3.2 Scaling from model to prototype

According to Equation (2.9), in order to scale the resistance of a model up to prototype resistance the resistance of the model would have to be measured at the same Froude number and Reynolds number as the prototype.

To satisfy the similarity conditions for Froude number we need

$$\frac{V_p}{\sqrt{g_p L_p}} = \frac{V_m}{\sqrt{g_m L_m}}$$

Since gravity is essentially constant on the earth it is not practical to change gravity, thus g_p is equal to g_m .

Defining λ to equal the ratio of the prototype length to the model length we get

$$\frac{V_p}{V_m} = \sqrt{\frac{L_p}{L_m}} = \lambda^{\frac{1}{2}} \qquad (2.10)$$

that is, the velocity of the model must be slower than that of the prototype. For example, consider a one in a hundred scale model of a 200 m ship which has a service speed of 15 m/s, the required model size would be 2 m and the model velocity 1,5 m/s.

Now considering similarity as determined by the Reynolds number

$$\frac{V_p L_p}{\nu_p} = \frac{V_m L_m}{\nu_m}$$

Assuming that the prototype and model are both operating in water at the same temperature, that is $\nu_p = \nu_m$

then $$\frac{V_p}{V_m} = \frac{L_m}{L_p} = \lambda^{-1} \qquad (2.11)$$

that is, the velocity of the model must be faster than the prototype velocity. Using the previous example the model velocity would have to be 1500 m/s. Clearly it is impossible for both Froude number and Reynolds number to be satisfied with one model, unless major changes are made to the effect of gravity on the model or the viscosity of the fluid that the model is tested in. Since changes to gravity and viscosity are impractical a different approach had to be found.

In Equation (2.9) there are the two important dimensionless ratios; Froude number and Reynolds number. Since Froude number contains g it can be reasonably expected that Froude number represents the wave-making resistance of the ship. Reynolds number contains viscosity and is, therefore, expected to represent the viscous resistance of the ship.

2.3.3 Froude's method

William Froude carried out tests on many geometrically similar models (geosims) and from this in 1868 he formulated his Law of Comparison (ref Todd 1966) which states:

"The resistance of geometrically similar ships is in the ratio of the cube of their linear dimensions if their speeds are in the ratio of the square roots of their linear dimensions".

that is if $$\frac{V_p}{V_m} = \lambda^{\frac{1}{2}}$$

then $$\frac{R_{Tp}}{R_{Tm}} = \lambda^3 \qquad (2.12)$$

If the model and prototype are run in fluid with the same density and at the same temperature then their displacements Δ, are also in the ratio λ^3

$$\frac{R_{Tp}}{R_{Tm}} = \frac{\Delta_p}{\Delta_m} \quad \text{or} \quad \frac{R_{Tp}}{\Delta_p} = \frac{R_{Tm}}{\Delta_m} \qquad (2.13)$$

Froude found that this law was not quite valid for his geosims and he believed that this was because the frictional resistance did not follow the same law of variation that the wave-making resistance followed. It is important to remember that when Froude was working on this problem many concepts today taken for granted did not exist, such as boundary layer theory,

Reynolds number and the ratio which was later to bear his name, Froude number. Froude proposed to separate the frictional resistance from the total resistance, and the modern interpretation of this may be shown by rewriting Equation (2.9)

$$R_T = \rho V^2 L^2 \left[f_1 (R_e) + f_2 (F_r) \right] \qquad (2.14)$$

In order to determine the variation of frictional resistance with speed, size and surface roughness, he carried out his famous plank experiments (ref Froude 1872). Froude found that the frictional resistance varied slightly less than the square of the speed and that the resistance per unit area decreased as the length of the plank increased. Froude presented his equation in the following form

$$R_F = f S_W V^n \qquad (2.15)$$

where R_F = frictional resistance of the plank or flat plate skin friction

S_W = wetted surface area

f = a dimensional coefficient which depended on the roughness of the surface and also decreased with increasing plank length

V = speed of plank through the water

n = an index which was 1,825 for smooth surfaces and 2,0 for rough surfaces.

It is important to note that the frictional resistance that Froude measured was the flat plate skin friction and not the true skin friction of a 3-dimensional body which will be slightly greater. Froude had now divided the total resistance

of a ship into frictional resistance R_F and the remainder which he carefully termed residuary resistance R_R since it contained viscous and wave-making components. This may be written as

$$R_T = R_F + R_R \qquad (2.16)$$

2.3.4 Extension of model resistance to prototype resistance

To predict the resistance of prototype ships from model results Froude proposed the following method which is based on Equation (2.16).

a. The model is made to a linear scale of λ and operated at a number of Froude numbers that are in the range of the prototype Froude numbers.

b. The total resistance R_{Tm} is measured during these runs.

c. The frictional resistance of the model R_{Fm} is calculated using Equation (2.15).

d. The residuary resistance of the model R_{Rm} is found by difference using Equation (2.16).

$$R_{Rm} = R_{Tm} - R_{Fm}$$

e. The residuary resistance of the prototype R_{Rp} is calculated using Equation (2.12) and the corresponding prototype speed V_p is calculated using Equation (2.10).

f. The frictional resistance of the prototype R_{Fp} is calculated using Equation (2.15).

g. The total resistance of the prototype R_{Tp} is found using Equation (2.16)

$$R_{Tp} = R_{Rp} + R_{Fp}$$

This method is the basis of predicting prototype resistance that is still used in all towing tanks today. There are a number of new frictional resistance formulations which will be discussed in Section 2.4.

In order to obtain dimensionless plots of resistance versus speed various resistance coefficients have been defined as follows

$$C_T = \text{Total resistance coefficient} = \frac{R_T}{\frac{1}{2} \rho V^2 S_W} \tag{2.17}$$

$$C_F = \text{Frictional resistance coefficient} = \frac{R_F}{\frac{1}{2} \rho V^2 S_W} \tag{2.18}$$

$$C_R = \text{Residuary resistance coefficient} = \frac{R_R}{\frac{1}{2} \rho V^2 S_W} \tag{2.19}$$

The frictional resistance coefficient is generally plotted against Reynolds number while the residuary resistance coefficient is plotted against Froude number.

It is important to note that there is an inaccuracy in the Froude method in that the residuary resistance contains components (viscous pressure resistance and an extra frictional force due to curvature) that are dependent on viscosity. These parts of the residuary resistance are scaled up with the wave-making resistance using Froude number scaling although they should be scaled using Reynolds number. Nevertheless this inaccuracy does not seem to have had a major influence on the results since the Froude scaling method has been used successfully for nearly a century. It does, however, represent an area where a refinement of the scaling method could be made.

2.4 Skin friction

Skin friction is a very important part of ship resistance since for most ships it is the major component of resistance. On cargo carriers, which form the major part of the world's mercantile fleet, skin friction can amount up to 85-90% of the total resistance. Even on higher speed passenger liners and warships where wave-making resistance becomes more influential, skin friction can account for up to 50% of the total resistance (ref Blevins 1984).

Skin friction also plays an important role in the modelling of ship resistance. The flow regime around all prototype ships is turbulent and when a model is tested care must be taken to ensure that flow around the model is turbulent (ref Allan and Conn 1950).

If results taken from a model which has been tested in laminar flow are extrapolated to full scale, the predicted full scale resistance will be significantly less than the actual resistance of the prototype.

A factor which has a significant effect on skin friction is the hull surface condition. On clean, new sister ships power differences of over 20% have been found and this is mainly attributed to differences in painting and hull surface finish. The change from riveted to welded construction has resulted in smoother hulls which give an estimated power reduction of 20% (ref Lackenby 1962). Corrosion and fouling of a ship's hull can also significantly affect the ship resistance. Figure 2.4, page 2.17, shows the increase in power required by a ship in relation to the number of years in service.

To demonstrate the nature of skin friction it is useful to consider a vertical flat plate placed in a moving stream of water. The resistance acting on the flat plate will be the flat plate skin friction as discussed in Section 2.2.2.1.

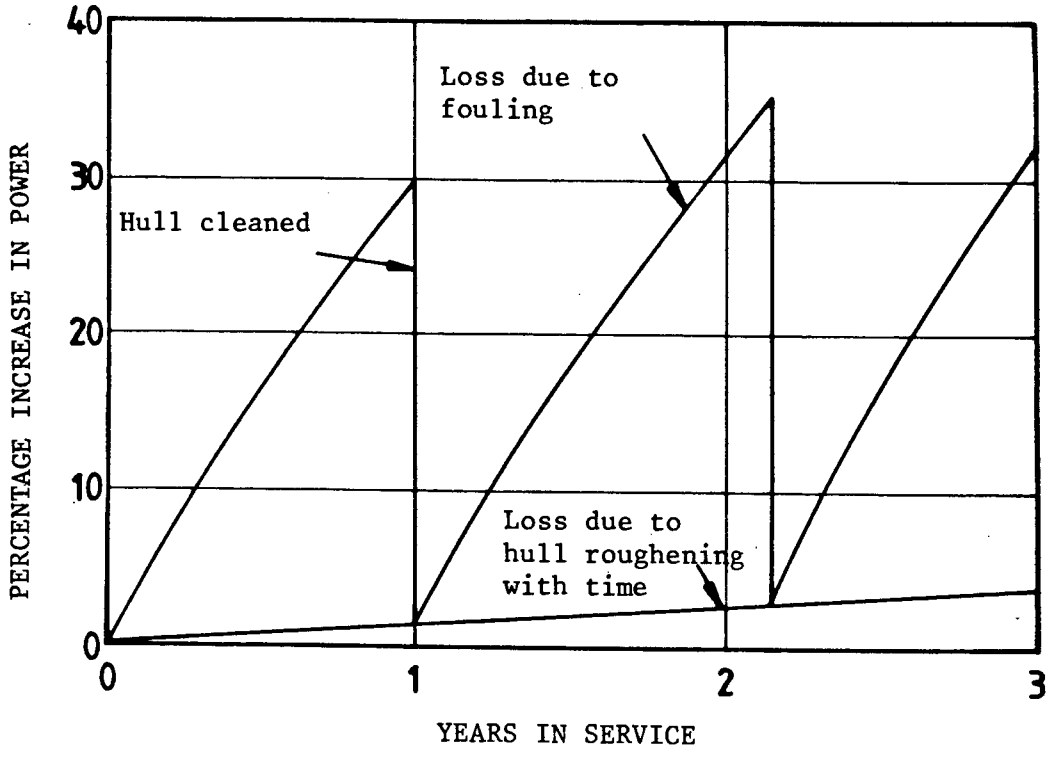

Figure 2.4 Loss in performance with time in service for a cross-channel ship (ref Lackenby 1962)

2.4.1 Skin friction acting on a flat plate

Consider the flow of water to be moving past the plate at steady speed. The fluid particles directly in contact with the plate remain fixed to the plate; however, at some small distance from the plate the velocity in the fluid will equal the free stream approach velocity. Thus there is a narrow belt of high velocity gradient transversely away from the plate which is termed the boundary layer. The boundary layer is characterised by high shearing stresses caused by the momentum interchange between the adjacent layers of differing speed. These shearing stresses in the boundary layer are the origin of the skin friction acting on the plate.

The boundary layer at the leading edge of the plate is zero and thickens away from the leading edge. The fluid flow near the leading edge will be laminar, and in this region the boundary layer is termed the laminar boundary layer. The laminar boundary layer continues to thicken until a critical

value of plate Reynolds number Re_x is reached at which the laminar flow breaks down and becomes generally turbulent. The fluid particles no longer move in streamlines but have an oscillatory motion about a mean flow path. The boundary layer becomes much thicker, thus increasing the amount of water entrained in the boundary layer, leading to a greater momentum demand and consequently the resistance to motion increases. Figure 2.5 shows the development of turbulent flow along a flat plate. Note that in the turbulent flow regime there is still a laminar sub-layer through which the final transfer of momentum is made.

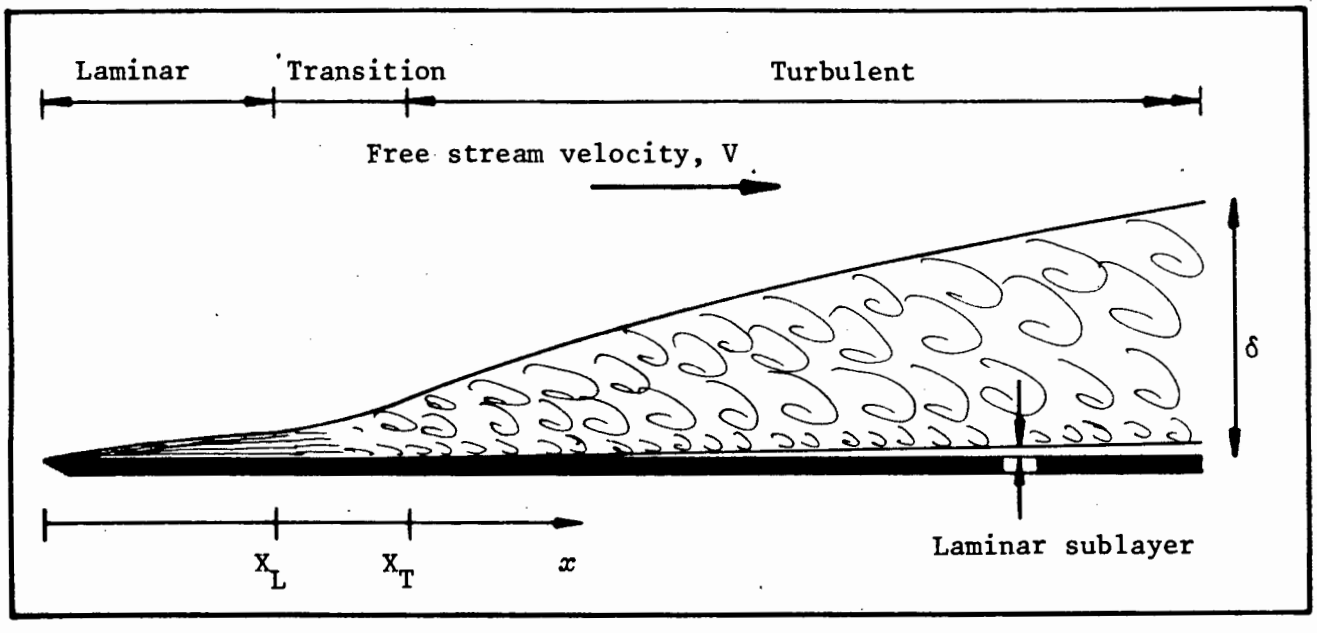

Figure 2.5 Development of boundary layer on a flat plate

The value of x_L i.e. the length of the laminar flow regime beyond the leading edge of the plate, is only influenced by the level of turbulence in the approaching fluid. The roughness of the surface has no effect on the magnitude of x_L .

The variation of values of x_L is given by (ref Kilner 1983)

$$Re_x = 5 \times 10^5 \text{ to } 2 \times 10^6$$

where Re_x = Plate Reynolds number

$$= \frac{Vx}{\nu} \qquad (2.20)$$

The lower value is for highly turbulent approach flow, while the higher value is for low levels of turbulence in the approaching flow.

Returning to the example discussed in Section 2.3.2 and considering the model to be tested under Froude number scaling, Vp = 15 m/s and Vm = 1,5 m/s. Assuming that both the model and prototype are in water at 15°C

$$x_{Lm} = \frac{\nu \ (5\text{x}10^5 \text{ to } 2\text{x}10^6)}{V}$$

$$= \frac{1{,}141\text{x}10^{-6} \ (5\text{x}10^5 \text{ to } 2\text{x}10^6)}{1{,}5}$$

$$= 0{,}380 \text{ to } 1{,}521 \text{ m}$$

$$x_{Lp} = 0{,}038 \text{ to } 0{,}152 \text{ m}$$

Therefore, the length of the laminar boundary layer along the hull is much smaller on the prototype (0,05% of its length) than the model (48% of its length on average). Therefore, the extensive existence of laminar flow over a ship model hull can be a source of error and care needs to be taken to ensure that the flow around a model is turbulent.

The boundary layer thickness, δ is not capable of exact definition and many approximations exist based on properties of the boundary layer (ref Blevins 1984).

a. 99% thickness
b. Displacement thickness
c. Momentum thickness
d. Kinetic energy thickness
e. Shear thickness.

In this thesis the 99% thickness will be used, which is the distance from the surface for the flow velocity to achieve 99% of the free stream velocity V .

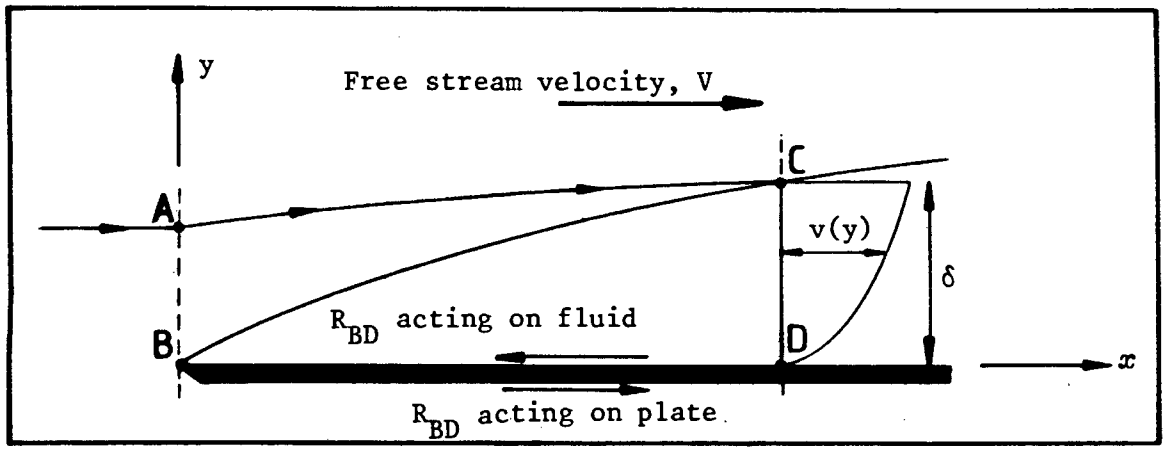

Figure 2.6 Streamline along a flat plate

Referring to Figure 2.6, two sections have been chosen on the plate: one at the leading edge AB and the other within the boundary layer CD. The discharge crossing AB is equal to the discharge crossing CD and, therefore, there is no flow across AC i.e. AC is a streamline. The deviation of the streamline is assumed to be small and, therefore, it may also be assumed that there is no pressure gradient along the plate.

Thus in applying the impulse momentum principle to ABCD only the resistance force on the plate and the momentum pressure forces at AB and CD need to be considered. To calculate the momentum pressure force at CD the velocity distribution in the boundary layer must be known. Applying the impulse momentum principle:

For unit width into the paper

$$\rho V^2 AB = R_{BD} + \int_o^\delta \rho [v(y)]^2 dy \qquad (2.21)$$

and $\rho V AB = \int_o^\delta \rho v dy$ from continuity

$$\rho V^2 AB = \int_o^\delta \rho v V dy \qquad (2.22)$$

Equating (2.21) and (2.22)

$$R_{BD} = \int_o^\delta (\rho v V - \rho v^2) dy = \rho \int_o^\delta v (V-v) dy \qquad (2.23)$$

i.e. the resistance acting on a single side of the plate per unit width. Note that this is a very general result depending only on velocity distribution at CD and not on the boundary layer type.

2.4.1.1 Laminar boundary layer

The velocity distribution in a laminar boundary layer may be solved exactly by the solution of the Navier Stokes equations governing the flow. The analytical evaluation of these equations was first obtained by Blasius and subsequently the solution procedure has been refined (ref Schlichting 1968). The solution of the velocity distribution is presented in Figure 2.7.

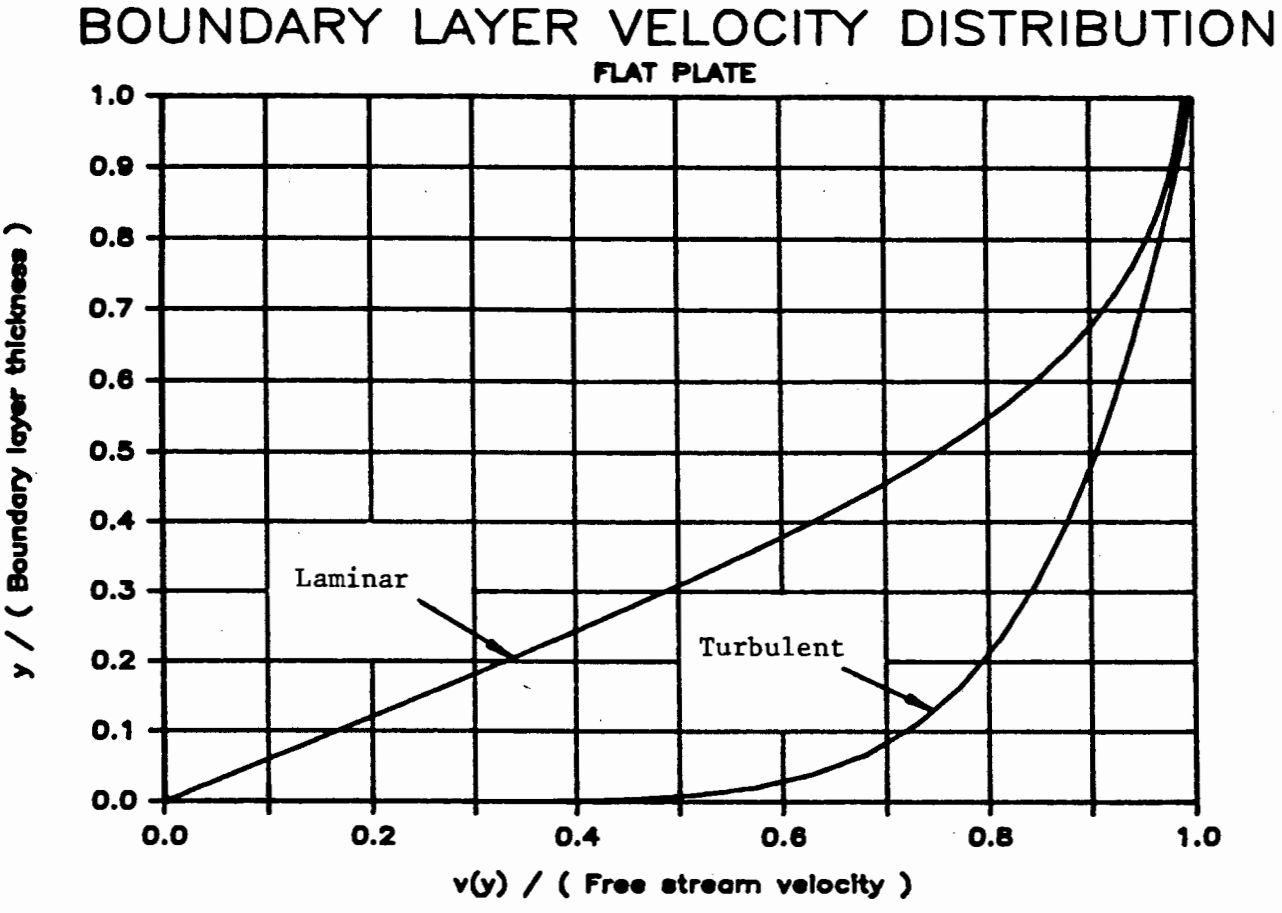

Figure 2.7 Boundary layer velocity distribution

The thickness of the boundary layer is given approximately by

$$\delta = 5\sqrt{\frac{\nu x}{V}} = 5x\sqrt{\frac{\nu}{Vx}} = 5x\ (Re_x)^{-\frac{1}{2}} \qquad (2.24)$$

Thus the boundary layer thickness in laminar flow increases with the square root of x .

The skin friction acting on the plate may now be calculated by returning to Equation 2.23 and using the velocity distribution given in Figure 2.7. The solution of the integral gives the following

$$R_F = 0{,}1328\ \rho\ V^2\ \delta$$

substituting in Equation 2.24

$$R_F = 0{,}1328\ \rho\ V^2\ 5x\ (Re_x)^{-\frac{1}{2}}$$

$$= 0{,}664\ \rho\ V^2\ x\ (Re_x)^{-\frac{1}{2}} \qquad (2.25)$$

giving the skin frictional force acting on one side of the plate.

The skin frictional resistance coefficient is

$$C_F = \frac{R_F}{\frac{1}{2}\ \rho\ V^2\ x} = 1{,}328\ (Re_x)^{-\frac{1}{2}} \qquad (2.26)$$

This is known as the Blasius line for laminar flow. See Figure 2.8 page 2.24.

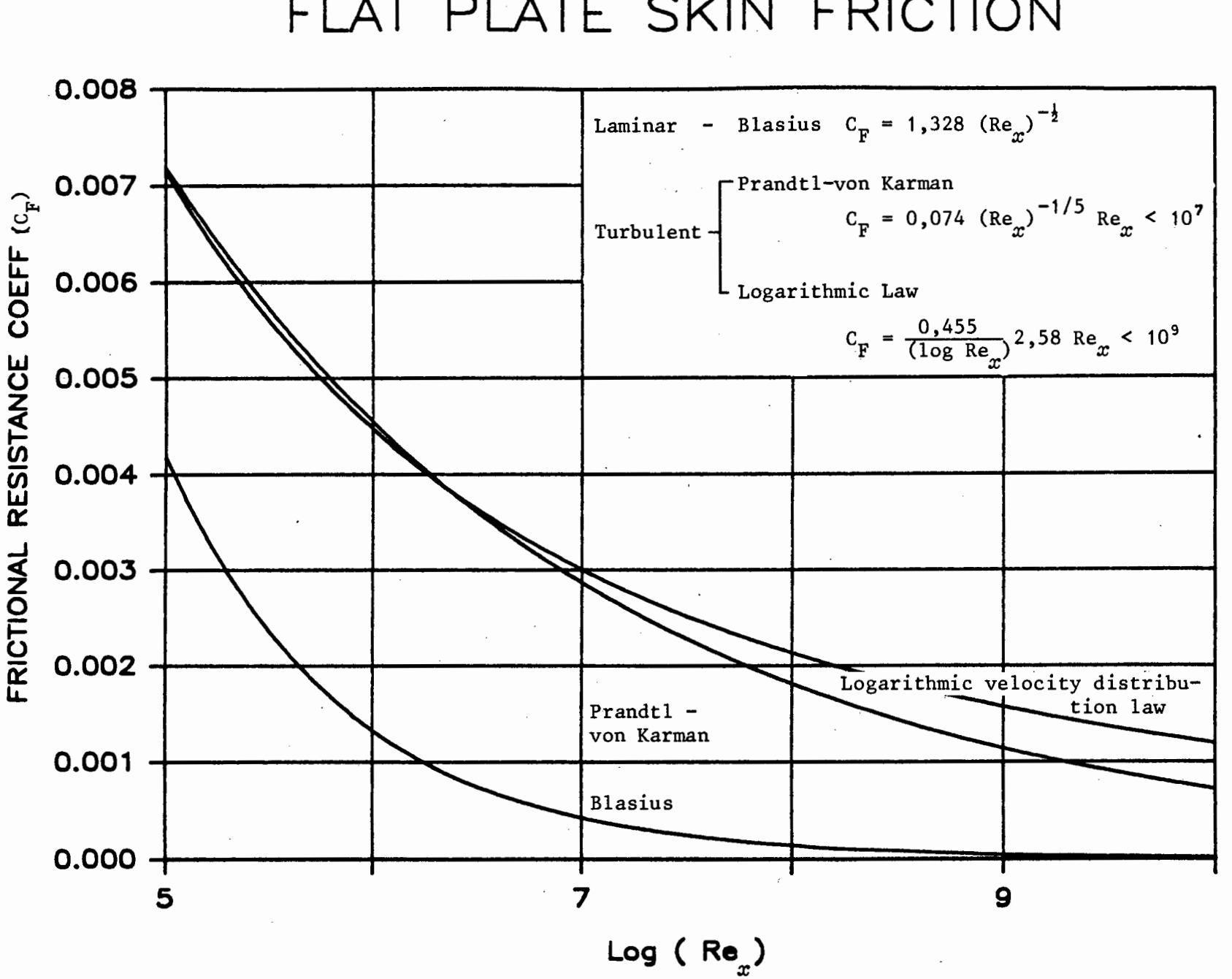

Figure 2.8 Flat plate skin friction formulations

2.4.1.2 Turbulent boundary layer on a smooth plate

There are two solutions available for turbulent flow on a smooth flat plate - one based on a power velocity distribution and the other on a logarithmic velocity distribution. The solution to the power velocity distribution will be discussed first and then, due to the complexity of the logarithmic velocity distribution, its solution will only be stated.

Nikuradse carried out experiments with turbulent flow through smooth pipes and measured the velocity profiles at different Reynolds numbers. He presented his answers in the empirical form.

$$\frac{v(y)}{V_{max}} = \left(\frac{y}{R}\right)^{1/n} \qquad (2.27)$$

where R = radius of pipe

V_{max} = maximum velocity in pipe

y = radius at which velocity is $v(y)$.

The value of n is function of Reynolds number and approximately equals 7 in the range $4 \times 10^3 < Re < 3 \times 10^7$ (ref Schlichting 1968). Prandtl made the assumption that the velocity distribution in the layer of a flat plate is identical to that of a circular pipe. Although this cannot be precisely correct since there is a pressure gradient in a pipe, it is nevertheless close enough to be used as an approximation.

Therefore, we have the following approximate velocity distribution in the turbulent boundary layer of a flat plate (see Figure 2.7 page 2.22).

$$\frac{v}{V_{max}} = \left(\frac{y}{\delta}\right)^{1/7} \tag{2.28}$$

substituting this into Equation 2.23 and solving

$$R_F = \rho V^2 \int_o^\delta \left(\frac{v}{V_{max}}\right)\left(1 - \frac{v}{V_{max}}\right) dy$$

$$= \rho V^2 \int_o^\delta \left[\left(\frac{y}{\delta}\right)^{1/7} - \left(\frac{y}{\delta}\right)^{2/7}\right] dy$$

$$= \rho V^2 \delta \left[\frac{7}{8}\left(\frac{y}{\delta}\right)^{8/7} - \frac{7}{9}\left(\frac{y}{\delta}\right)^{9/7}\right]_o^\delta$$

$$= \frac{7}{72} \rho V^2 \delta \tag{2.29}$$

To obtain information about the wall shear stress τ_o, we use the relationship established by Blasius for Reynolds number in pipe flow

$$\frac{\tau_o}{\frac{1}{2}\rho \bar{V}^2} = 0{,}08\ (Re)^{-1/4} \tag{2.30}$$

where Re = Reynolds number of pipe = $\frac{\bar{V}D}{\nu}$

$\bar{V}$ = Mean velocity

D = Diameter of pipe.

We need Equation 2.30 in terms of radius and maximum velocity. Using the relationship (ref Kilner notes 1983)

$$\frac{V_{max}}{\bar{V}} = 1,24 \quad \text{for} \quad Re < 3 \times 10^7$$

and $D = 2R$

$$\therefore \quad Re = \frac{V_{max}}{\frac{1,24}{\nu}} 2R = \frac{1,6129\ V_{max}\ R}{\nu}$$

Rewriting Equation 2.30

$$\frac{\tau_o}{\frac{1}{2}\rho V^2_{max}} = 0,0462 \left(\frac{V_{max}\ R}{\nu}\right)^{-1/4} \qquad (2.31)$$

And now using the analogy between the flat plate and circular pipe we take V_{max} as the free stream velocity V and δ as the thickness of the boundary layer. Therefore, we can now write Equation 2.31 as applied to a flat plate

$$\tau_o = 0,0231\ \rho\ V^2 \left(\frac{V\ \delta}{\nu}\right)^{-1/4} \qquad (2.32)$$

Differentiating Equation 2.29 with respect to x we get

$$\tau_o = \frac{dF}{dx} = \frac{7}{72}\ \rho\ V^2\ \frac{d\delta}{dx} \qquad (2.33)$$

Equating Equations 2.32 and 2.33

$$\frac{0,0231}{(\frac{V\delta}{\nu})1/4} = \frac{7}{72}\frac{d\delta}{dx}$$

$$\int_o^x 0,2374\ dx = \int_o^\delta (\frac{V\delta}{\nu})^{1/4}\ d\delta$$

$$0,2374\ x = (\frac{V}{\nu})^{1/4}\frac{4}{5}\delta^{5/4}$$

Raising to 4/5 :

$$0,3165\ x^{4/5} = (\frac{V}{\nu})^{1/5}\ (0,8365)\delta$$

$$\therefore\ \delta = 0,37\ x\ (Re_x)^{-1/5} \qquad (2.34)$$

Therefore, in a turbulent boundary layer δ increases with x to the 0,8 power compared to the laminar boundary layer case where δ increases with x to 0,5 power.

Substituting Equation 2.34 into Equation 2.29

$$R_F = 0,036\ \rho\ V^2\ x\ (Re_x)^{-1/5} \qquad (2.35)$$

giving the skin friction acting on one side of the plate. Thus the skin friction coefficient is given by

$$C_F = \frac{R_F}{\frac{1}{2}\ \rho\ V^2} = 0,072\ (Re_x)^{-1/5} \qquad (2.36)$$

$$Re_x < 10^7$$

A better correlation with experimental results has been found by changing the numerical constant to 0,074, therefore

$$C_F = 0{,}074\ (Re_x)^{-1/5} \qquad Re_x < 10^7 \qquad (2.37)$$

Equation 2.36 is known as the Prandtl-von Karman line and is illustrated in Figure 2.8 page 2.24.

The solution to the logarithmic velocity distribution has been found to fit an empirical equation of the form

$$C_F = \frac{0{,}455}{(\log Re_x)^{2{,}58}} \qquad (2.38)$$

This equation is valid for the whole range of Reynolds numbers up to $Re_x = 10^9$. See Figure 2.8 page 2.24.

2.4.1.3 Laminar and turbulent flow on a smooth flat plate

Unless the flow is disturbed before reaching the plate the flow after the leading edge will be laminar and if the critical value of Reynolds number is reached further down the plate the transition from laminar to turbulent flow will take place. In order to allow for the initial length of laminar flow we need to make the following correction (ref Schlichting 1968).

$$C_F = \frac{0{,}455}{(\log Re_x)^{2{,}58}} - \frac{A}{Re_x} \qquad (2.39)$$

The values of A are given in Table 2.1. This equation is known as the Prandtl-Schlichting skin friction formula for a smooth flat plate at zero incidence.

Re at transition	$3x10^5$	$5x10^5$	10^6	$3x10^6$
A	1050	1700	3300	8700

Table 2.1 A versus Re at transition

2.4.1.4 Turbulent flow on a rough plate

For fully developed turbulent flow on rough plates the following equation has been obtained by empirical methods (see Figure 2.9 page 2.31).

$$C_F = [1,89 + 1,62 \log (x/k)]^{-2.5} \qquad (2.40)$$

valid for $10^2 < x/k < 10^6$

where k = effective roughness of plate (m)

$\frac{k}{x}$ = relative roughness

Providing the protuberances constituting the roughness are within the depth of the laminar sub-layer, they will have no influence on the skin friction. As Reynolds number increases, the relative roughness ratio at which the surface ceases to behave as a smooth one decreases. If the roughness at which this particular value of $\frac{k}{x}$ occurs, is called the admissible roughness, k_{adm}, its variation with Reynolds number can approximately

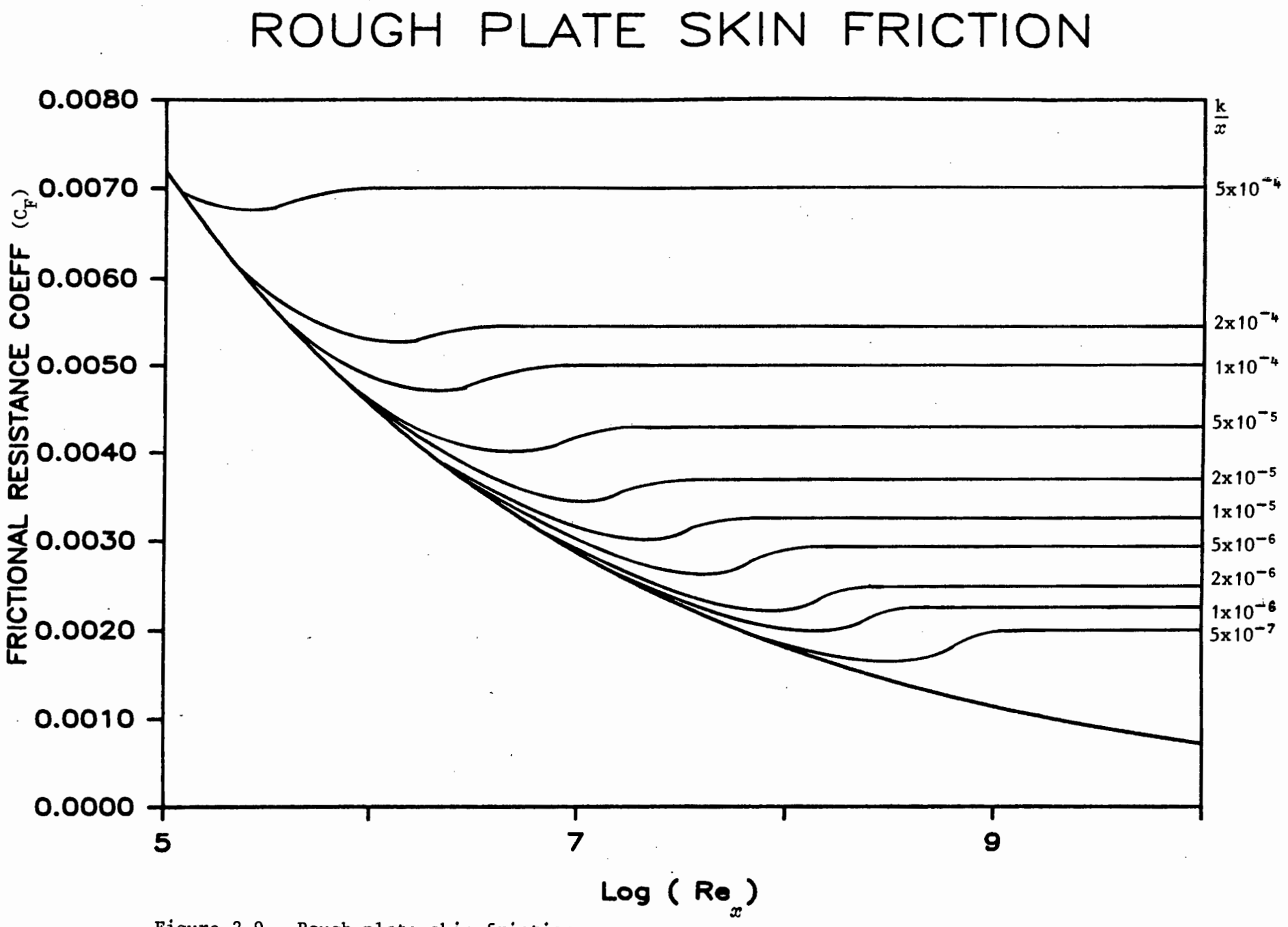

Figure 2.9 Rough plate skin friction

be given by the following formula (ref Todd 1966)

$$\frac{V\, k_{adm}}{\nu} = 100 \qquad (2.41)$$

Therefore, the admissible roughness does not depend on the length of the plate. A ship travelling at a speed of 14 m/s will have an admissible roughness of 0,007 mm, and while travelling at 5 m/s an admissible roughness of 0,02 mm. Clearly it is impossible to obtain a hydraulically smooth ship hull and, therefore, a correction due to hull roughness will always have to be made when predicting ship skin friction.

2.4.2 Skin friction acting on a ship

The nature of the skin friction acting on a ship is similar to that of a flat plate - the only difference being the curvature of the hull which leads to radial pressure gradients and velocities around the hull which are slightly greater than the ship's speed through the water. If the velocity distribution within the boundary layer is known then it is possible to exactly calculate the skin friction acting on the ship.

To determine the velocity distribution around a single hull involves a substantial amount of work and time and is, therefore, not a practical method of determining the skin friction of a large number of hull forms. In order to provide quick numerical values for skin friction, various skin friction formulations have been developed.

The first of these formulations was developed by Froude after his famous plank experiments in 1872 as was discussed in Section 2.3.4. The form of Froude's equation is as follows

$$R_F = f\, S_W\, V^n \qquad (2.42)$$

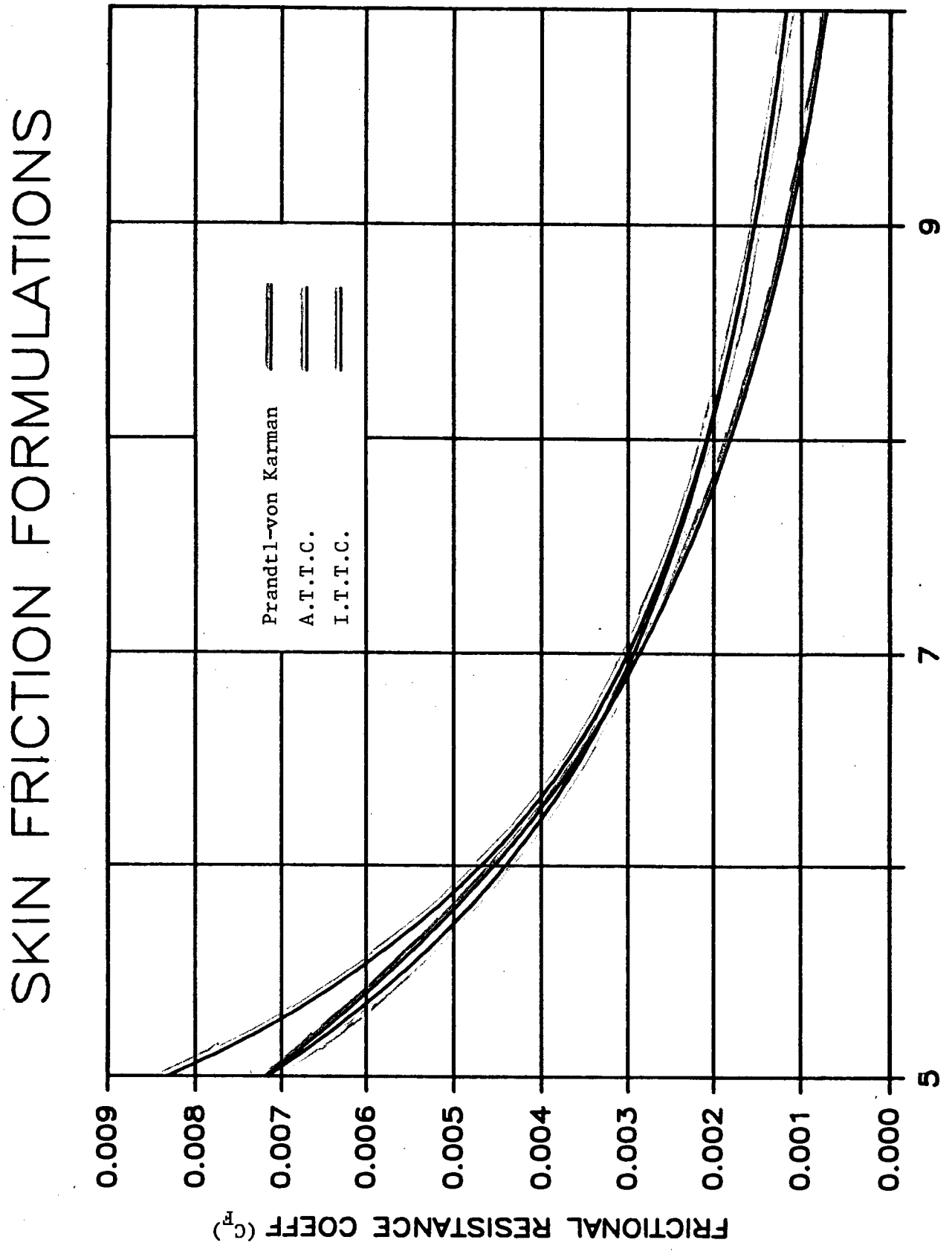

Figure 2.10 Skin friction formulations

The coefficients f and n make allowance for different lengths of plank and plank surface roughness. Froude's equation is essentially a flat plate skin friction formulation. In 1921 Prandtl and von Karman separately published Equation 2.43. This formulation is based on a smooth flat plate with fully developed turbulent flow. The equation is valid for Reynolds numbers below 10^7 . See Figure 2.10 page 2.33.

$$C_F = 0{,}074\ (Re_L)^{-1/5} \tag{2.43}$$

Schoenherr in 1932 collected most of the data from plank tests available and set out to obtain a formulation using Reynolds number and a frictional resistance coefficient. His formulation later became known as the A.T.T.C. (American Towing Tank Conference) line, Equation 2.44. Schoenherr's formulation is based on smooth flat plate data and, therefore, a correction needs to be made for roughness. See Figure 2.10 page 2.33.

$$\frac{0{,}024}{\sqrt{C_F}} = \log\ (Re_L\ C_F) \tag{2.44}$$

At the 1957 International Towing Tank Conference (I.T.T.C.) a new formulation was presented, Equation 2.45. This formulation is a model-ship correlation and does not claim to represent the frictional resistance of either a flat plate or a curved surface. See Figure 2.10 page 2.33.

$$C_F = \frac{0{,}075}{[\log\ Re_L - 2]^2} \tag{2.45}$$

The 1957 I.T.T.C. line has not been accepted by all towing tanks and many still use frictional formulations that are based on their own data collected during tests. Therefore, there is, as yet, no completely standard formulation for skin friction prediction.

2.5 Viscous pressure resistance

Viscous pressure resistance is due to the failure of the streamlines to close behind a ship. This results in a lack of pressure recovery at the stern, i.e. the pressures acting on the bow are greater than the pressures acting on the stern. See Figure 2.11.

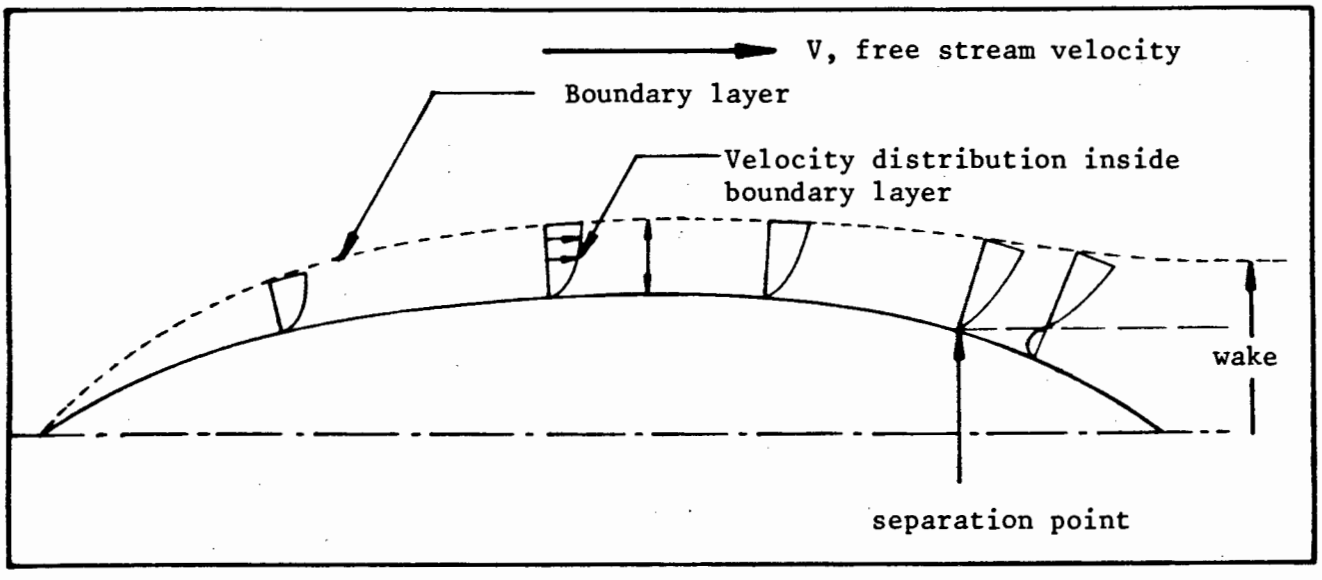

Figure 2.11 Separation on a ship form

The boundary layer has no thickness at the bow and gradually increases towards the stern as more fluid is caught up in the momentum interchange between the ship and the surrounding fluid. Fluid particles moving from the bow to the stern have their velocities reduced by the pressure gradient (i.e. moving towards higher pressure) and the shearing stresses. At some point along the hull fluid particles may have insufficient kinetic energy to move along the hull and they come to rest against the ship's hull. At this point separation takes

place, particles following are subsequently diverted away from the hull causing vortices in the boundary layer and wake. Thus from the separation point the flow lines leave the hull and distort the pressure distribution in this zone, thus causing the failure of the pressures at the stern to match the pressures at the bow.

The above phenomenon would not take place in an ideal fluid and would also not arise on a flat plate. Therefore, viscous pressure resistance is dependent on the viscosity of the fluid and the ship form, increasing as viscosity increases and as the hull form becomes more bluff.

2.6 Wave-making resistance

Wave-making resistance forms one of the most important components of a ship's resistance even though it only becomes dominant at high speeds. The viscous resistance of a conventional ship's hull cannot be reduced significantly by changes to the hull shape. However, the wave-making resistance can be reduced appreciably by modifications to the hull shape. This has led to development of the bulbous bow and wave-less forms (ref Inui 1962). Therefore, the importance of wave-making resistance is that a knowledge of the relationship between hull geometry and wave-making resistance can lead to the development of optimum shaped hulls.

2.6.1 The nature of wave-making resistance

A ship advancing with steady speed through calm sea disturbs the surface in a regular wave pattern which moves with the ship. The wave pattern consists of two systems of diverging and transverse waves which are well illustrated in Plate 2.1 (ref Saunders 1972).

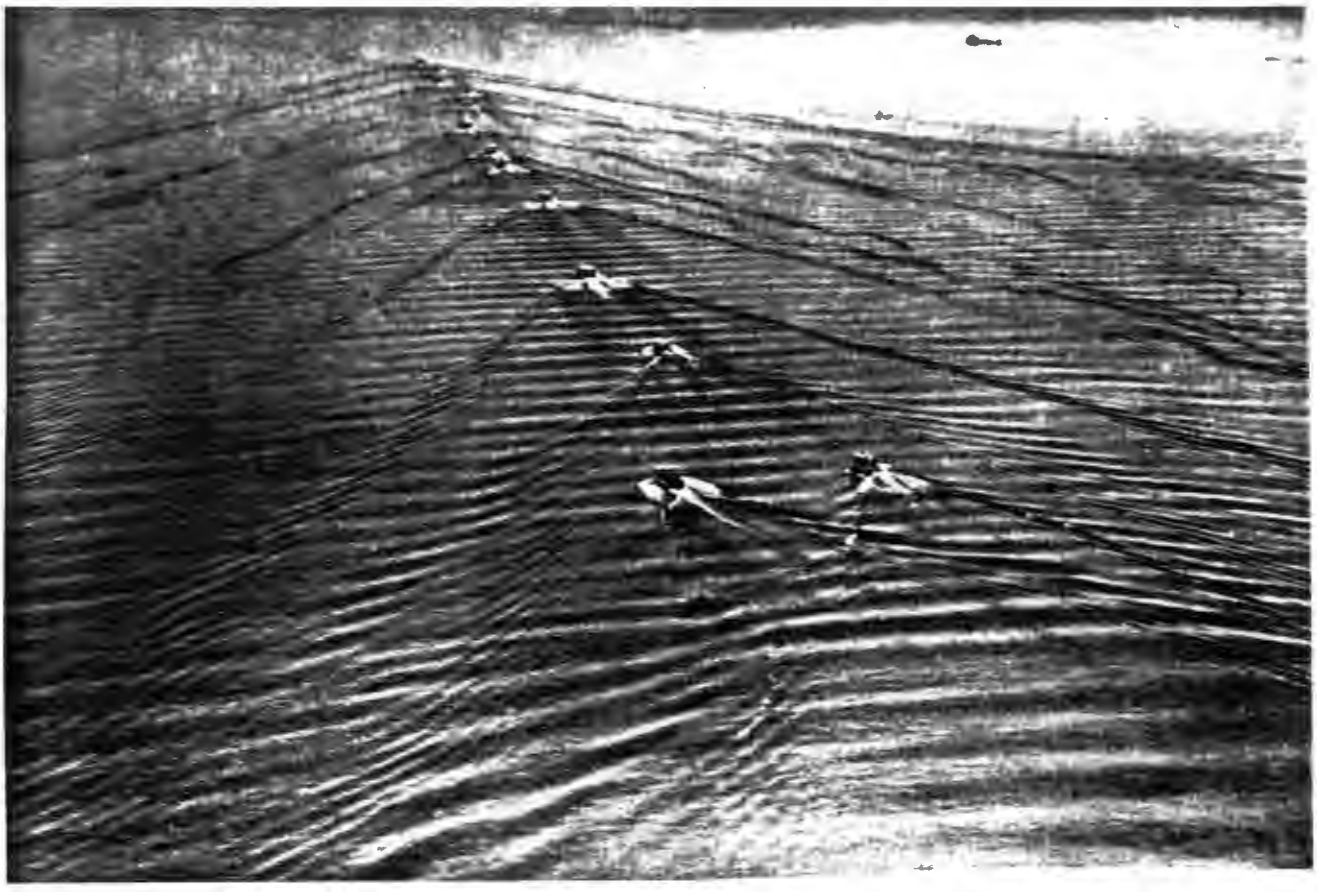

Plate 2.1 13 sets of diverging and transverse ship generated waves

The origin of this wave system may be found by first considering a deeply submerged body moving through an ideal fluid. The pressures acting on the front of the body are compensated by the pressure at the back and, therefore, the body has no resistance. However, when this body is moving at the surface of the fluid the pressure generated at the front of the body causes changes in the local fluid elevation, in effect waves. These waves then cause changes in the pressure distribution along the length of the model, resulting in a net backwards force on the hull referred to as the wave-making resistance of the body.

The ship generated wave system and, therefore, also the wave-making resistance is a function of:

a. Speed with which the ship moves through the water

b. The depth of the water

c. Geometric proportions of the ship

d. Size of the ship.

The wave system will remain constant for a ship moving at constant speed and through water of uniform depth.

The earliest description of ship waves was given by Lord Kelvin in 1887 and then later elaborated by him in 1904 (ref Comstock 1980). Kelvin considered a single pressure point travelling in a straight line over the surface of the water sending out waves which combine to form a characteristic wave pattern shown in Figure 2.12. The wave pattern consists of a system of transverse waves following behind the point and a series of divergent waves radiating away from the point.

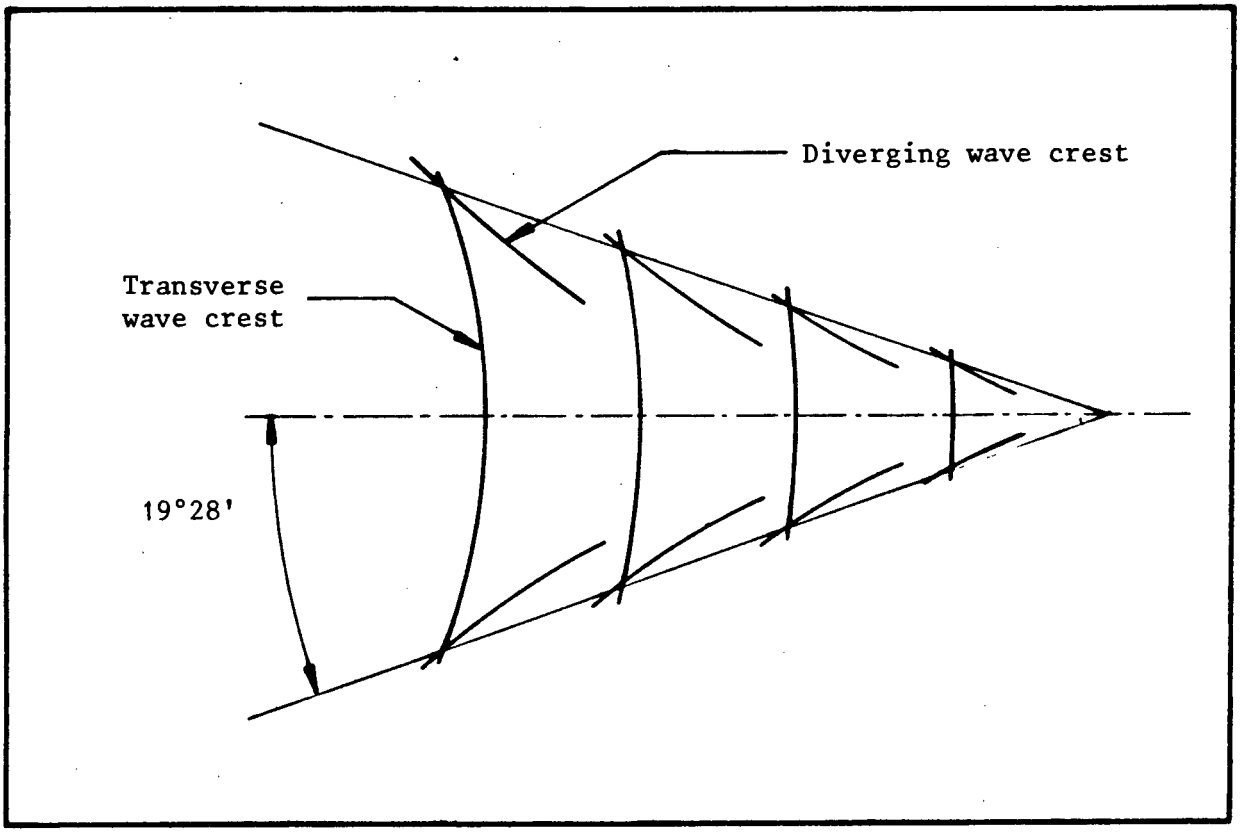

Figure 2.12 Kelvin wave pattern

William Froude in 1887 presented the first discussion and sketch of the system of waves generated by the bow of a ship moving in deep water. See Figure 2.13 (ref Froude 1887). Froude suspected, and it has also been shown in practice, that the stern generates another set of diverging and transverse waves - these two wave systems are illustrated in Figure 2.14.

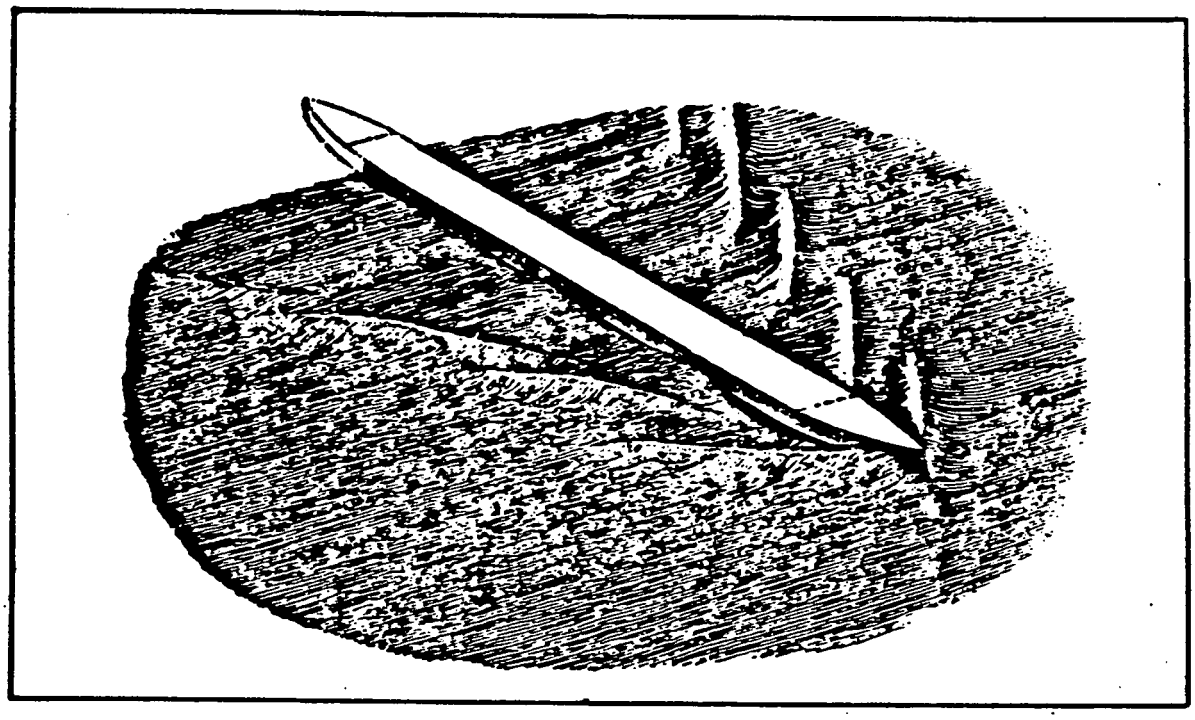

Figure 2.13 Froude's original sketch of a bow wave train

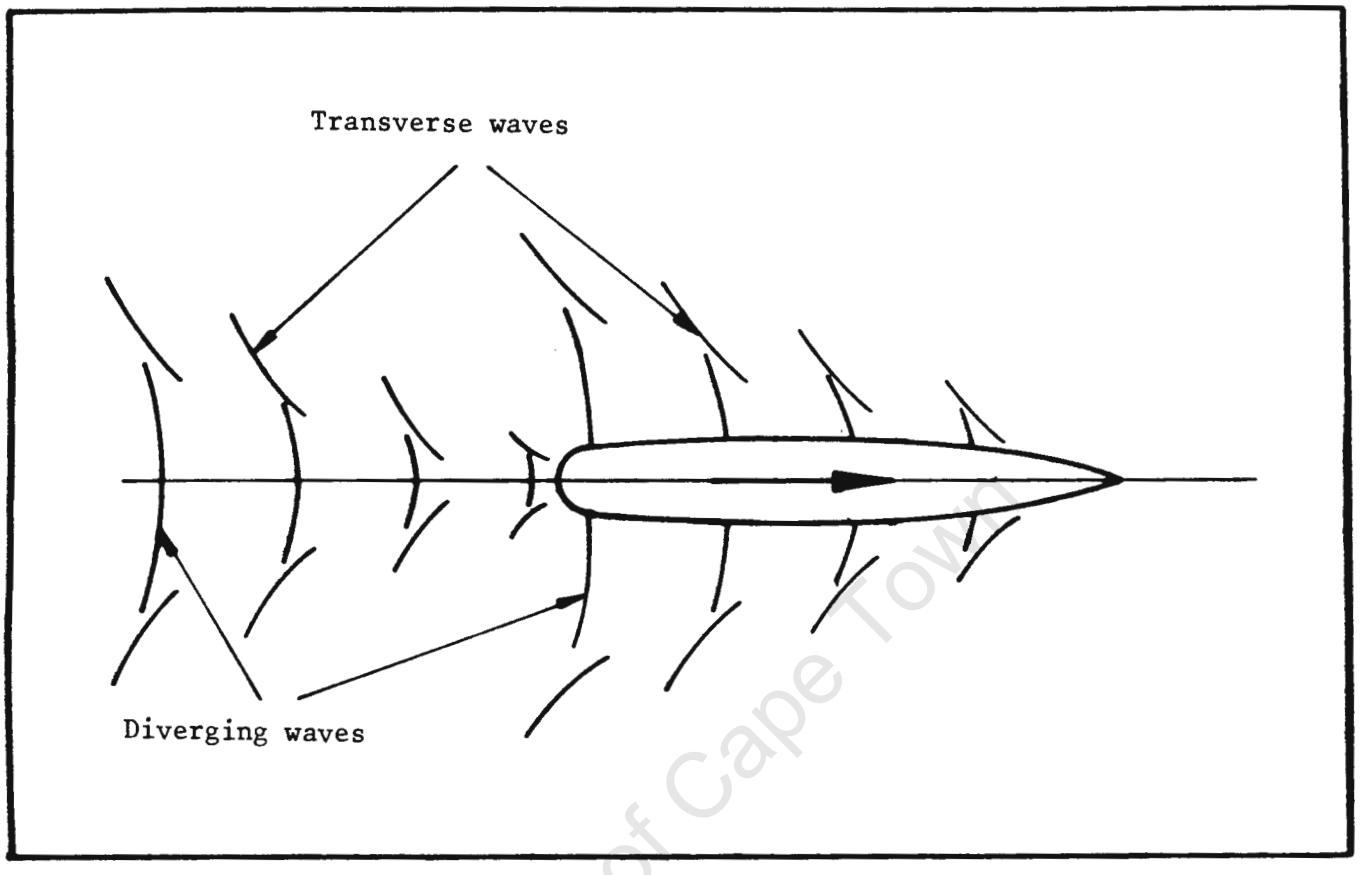

Figure 2.14 Ship wave pattern

University of Cape Town

2.6.2 Theoretical calculation of wave-making resistance

Mitchell was the first person to obtain an analytical expression for the wave-making resistance of a surface body. Mitchell obtained his result in 1898 by direct solution of the differential equation for the velocity potential using a double Fourier series. (ref Wigley 1942).

Considering forms that are symmetrical about centre line and and also about midships, and using cartesian coordinates as shown in Figure 2.15:

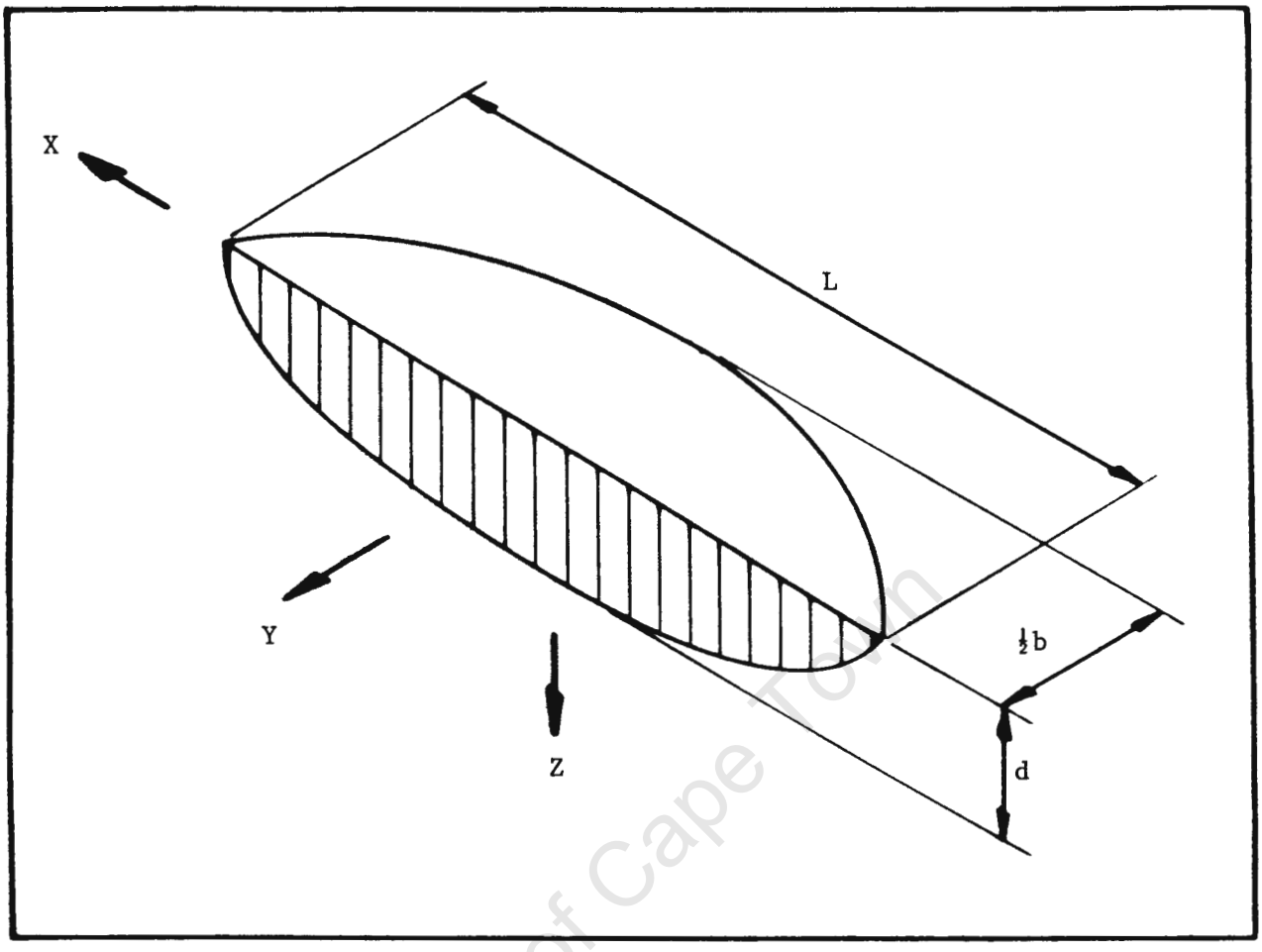

Figure 2.15 Dimensionless coordinate system

University of Cape Town

Defining dimensionless coordinates

$$X = 2x/L$$

$$Y = 2y/b$$

$$Z = z/b$$

and writing the equation of one half of the surface of the form as

$$Y = f(X,Z)$$

The wave resistance of the form specified in the above equation is given by

$$R_T = \frac{4\rho g^2}{\pi V^2} \int_0^{\pi/2} (I^2 + J^2) \sec^3\theta d\theta$$

where

$$J = \frac{bd}{2} \int_0^1 \int_{-1}^{+1} \left(\frac{\delta Y}{\delta X}\right) e^{-dgZ\sec^2\theta/V^2} \sin(LgX\sec\theta/ZV^2) dXdZ \qquad (2.46)$$

$$I = \frac{bd}{2} \int_0^1 \int_{-1}^{+1} \left(\frac{\delta Y}{\delta X}\right) e^{-dgZ\sec^2\theta/V^2} \cos(LgX\sec\theta/ZV^2) dXdZ$$

This solution is based on the following assumptions:

a. The wave height is small compared with wave-length

b. The water velocities due to wave motion are small compared with the speed of advance

c. The effects of turbulence and viscosity can be neglected

d. Trim and sinkage of the form do not alter its wave-making characteristics appreciably.

2.6.3 "Humps and hollows" in resistance curves

Figure 2.16 shows the theoretical wave-making resistance computed from Equation 2.46. The form of the model is one used in the author's experiments which are discussed in Chapter 5. The curve displays the characteristic "humps and hollows" of a total resistance curve, although the amplitude of the deviations are exaggerated, since no allowance is made for viscosity in the calculation. The

University of Cape Town

source of these undulations in the resistance curve may be explained by considering the wave length of the transverse waves in relation to the length of the ship. The speed of the transverse waves can reasonably be expected to have the same speed as the ship has moving through the water. The wave length and speed of a deep water wave is given by (ref Sorenson 1973)

$$c_o = \frac{gT}{2\Pi} \quad = \text{speed of deep water wave}$$

$$\lambda_o = \frac{g}{2\Pi} T^2 \quad = \text{wave length of deep water wave}$$

Combining these two equations and recognising that $c_o = V$

$$\lambda_o = \frac{2\Pi V^2}{g} \tag{2.47}$$

The transverse wave length is plotted along the length of the ship's hull in Figure 2.17 for a number of Froude numbers. From this diagram it is clear that the humps in the resistance curve occur when the surface levels at the stern are low, while hollows occur when the surface level is relatively high at the stern. Noting that the pressures at the stern are significantly affected by the local water height, it is apparent that the undulations of the resistance curve are a function of the positioning of the transverse waves along the ship's length as generated by the bow.

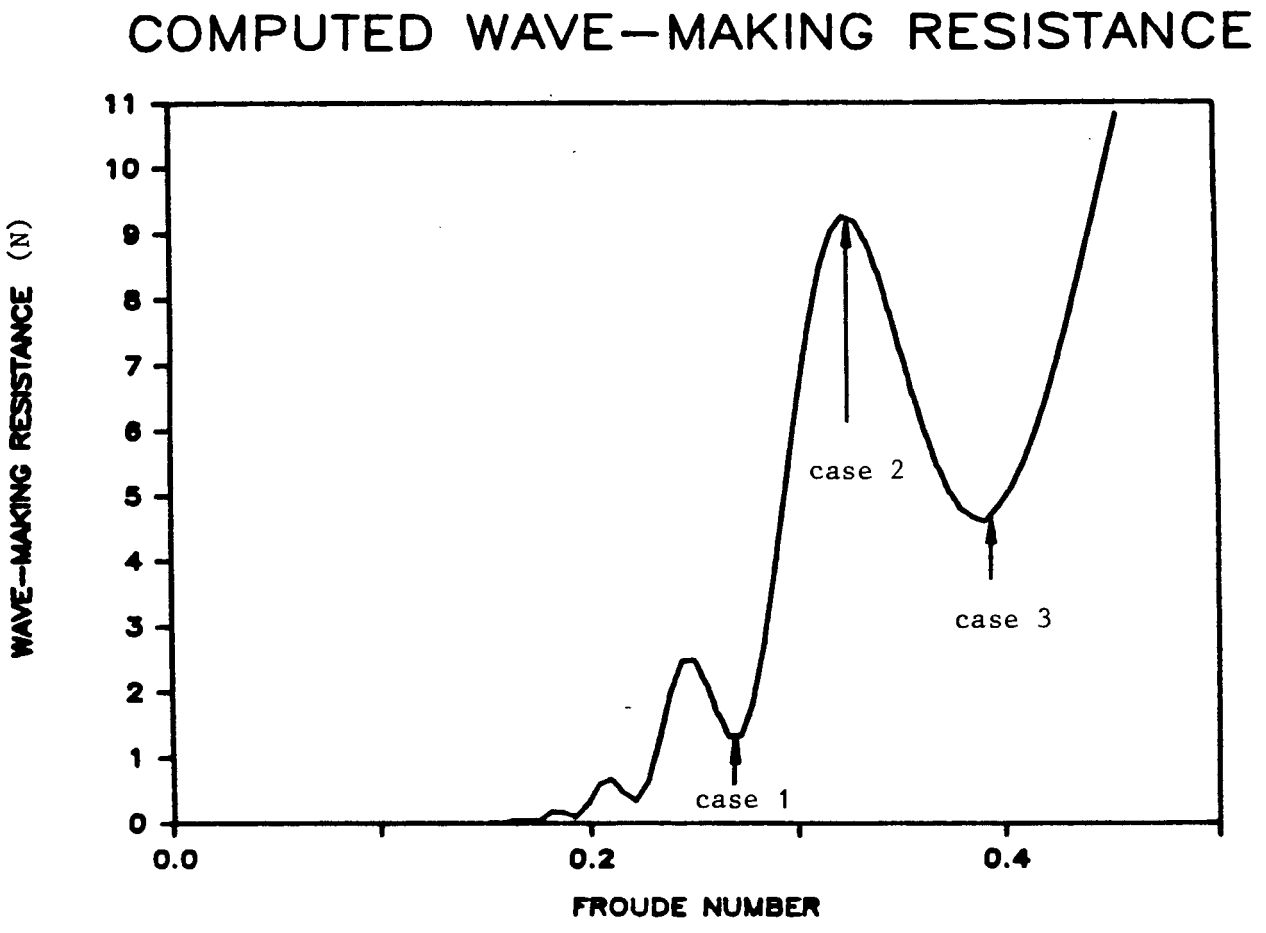

Figure 2.16 Characteristic total resistance curve

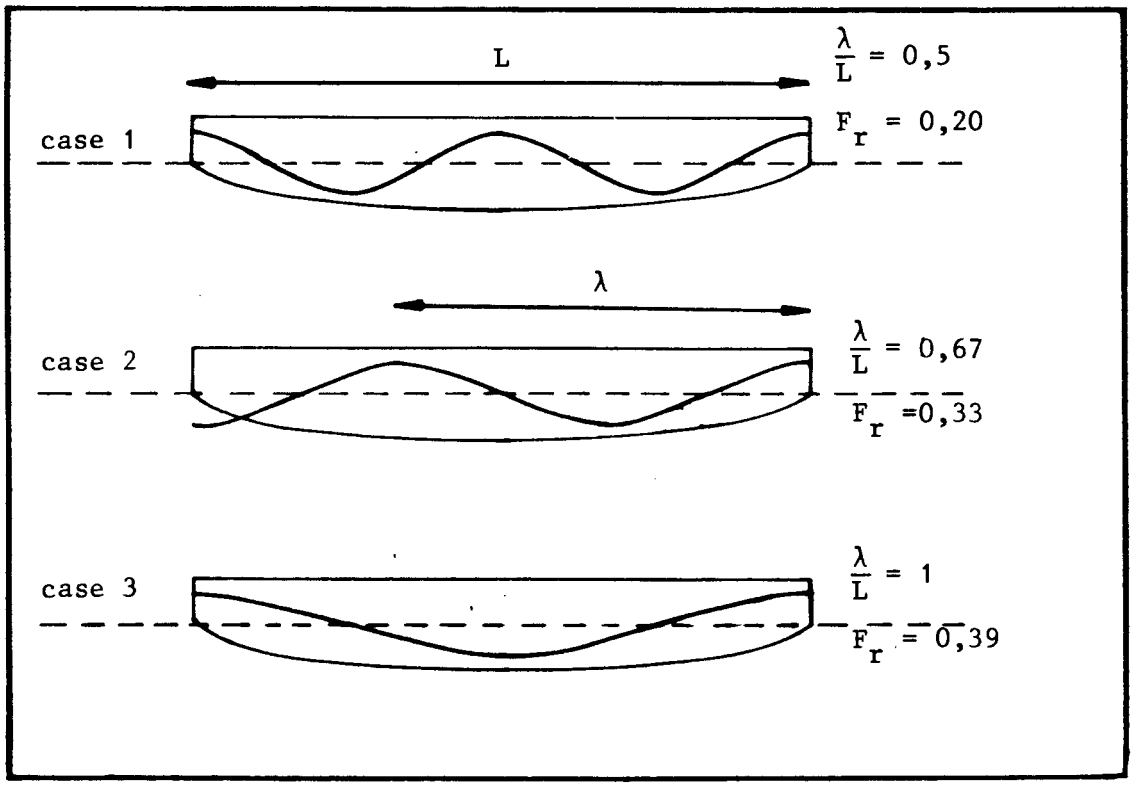

Figure 2.17 Profiles along model's hull

CHAPTER 3

EXPERIMENTAL MEASUREMENT TECHNIQUES

3.1 Total resistance

The total resistance of a model ship is probably the easiest of all the resistance components to measure. Froude, in 1872, presented a sketch of the dynamometer that he used in his Torquay experiments (see Figure 3.1). Froude measured resistance by means of a spring (component H in Figure 3.1), the extension of which was recorded on a revolving drum.

In more recent times with the advent of electronics the measurement of the total resistance of a model has become more sophisticated. The resistance is usually obtained by measuring the strain on a sensing element using electrical resistance strain gauges. The electrical analog signal is then usually converted to a digital signal which is then processed with the aid of a computer. Plate 3.1 illustrates a modern dynamometer as used by Grim, Oltmann, Sharma and Wolff (1976).

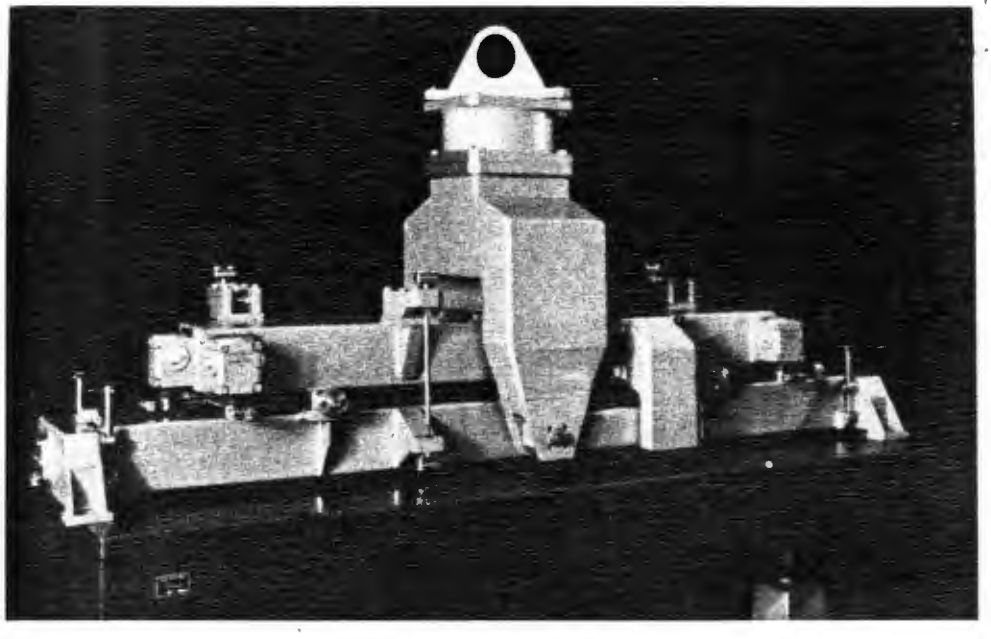

Plate 3.1 Modern dynamometer

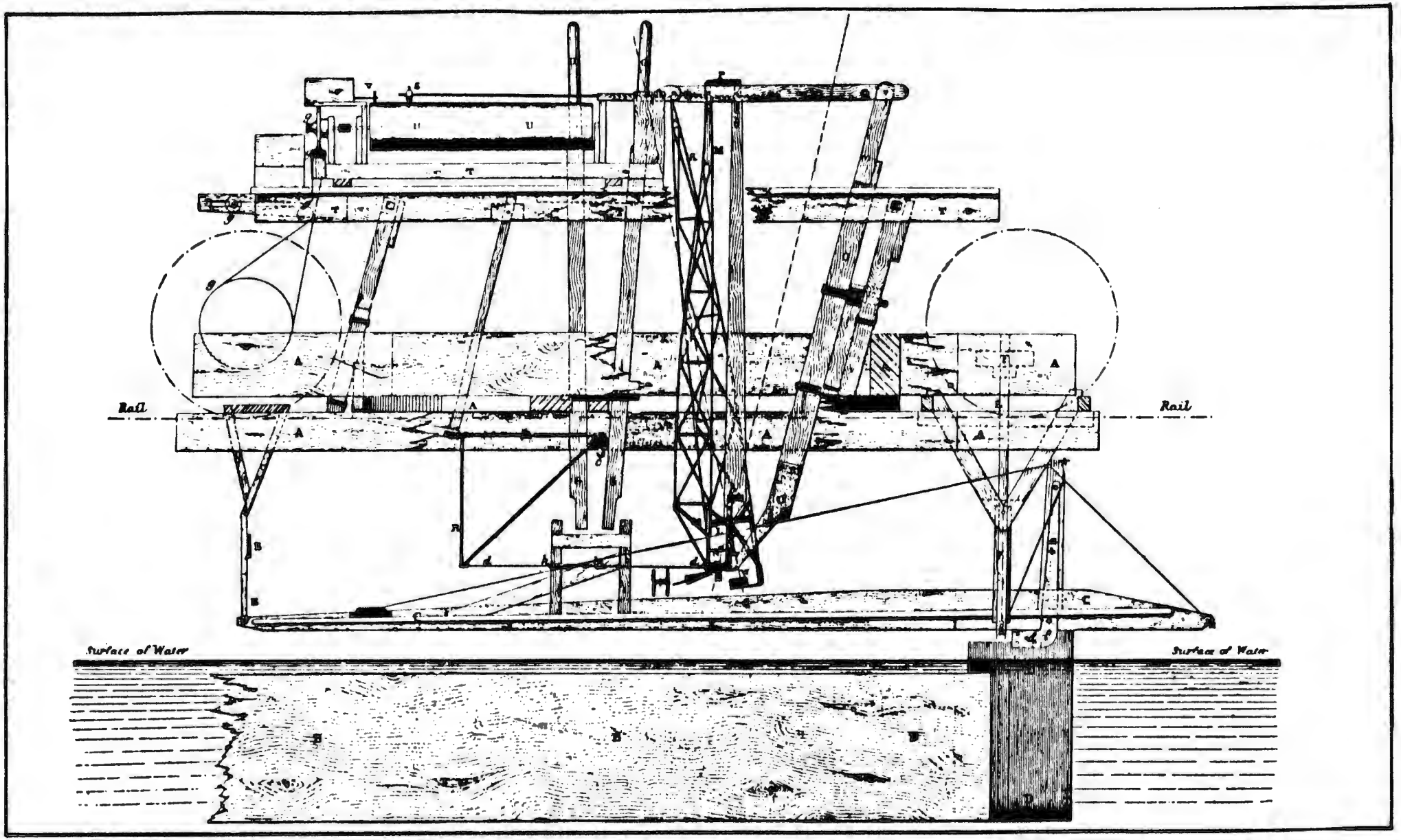

Figure 3.1 Froude's dynamometer (ref Froude 1872)

3.2 Total viscous resistance

The total viscous resistance of a model ship can be deduced by measuring the resistance of a reflex or double model of the ship in a wind tunnel. Since the model is submerged there is no wave-making resistance and hence the total resistance equals twice the total viscous resistance. Larsson (1976) used a reflex model to study three-dimensional boundary layers of a ship in a wind tunnel. The concept of measuring the total viscous resistance of a ship with a reflex model in a wind tunnel has been used by the following authors: Lackenby (1965), Shearer and Cross (1965) and Matheson and Joubert (1973).

University of Cape Town

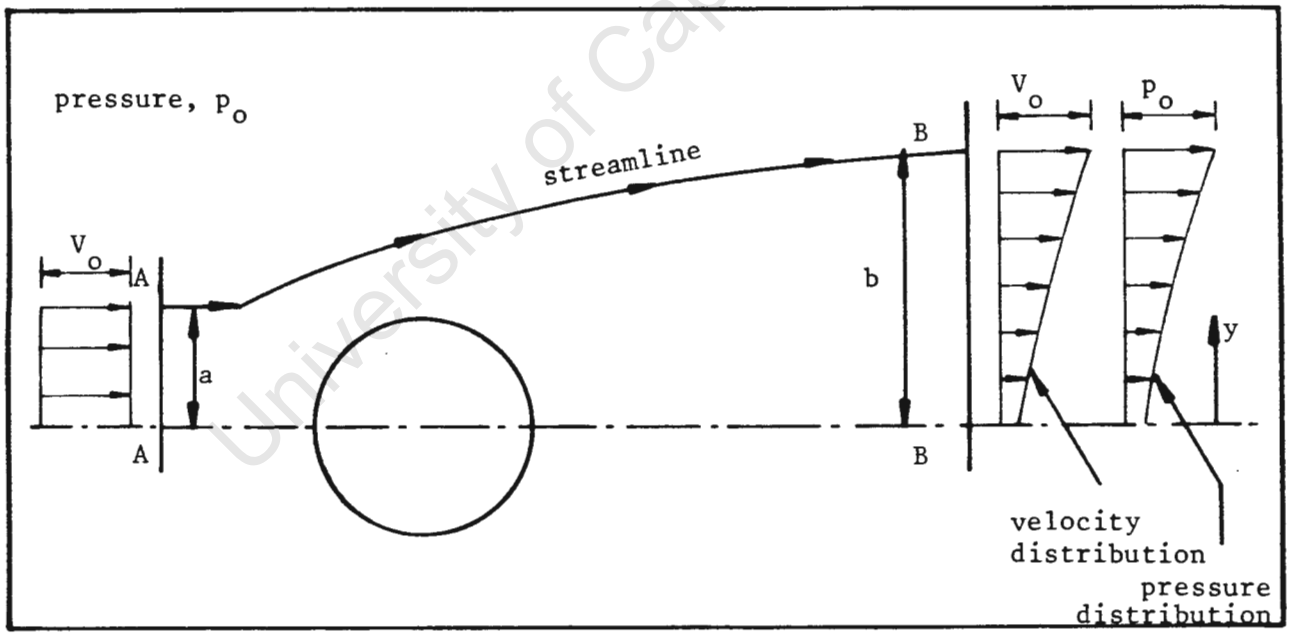

Figure 3.2 Flow past a cylinder

Consider a two-dimensional cylinder placed in a moving stream (see Figure 3.2). Section AA is chosen to be sufficiently far upstream to be unaffected by the cylinder. Section BB is chosen at some distance downstream from the body beyond the zone of vortex shedding. The velocities and pressures at AA will be uniform i.e. V_o and p_o. At section BB both the velocities and pressures will no longer be uniform and will be a function of y as shown in Figure 3.2. The discharges crossing AA and BB are equal and, therefore, line AB is a streamline and has a uniform velocity V_o along it and, therefore, has uniform pressure p_o acting along it. Applying the total force principle for 1 m dimension into the page we get:

$$2p_o a + \tfrac{1}{2}\rho V_o^2\, 2a + 2p_o(b-a) = 2\int_o^b p(y)dy + \int_o^b \rho v(y)dy + R \qquad (3.1)$$

where R = resistance force on the cylinder

$$\therefore \quad R = 2\left[p_o a + \tfrac{1}{2}\rho V_o^2 a + p_o(b-a) - \int_o^b p(y)dy - \tfrac{1}{2}\rho \int_o^b v(y)^2 dy\right]$$

Considering continuity

$$2V_o a = 2\int_o^b v(y)dy$$

$$\therefore \quad V_o^2 a = \int_o^b V_o v(y)dy$$

$$\therefore \quad R = 2\left[\int_o^b (p_o - p(y))dy + \tfrac{1}{2}\rho \int_o^b v(y)\,(V_o - v(y))dy\right] \qquad (3.2)$$

Therefore, by measuring the variation of velocity and pressure in the wake the resistance force acting on the body can be determined. This method is known as the Pitot traverse and was first used by Betz for the drag on aerofoils and the method was later refined by Jones (ref Schlichting 1968). Regarding the application of this method to

three-dimensional bodies Lackenby (1965) has shown that the results agree closely with those obtained by a dynamometer. Tulin (1951) has also suggested that the method can be applied to the determination of the total viscous resistance of a surface body and thus represents a method of separating wave-making and viscous resistance. The Pitot traverse method has been used by Lackenby (1965), Shearer (1965) and Townsin (1971).

3.3 Skin friction

When a fluid flows past a ship's hull it exerts normal and shear stresses on the hull surface. The measurement of the normal stress or pressure is relatively simple (discussed in Section 3.4), however, the measurement of the shear stress or the local skin friction is a more complicated task. If the velocity distribution at a point along the hull is known, the local shear stress may be calculated using Equation 3.3. By integrating the local shear stress over a small area dA the local skin friction can be calculated

$$\tau_o = \mu \frac{dV}{dy} \tag{3.3}$$

This method entails making numerous measurements to obtain the velocity distribution close to the hull which gives the value of the local shear stress at one point only. To obtain the variation of the skin friction over the hull the above procedure has to be repeated at other locations along the hull. Obviously this method is time consuming and hence expensive. As a result simpler and less time consuming methods have been developed to measure local skin friction.

3.3.1 Direct measurements

The shear stress at the hull can be measured directly by using a transducer. The transducer is usually calibrated by direct force application. Since the transducers do not reply on the behaviour of the boundary layer they are in principle the most reliable method of measuring shear stress.

There are, however, some distinct disadvantages to the use of these transducers.

The transducer's sensing element must have a gap around its perimeter and this gap may cause effects under flow conditions which are not taken into account in its calibration. The sensing element must be perfectly aligned to the contour of the wall so as not to give rise to additional forces due to flow disturbances. Along a ship's hull there are several regions of high surface curvature and to place a flat sensing element in these locations causes a discontinuity in the surface which can again lead to extraneous forces on the sensing element.

Although commercially manufactured skin friction gauges are available (see Figure 3.3 ref Goldstein 1983), they do not seem to have been used frequently for the measurement of skin friction of model ships.

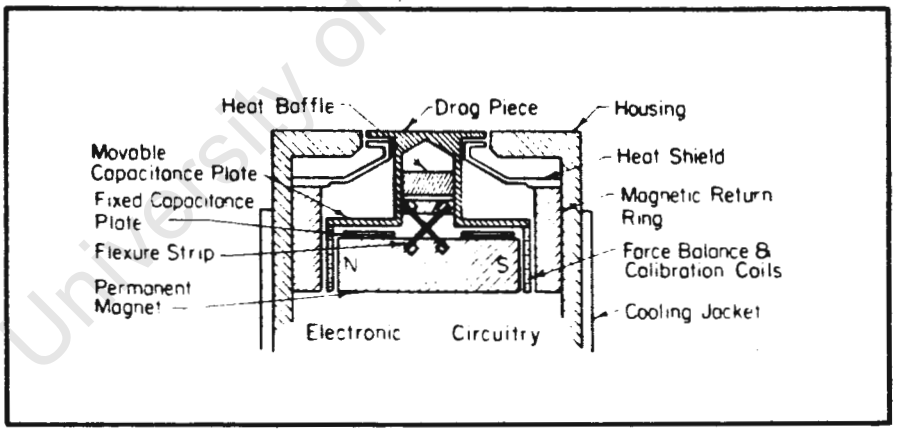

Figure 3.3 Skin friction gauge (Goldstein 1983)

3.3.2 Stanton gauge

The Stanton gauge is a forward facing knife edged opening designed to lie within the laminar sub-layer (see Figure 3.4). The static pressure is first measured with the knife edge removed and then the pressure measured with the knife edge in place. The difference in the two readings is related to the local skin friction. The gauge is usually calibrated in pipe in which the skin friction shear stresses are known.

University of Cape Town

The pressure differences are generally very small and, therefore, it is necessary to use a micromanometer with an accuracy of ± 0,01 mm (ref Goldstein 1983). Great care needs to be taken to keep the distance of the knife edge above the hole constant. Problems arise in water in that the suspended solids, such as are usually present, may clog the knife edge (ref Steele and Pearce 1967).

The Stanton gauge has largely been superseded by the Preston tube as a method of measuring skin friction on model ships.

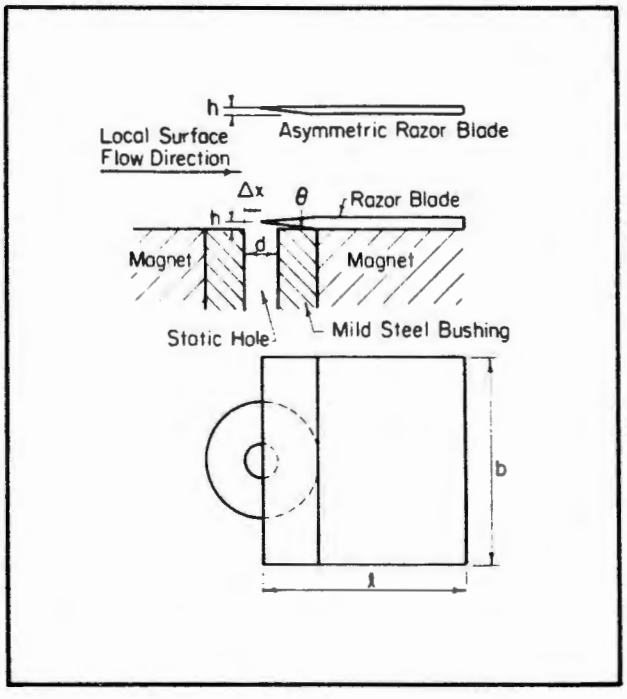

Figure 3.4 Stanton gauge (Goldstein 1983)

3.3.3 Preston tube

The Preston tube is a forward-facing total head tube placed adjacent to the surface of a body where the skin friction measurement is to be made (see Figure 3.5). The Preston tube is larger than the Stanton gauge and does not remain within the laminar sub-layer. The static pressure is first measured and then compared to the pressure measured with the total head tube in place. The pressure difference is then related to the local skin friction. The Preston tube is usually calibrated in a pipe and was first done so by Preston

using air. This method of calibration depends on the assumption of a universal inner velocity law being common to boundary layers and fully developed pipe flow. Mead and Rechenberg (1962) investigated this assumption and found "that for a given skin friction the Pitot tube (Preston tube) reading was the same for both boundary layer and pipe flows, thus vindicating Preston's method and confirming the existence of a universal region of wall similarity".

The Preston tube may only be reliably used in turbulent flow and care must be taken to ensure that the flow is turbulent both in the calibration and on the model. Since the static pressure and Preston tube pressure cannot be measured simultaneously, it is important to ensure that the flow conditions are the same when the measurements are made. As with the Stanton gauge the pressure differences are small and should be measured with a micromanometer.

The Preston tube was initially used in the field of aeronautics to measure skin friction on models in wind tunnels. More recently it has been used to measure the skin friction of ship models - Steele and Pearce (1968), Shearer and Steele (1970) and Cole and Millward (1977). The Preston tube seems to be firmly established as one of the tools used for ship resistance investigations.

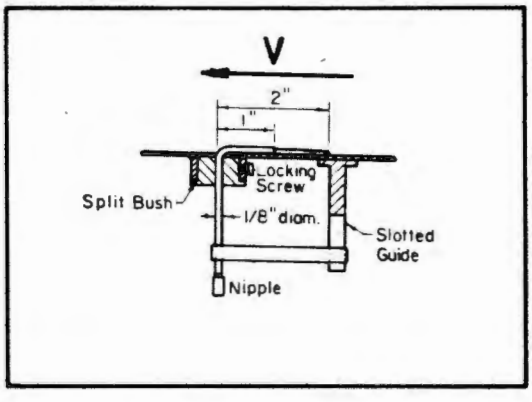

Figure 3.5 Preston tube (Goldstein 1983)

3.3.4 Thin film probes

The thin film probe consists of a film or element which is heated electrically. The amount of heat transfer varies with the local flow conditions as the fluid passes over the probe. Bellhouse and Shultz (1966) have shown that the following relationship relates the electrical current variation to the local shear stress at the wall

$$\tau_o^{1/3} = A\,(i^2R/\Delta T) + B \qquad (3.4)$$

where i = electrical current (A)

R = electrical resistance of film (Ω)

ΔT = the temperature difference between the film and the oncoming stream (°C)

A,B = constants.

In order to calibrate the probe a constant shear stress, τ_o, is applied (such as in a pipe). The values of i, R and ΔT are measured. The constants A and B are determined by plotting $\frac{i^2R}{\Delta T}$ against $\tau_o^{1/3}$.

The thin film is mounted flush in the wall of a model and, therefore, does not influence the local boundary layer as happens with the Stanton gauge and Preston tube. The thin film probe can also be used to determine whether the flow is laminar or turbulent. The response time of the probe is very fast (Bellhouse and Shultz quote 0,04 sec) and it is, therefore, suited to dynamic measurements using a data logging system. Because the time period required to take the readings is small, measurements of local skin friction can be made in a short duration facility such as a towing tank.

Most of the work done using thin film probes has been done in air e.g. Davies and Kimber (1976). However, Pope and Bellhouse (1971) used thin film probes to measure local skin friction on a model ship. They found good agreement with the results obtained from Preston tubes. The major problem encountered was that small bubbles of air present in the water collected on the model. These air bubbles had to be removed prior to each test to ensure that the bubbles did not cause any inaccuracies as they would have greatly influenced the heat transfer rate.

Although the thin film probes are relatively expensive to manufacture, they have great potential for the measurement of local skin friction. They offer a fast and simple measurement because the instrument output is electrical.

3.4 Total pressure resistance

Consider a small hole or tapping made in the side of a model and connected to a manometer - the fluid level in the manometer will equal the still water level when the model is stationery. If the model is now moved through the fluid the water level will either rise or drop relative to the still water level depending on the location of the tapping on the hull. The pressure difference Δp is related to pressure resistance experienced by the model and will be positive at the bow and usually negative at the stern.

If the model's hull is covered with an array of pressure tappings each having a defined area, dA and the pressure differences are recorded when the model is moving through a fluid the total pressure resistance can be found by the following equation

$$R_p = \int_{S_W} \Delta p \cos\phi \, dA \qquad (3.5)$$

where S_W = wetted surface area

ϕ = angle between the normal to the surface dA and direction of motion.

Therefore, the evaluation of the total pressure resistance is relatively simple. However, great care must be taken to ensure that the tappings are drilled normal to the surface and that there are no burrs around the holes as this would affect the measured pressure. Generally the pressures are measured using a manometer which has the advantage of accuracy but has a slow response and can, therefore, only be used in situations where steady state can be achieved for a reasonable length of time. Electronic pressure transducers may be used instead of manometers if steady state can only be achieved for a short duration as their response time is much faster.

Some of the authors that have conducted pressure tapping experiments on model ships are Froude (1874), Lackenby (1965), Shearer and Cross (1965), and Matheson and Joubert (1973).

3.5 Wave-making resistance

A ship moving through still water generates a set of gravity waves and in doing so, therefore, expends energy which is associated with wave-making resistance for a known ship movement. If the change in amount of energy stored in the ship wave pattern could be measured, the wave-making resistance of the ship could be determined. Therefore, the problem has two components: firstly, to determine the wave pattern and secondly, having obtained the wave pattern, to calculate the wave-making resistance.

A common way to obtain the ship wave pattern is to place wave-height recorders at fixed points and then measure the wave pattern as the model passes. A novel method of determining the wave pattern has been developed at the University of Cape Town by Paterson (1986). A model is towed across a basin filled with an opaque fluid and a pair of stereo photographs taken. These photographs are later analysed in a stereo comparator and a contour map of the wave pattern produced. The method is interesting because the possibility exists of taking stereo photographs of full scale ships in protected waters.

The methods of analysis vary but generally they consist of either taking a transverse cut or a longitudinal cut of the wave pattern, ref Wehausen (1973).

University of Cape Town

CHAPTER 4

EXPERIMENTAL OBJECTIVES

4.1 Objectives

The purpose of the experimental investigation was to measure directly as many of the resistance components as possible, or failing this, to be able to deduce the resistance components not directly measured. From the start it was felt that the direct measurement of skin friction and wave-making resistance were beyond the scope of the investigation and, therefore, these two components would have to be obtained by difference. This lead to two sets of experiments - one aimed at deducing the wave-making resistance and the other at inferring skin friction. For practical reasons these two sets of experiments were conducted at different scales, in different facilities, in the geometric ratio of 2,7 to 1.

To determine the skin friction component of total resistance a model had pressure tappings located on it and thus the total pressure resistance measured. By measuring the total resistance and subtracting the pressure component the skin friction could be deduced. In order to measure the pressure distribution a fairly long steady state time period is required and to achieve this a glass flume in the U C T hydraulics laboratory was used. Water is supplied to the glass flume from a constant head tank and, therefore, the same flow conditions can be maintained indefinitely.

The wave-making resistance was to be found by measuring the total resistance of a model placed at the water surface and then measuring the total resistance of the corresponding reflex model deeply submerged.

Half of the total resistance of the deeply submerged body would equal the total viscous resistance of the surface body and, therefore, if subtracted from the total resistance of the surface body the difference would be the wave-making resistance. Since the length of steady state is not too critical for the reflex experiment, use was made of the towing channel facility in U C T Civil Engineering laboratory.

4.2 Choice of model form

The decision had been made to measure the deeply submerged resistance of a reflex model and, since a body of revolution would ideally suit this purpose, it was chosen as the model form. The surface models are made from half a body of revolution with vertical sided superstructure walls.

The most important reason for choosing a body of revolution as the model form is that the models can be machined on a lathe to a very high degree of precision. As two models were to be made it was essential that their forms were identical so that valid comparison could be made between them.

In order to achieve a reasonable percentage of wave-making resistance a model with a blockage coefficient of 0,621, which is typical of cargo ships, was chosen. Figure 4.1 illustrates the form of the model and the front views of a surface model and a submerged model. Table 4.1 compares the principal dimensions of the towing channel model and the glass flume model.

		Glass Flume Model	Towing Channel Model
Water line length	L (m)	0,700	1,890
Max beam	b (m)	0,100	0,270
Max drift	d (m)	0,050	0,135
Displacement	Δ (dm^3)	2,175	44,848
Wetted surface area	S_W (m^2)	$94,247 \times 10^{-3}$	1,440
Frontal area	A_F (m^2)	$3,927 \times 10^{-3}$	$28,63 \times 10^{-3}$

Table 4.1 Principal dimensions of models

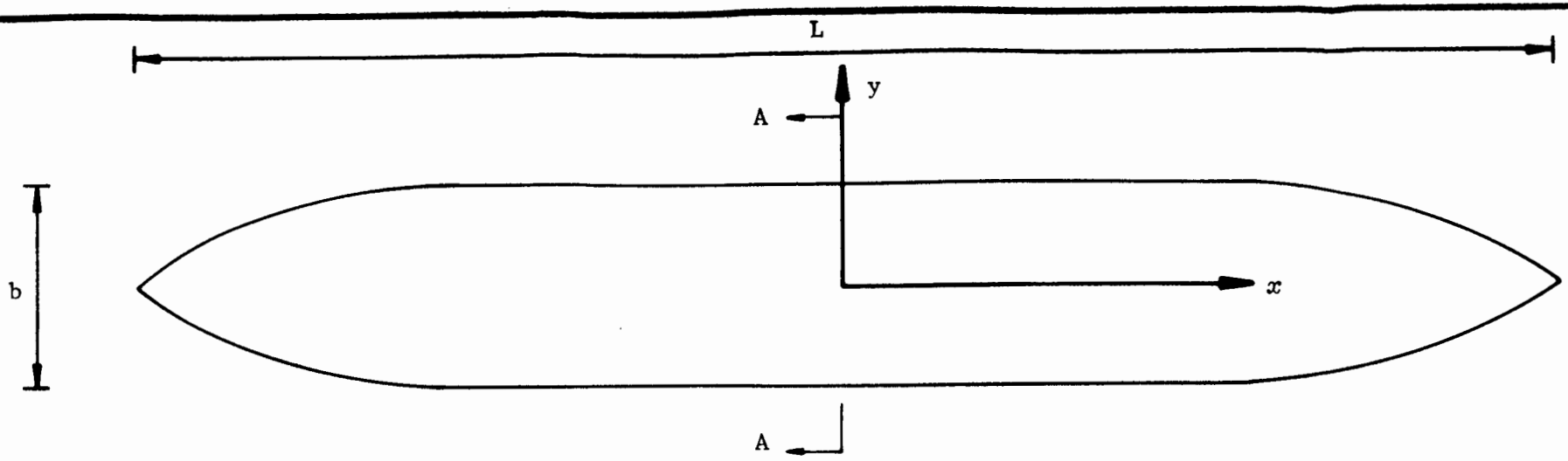

Plan view of body of revolution

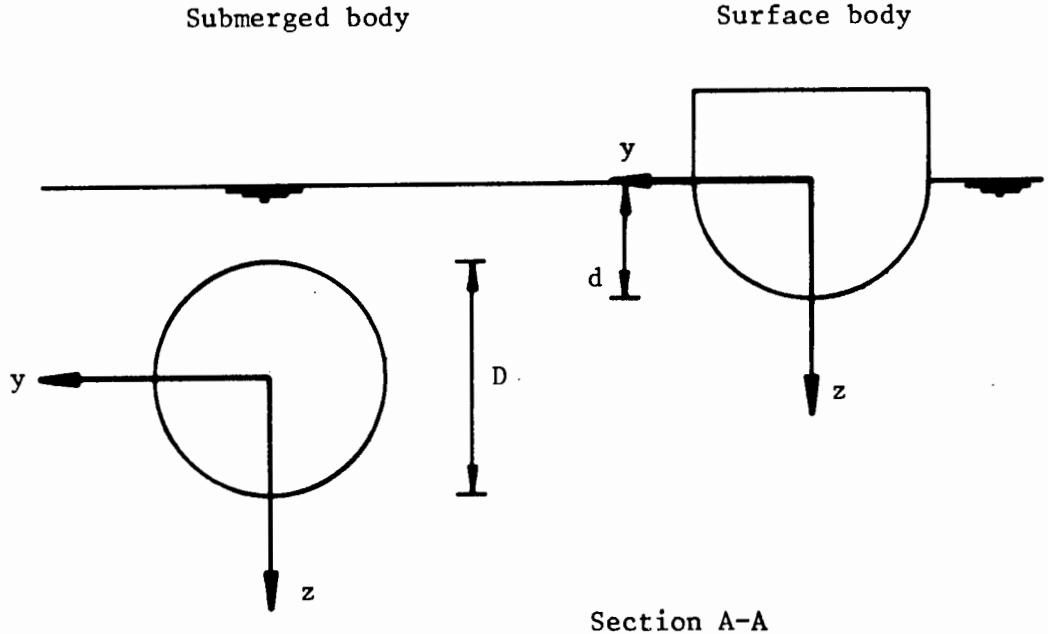

Section A-A

NOTES

1. Equation of line:

$$y = \frac{b}{2}\left(1 - \frac{x^6}{L^6}\right)$$

2. $C_B = 0{,}621$

3. $b/L = 0{,}143$

Figure 4.1 Form of models

By using a mathematical function to define the form of the model an estimate of the theoretical wave-making resistance could be made using Equation 2.46. In order to simplify the calculation a two-dimensional vertical sided form was used for the calculations. The results of these calculations are presented in Figure 4.2.

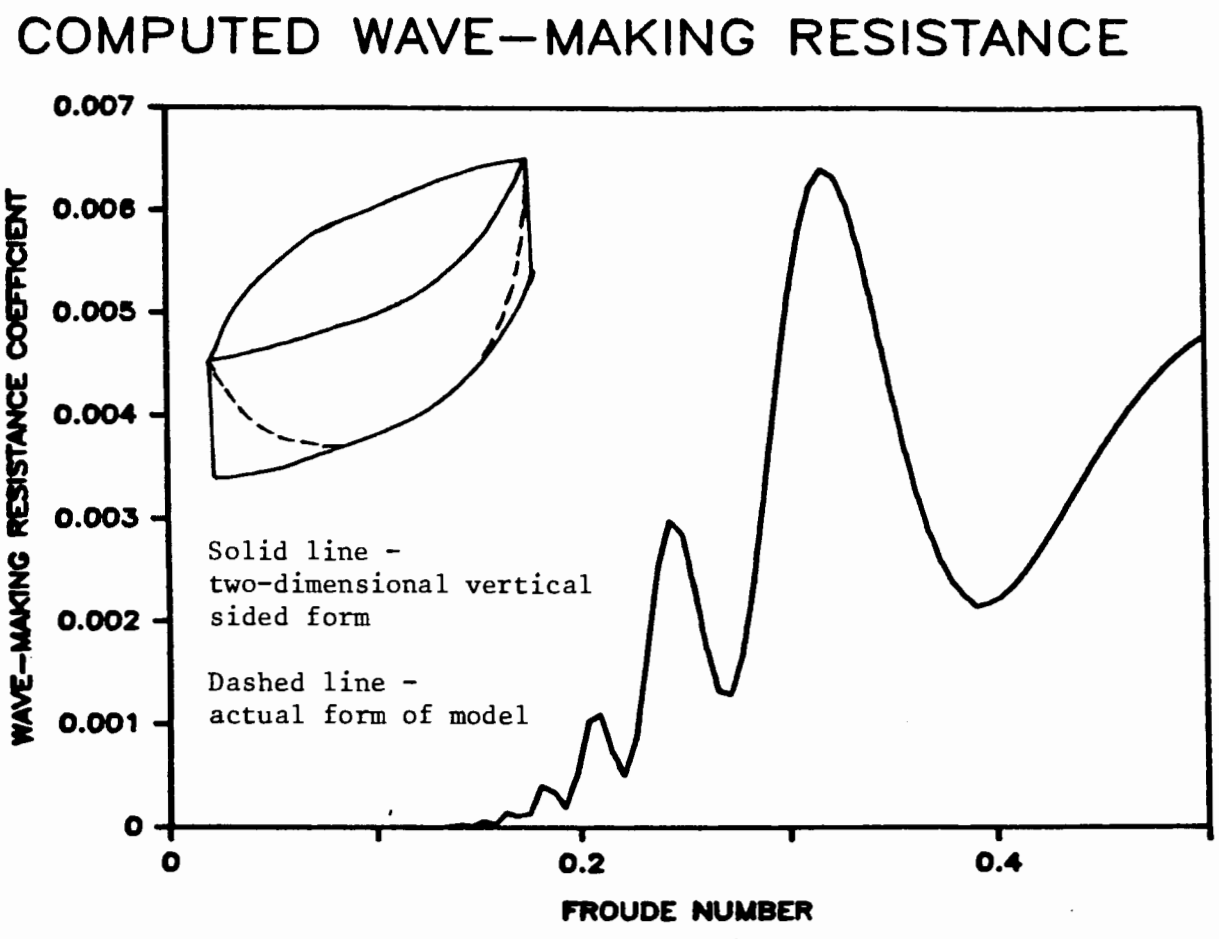

Figure 4.2 Computed wave-making resistance

Because a submerged reflex model was to be tested it was decided that for all the tests the models would be held in a support that restricted both squat and trim.

The dimensions of the models relative to the dimensions of the flume and towing channel are shown in Figure 4.3. Due to practical reasons the ratios are slightly different.

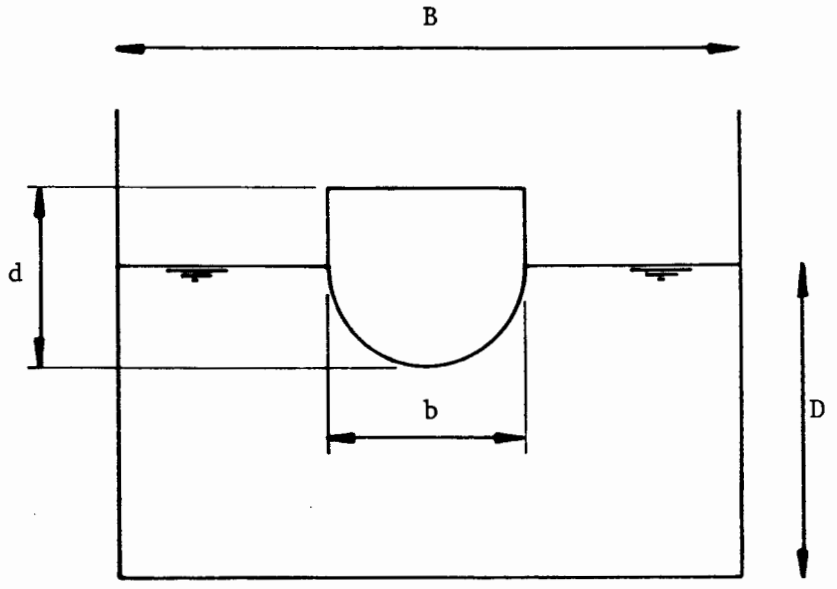

Glass flume model	Towing channel model
b = 0,100 B = 0,600	b = 0,270 B = 1,50
$\frac{b}{B} = \frac{1}{6}$	$\frac{b}{B} = \frac{1}{5,5}$
d = 0,050 D = 0,200	d = 0,135 D = 0,600
$\frac{d}{D} = \frac{1}{4}$	$\frac{d}{D} = \frac{1}{4,4}$

Figure 4.3 Relative dimensions of models

CHAPTER 5

GLASS FLUME EXPERIMENT

5.1 Glass flume

The flume is supplied with water from a constant head tank with a water level 15 m above laboratory floor which forms part of a recirculating system (see Figure 5.1). With the pump running the same flow conditions can be maintained in the flume indefinitely. The flow to the flume may be varied using the control valve (A). The water level in the flume is controlled using the adjustable tailgate (B). The gradient of the flume may be adjusted using the motorised jack (C). Parallel wire mesh sheets have been placed at the inlet of the flume to reduce the wave action in the flume.

The flume is constructed from glass panels in an aluminium and steel framework. The glass panels allow visual inspection of flow conditions in the flume from both the sides and the bottom of the flume (see Plate 5.1). The flume has a constant width of 610 mm and height of 500 mm over its length of 18 m.

Plate 5.1 Glass flume

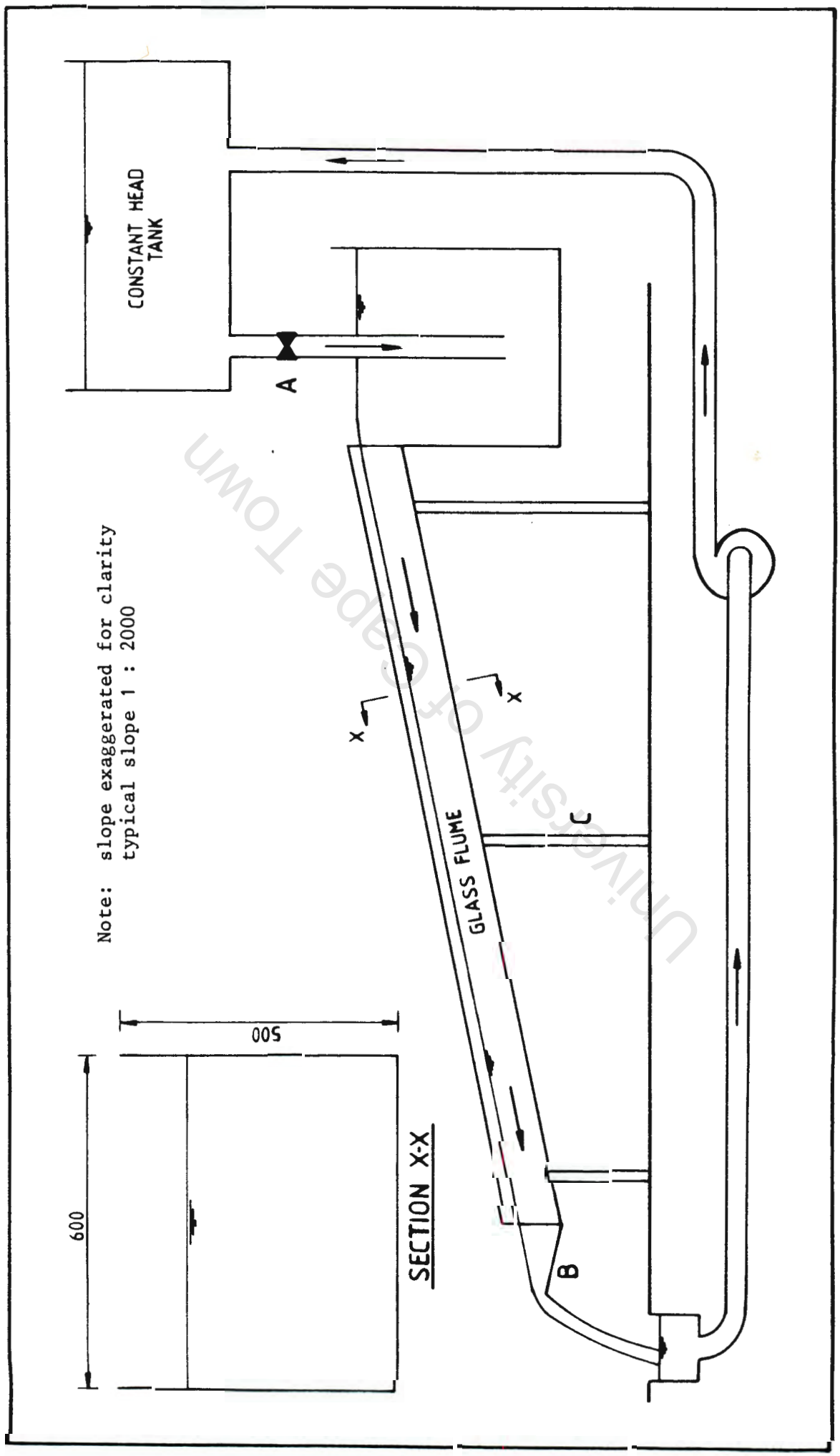

Figure 5.1 Recirculating water system

University of Cape Town

5.2 Model ship

The model ship is fabricated from jelutong (a soft wood) and aluminium according to the form and dimensions discussed in Chapter 4. Below the still water line the model is entirely made from aluminium, while above the still water line the vertical walls are made from jelutong. The aluminium section of the model was made in three components as shown in Plate 5.2. The components were joined using an aluminium based epoxy and then the jelutong sides glued on using epoxy glue - see Plate 5.3.

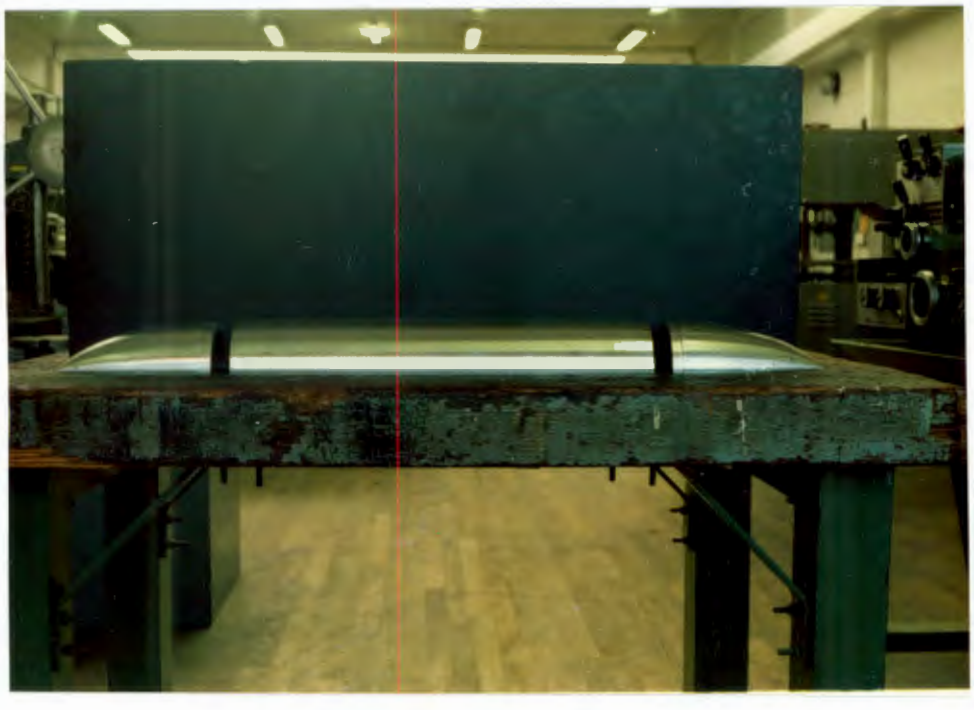

Plate 5.2 Components of model hull before assembly

Plate 5.3 Assembled components of model hull

The model has 40 pressure tappings located on its hull below the still water level. The holes were drilled into the model before the three aluminium components were assembled. The holes were drilled at predetermined locations and angles in a milling machine which ensured a high degree of accuracy in both the tapping angle and location. (See Plate 5.4). The holes were drilled to a diameter of 0,8 mm. A hypodermic needle was then pushed into the hole and a plastic tube connected to the back of the needle.

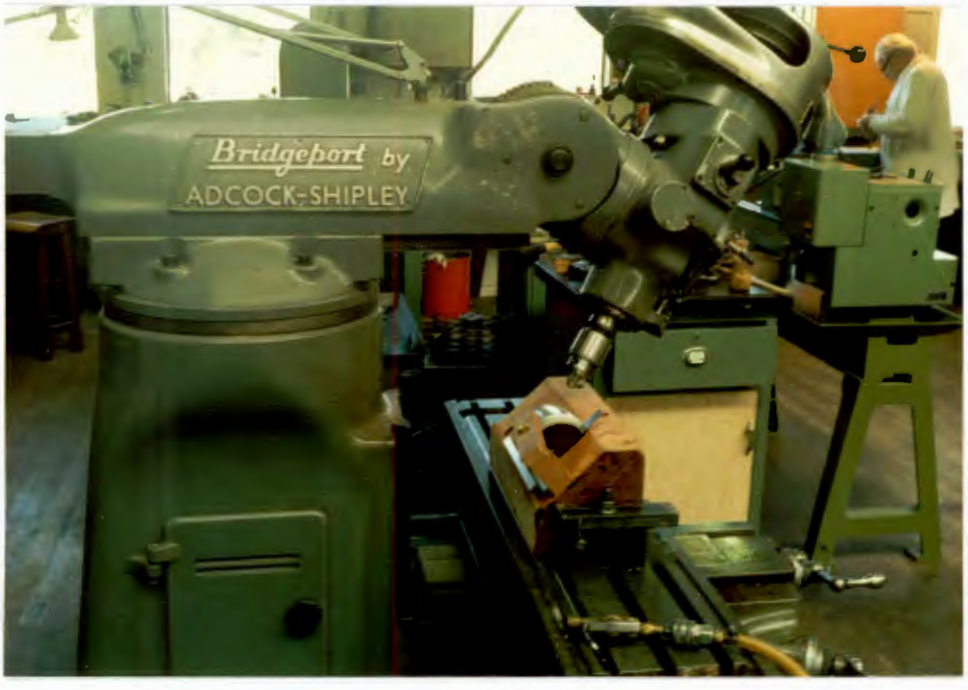

Plate 5.4 Drilling of pressure tapping holes

To minimise the number of tappings each tapping location is unique in that it does not appear on the other side of the centre-line of the model. (See Figure 5.2). The list of pressure tapping locations appears in Appendix B.1.

5.3 Measurement of water speed in the flume

The water speed relative to the model in the flume is measured using a pitot tube. The tube has a frontal tapping which measures the dynamic and static head (i.e. total head) and a circumferential tapping which only measures the static head. Therefore, the difference between the two readings is the dynamic head, Δh . The local water velocity can be related to the dynamic head by the following equation

$$\Delta h = K \frac{V^2}{2g} \quad \text{(metres of water)} \tag{5.1}$$

where K = a coefficient taken to be unity.

The head differences were measured by leading the two tappings to a manometer board (see section 5.5) where the water heights were measured using a depth gauge capable of reading to 0,1 mm. The pitot tube was mounted onto a depth gauge and positioned in the centre of the flume upstream from the model. By adjusting the depth gauge the pitot tube height could be accurately positioned to within 0,1 mm. The pitot tube was arranged to be on the model centreline and half of the model draught below the water surface.

5.4 Measurement of total resistance

An integral part of the measurement of total resistance is the method by which the model is supported. The support method may allow movement in the direction of motion of the model (i.e. the x direction) and restrain movement in other directions. The support method should also allow the measurement of resistance to be relatively simple.

University of Cape Town

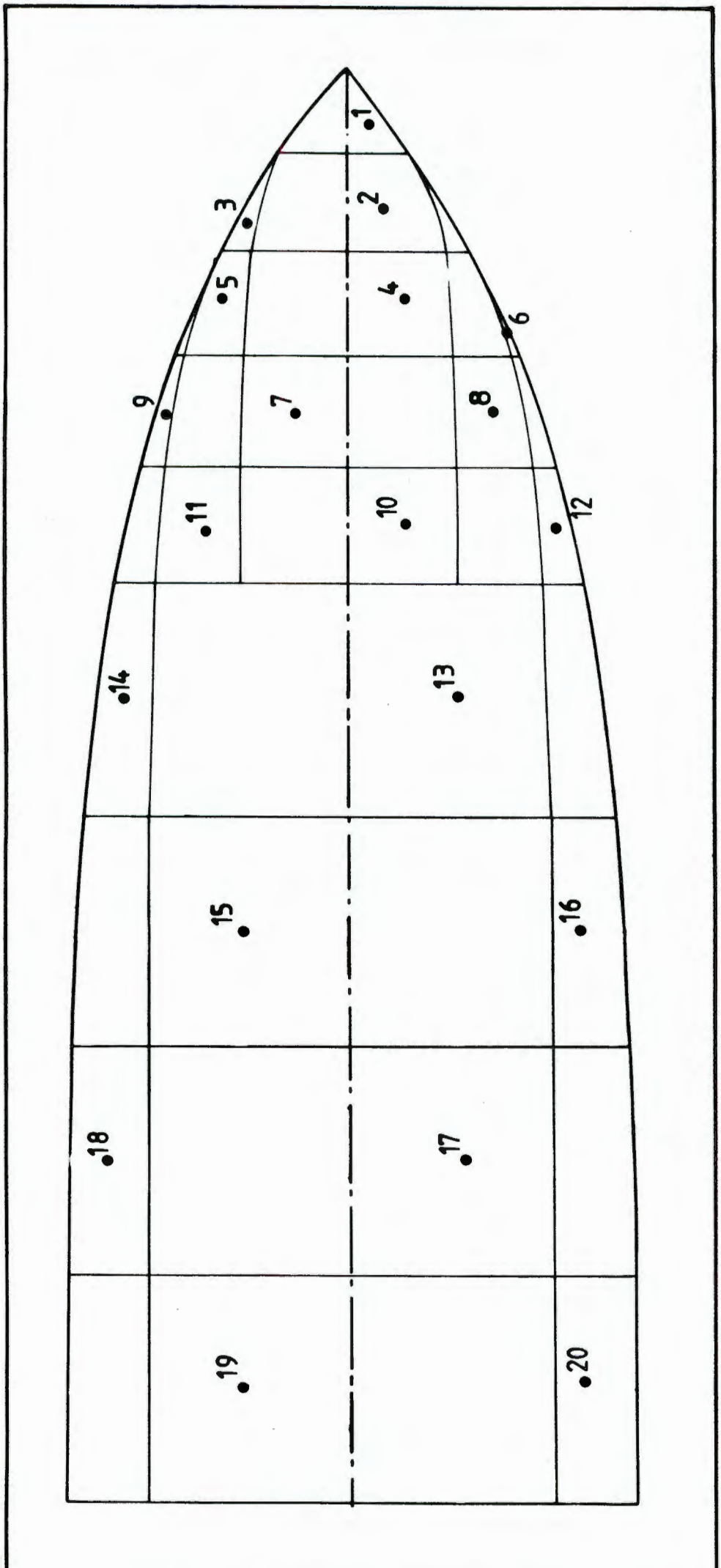

Figure 5.2 Pressure tapping locations

5.4.1 Alternative model support methods

Four alternative methods are illustrated in Figure 5.3. The cantilever and pendulum methods are similar in that they both allow rotation about a single point. The cantilever makes use of its stiffness to measure the total resistance by means of strain gauges positioned as shown in Figure 5.3. The pendulum method relies on an external load sensing device to keep its position and measure the total resistance. The cantilever method has the advantage of having no friction in the system and, therefore, allowing pure measurement of total resistance, however, care must be taken to ensure that the cantilever is not put into torsion as this will result in erroneous resistance measurements. The pendulum system will transmit torsional forces to the bearings and not to the resistance measurement device ensuring that only the total resistance is measured. The major drawback for both of these devices lies in the fact that in order to measure the resistance a deflection of the load sensing device is required. Any movement of the model in the x direction means that its elevation changes because the movement of the model is along the arc of a circle, this immediately places a restoring force on the model tending to return it to the lowest point of the arc. Therefore, both of these methods are only suitable if the deflection of the model can be kept to a minimum while still allowing accurate measurement of the total resistance.

The rolling bearing method shown in Figure 5.3 makes use of a horizontal plane on which bearings rest. The resistance force acting on the model its transmitted to the bearings which then roll along the horizontal plane. The total resistance may be measured using a load sensing device which will restrain the movement of the model. The mass of the system must be large enough to prevent a set of bearings lifting off the horizontal plane due to the moment caused by the resistance force acting on the model. The method has

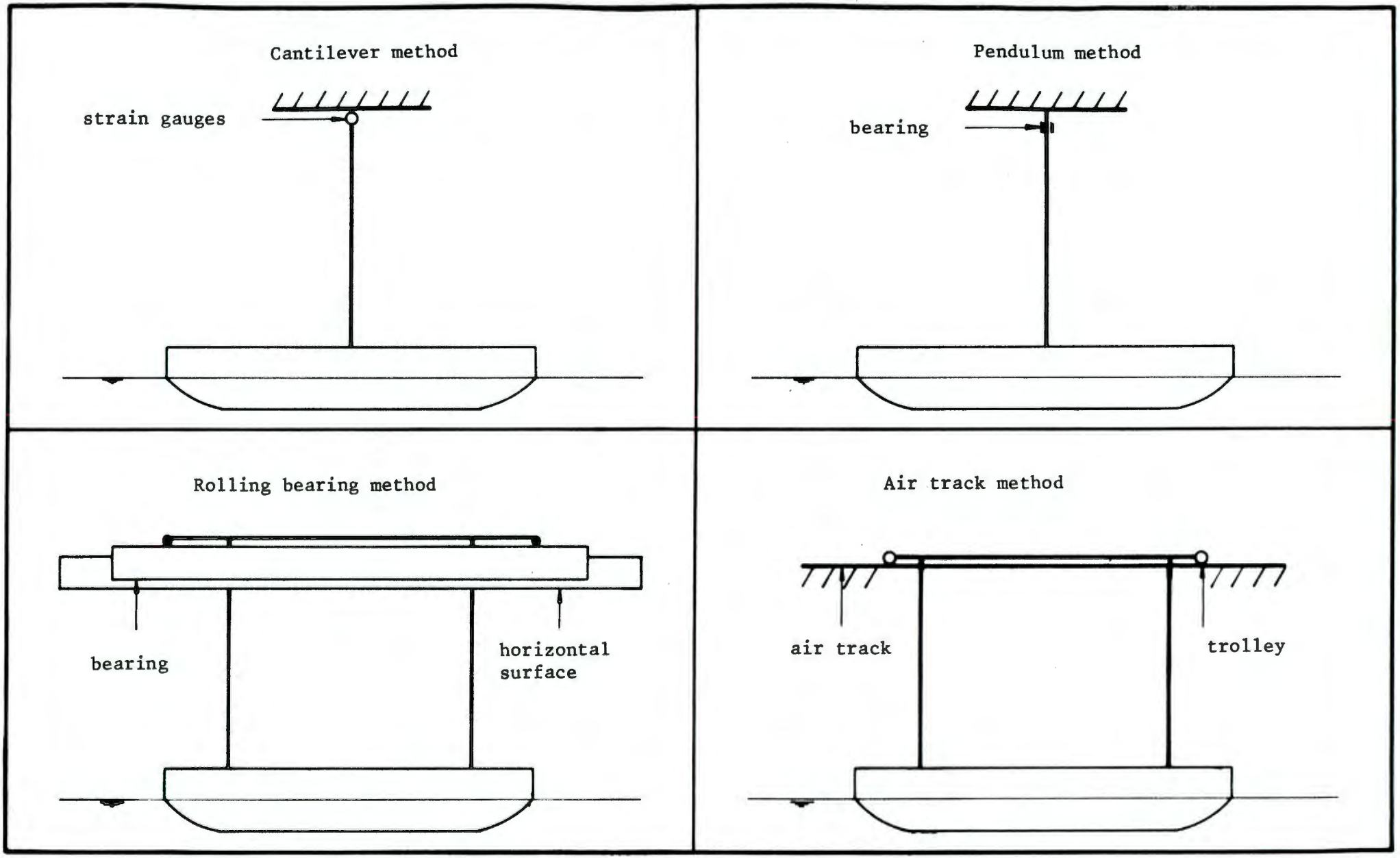

Figure 5.3 Alternative support methods

the advantage that the force transmitted to the load sensing device is a pure force with no moments acting on it. The main disadvantage with the method is the frictional resistance of the bearings which could cause an error in the total resistance measurement.

The fourth idea, namely the air track, overcomes the frictional disadvantage of the rolling bearing system while retaining all its advantages. The air track is commonly used as a demonstration of frictionless phenomena in introductory physics courses. The basic principle is that air is pumped through a track on which the trolley rides. By balancing the flow of air with the trolley mass the trolley can be made to "float" on top of the track and thus provide a frictionless method of supporting the model and allowing accurate measurements of total resistance to be made.

5.4.2 Alternative load sensing devices

The options available for use as load sensing devices are: commercial load cells, commercial spring balances and strain gauges mounted on a sensing element.

Commercial load cells that would achieve the desired accuracy (0,01 N) are available. The load cells are an attractive option for measuring the total resistance since they have negligible deflection when loaded, therefore, the movement of the support system would be very small. The load cells would also not introduce any additional friction to the system. They are, however, relatively expensive.

A Salter spring balance was investigated as a means of measuring the total resistance. The spring balance had a maximum load rating of 1 N and was graduated in 0,01 N steps. It was found that the spring balance was not at all suitable for use horizontally. The spring balance could be used in the vertical position with reasonable accuracy; however,

this would entail the use of a pulley to change the horizontal resistance force into a vertical force.

Strain gauges mounted on a sensing element provide a relatively cheap method of producing "load cells". The sensing element is usually put into bending (such as the base of a cantilever) and the compression and tension strains measured using strain gauges (see Figure 5.4). Four strain gauges are usually mounted to form a bridge - two gauges on the tension side and two gauges on the compression side. See Appendix D for the theory of the strain gauge bridge. The strain gauge bridge provides an output voltage that varies linearly with strain, provided care is taken to ensure that the sensing element is not loaded beyond its elastic limit.

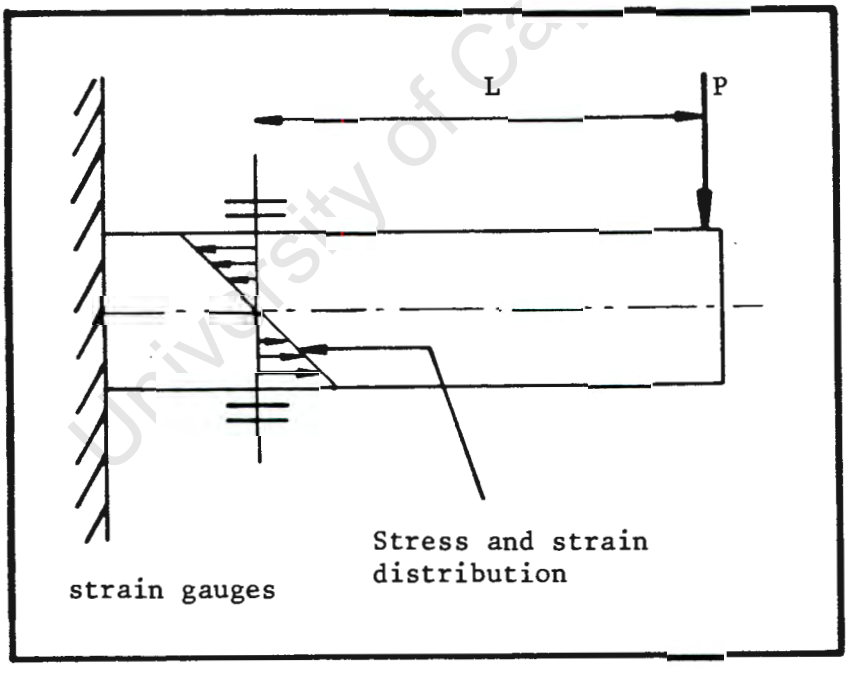

Figure 5.4 Cantilever load sensing device

University of Cape Town

5.4.3 Choice of measurement system

Both the pendulum and cantilever methods of supporting the model were discarded due to the unacceptably high restoring forces which would have made the resistance force measurements difficult to interpret. The rolling bearing method was an acceptable solution, the only problem being the friction of the bearings. Since the air track support method solved the frictional problem of the rolling bearing method while retaining all its advantages, the air track support method was the obvious choice.

The cost of commercial load cells proved prohibitive and were, therefore, not considered as an option to measure the total resistance. By choosing the air track system to support the model and, therefore, having a frictionless system, the use of a spring balance with a pulley wheel was not a viable option since it introduced friction into the system. Therefore, a strain gauge bridge mounted on a sensing element was chosen as the force measurement device.

To ensure stability the final choice of model support method was two air tracks parallel to each other. A trolley glides on each of the air tracks and the framework to support the model is fixed to the trolleys. The load sensing device chosen was a cantilever with strain gauges mounted on its base. This system has two advantages: one is that the system is totally frictionless and also, as the output of the strain gauge bridge is an electrical system, the total resistance of the model may be measured using data logging facilities.

5.4.4 Fabrication of total resistance measurement system

5.4.4.1 Air tracks

Each air track is made from a 1 m length of aluminium equal leg angle section (50 x 50 x 3 mm) and a mild steel channel section (100 x 50 x 5 mm) - see Figure 5.5. The angle section is mounted with its apex uppermost on the flat side of the channel section. The channel section provides a rigid base to support the angle section, and also forms part of the hollow triangular section inside the air track. The angle section which forms the track has two rows of holes (1 mm diameter) at 25 mm spacings drilled in the middle 800 mm section of each angle section on both faces. At each end of the angle section end plates are positioned, one of these having an adaptor for an inlet pipe. The angle section, end plates and channel section are bonded together using "Araldite" epoxy glue which provides an air tight seal.

The two air tracks are mounted parallel to each other on a cross member which is clamped to the flume. Each air track has three adjusting bolts which allow changes to the air track's elevation and allow the air track to be levelled accurately. The trolleys are made from the same aluminium angle section as the air track and are 760 mm long.

The inlet pipes of both of the air tracks are connected to a Hydrovane compressor which has a pressure range from 0 to 240 kPa. The flow of air to the tracks is controlled by a ball valve near the air tracks (see Figure 5.6 and Plate 5.5). By adjusting the flow of air into the air tracks the thickness of the air cushion on which the air track glides can be adjusted. To ensure maximum stability the air tracks are operated at the point at which the trolleys just lift off the air track.

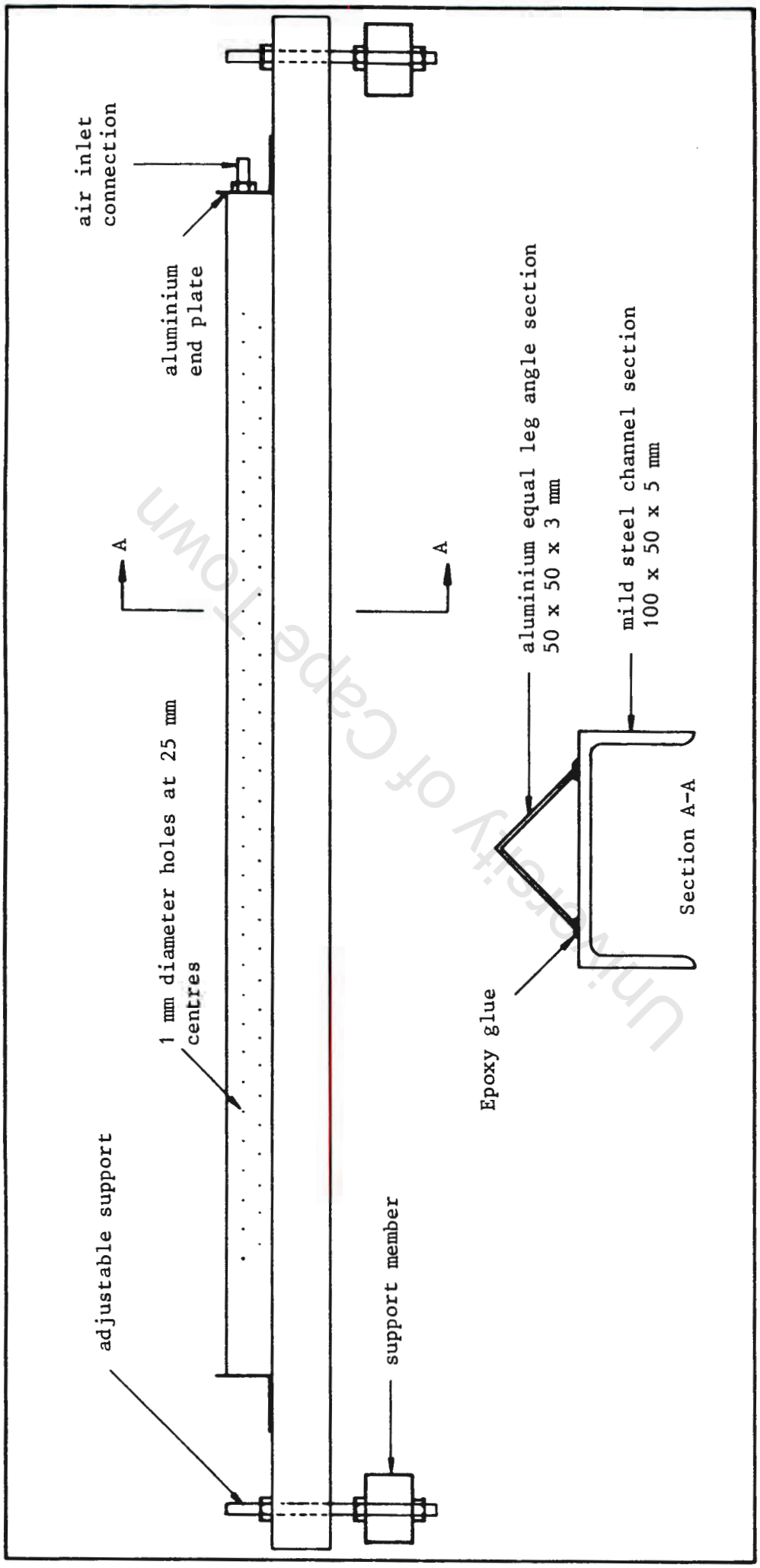

Figure 5.5 Air track

University of Cape Town

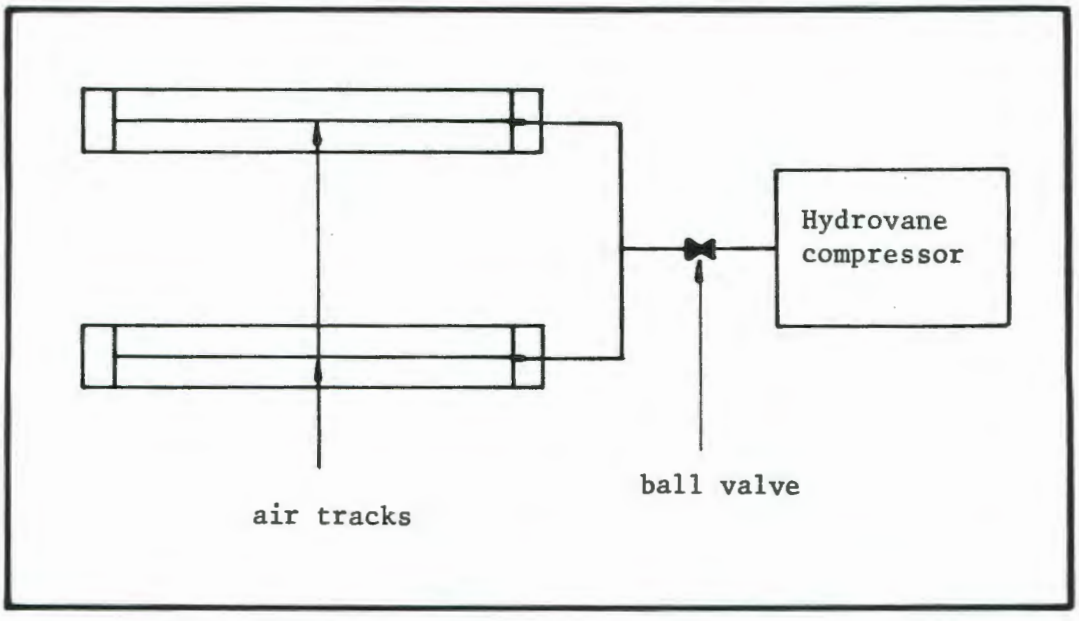

Figure 5.6 Compressor connection to air tracks

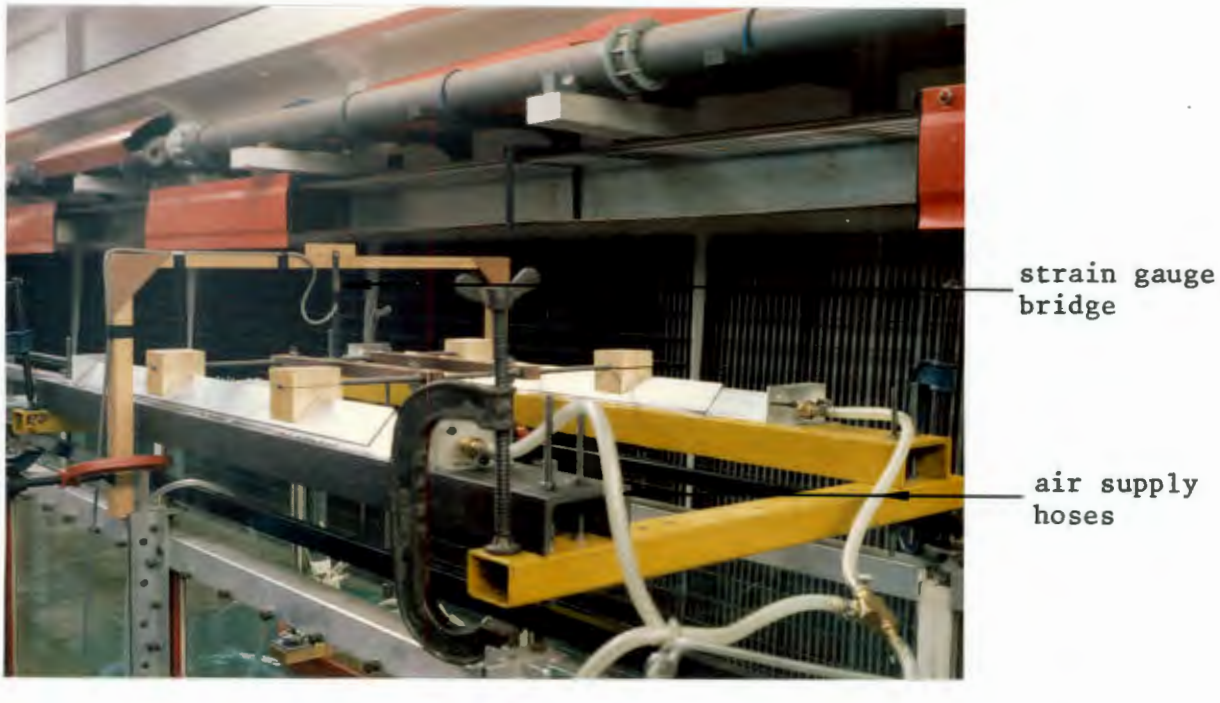

Plate 5.5 The dual air tracks

5.4.4.2 Model support

The model support system using dual air tracks is illustrated in Figure 5.7. The framework consists of 8 mm threaded mild steel rod with wooden connecting blocks. The framework allows a wide range of water depths to be used to test the model.

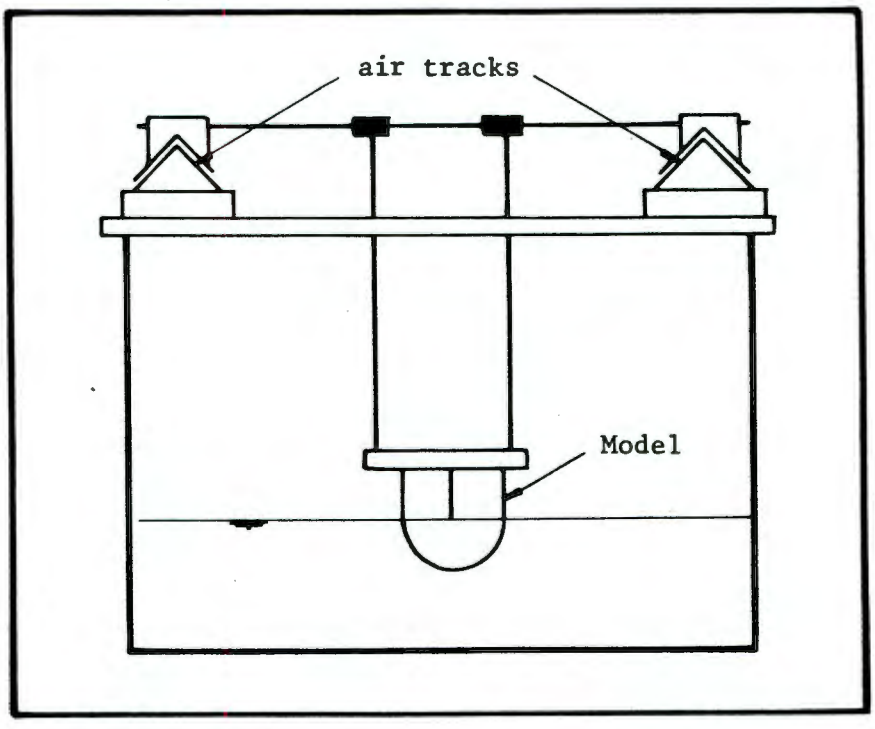

Figure 5.7 Dual air track model support system

5.4.4.3 Cantilever resistance measuring device

The cantilever is mounted on a wooden frame above the flume - see Plate 5.5 page 5.14. When the model has a resistance force acting on it, the system tends to move backwards - the cantilever provides the restraint and, therefore, measures the force acting on the model. The strain gauges used are temperature compensated with a gauge resistance of 120 ohm and a gauge factor of 2,10. The sensing device used for the cantilever is a hacksaw blade which is ideal for this application since it is manufactured from high tensile steel and can, therefore, tolerate high strains while remaining elastic.

The strain gauge bridge wiring diagram and connection to the data logging system is shown in Figure 5.8. The input voltage used is about 5 V and is supplied by a stabilised power supply. The output voltage (typically 0 - 20 mV) is measured using a Hewlett Packard 3497 Data Acquisition/Control Unit which is capable of reading to 100 μV. The measurements are relayed to a Hewlett Packard 150 personal computer which converts the voltage measurements into resistance forces using a previous calibration.

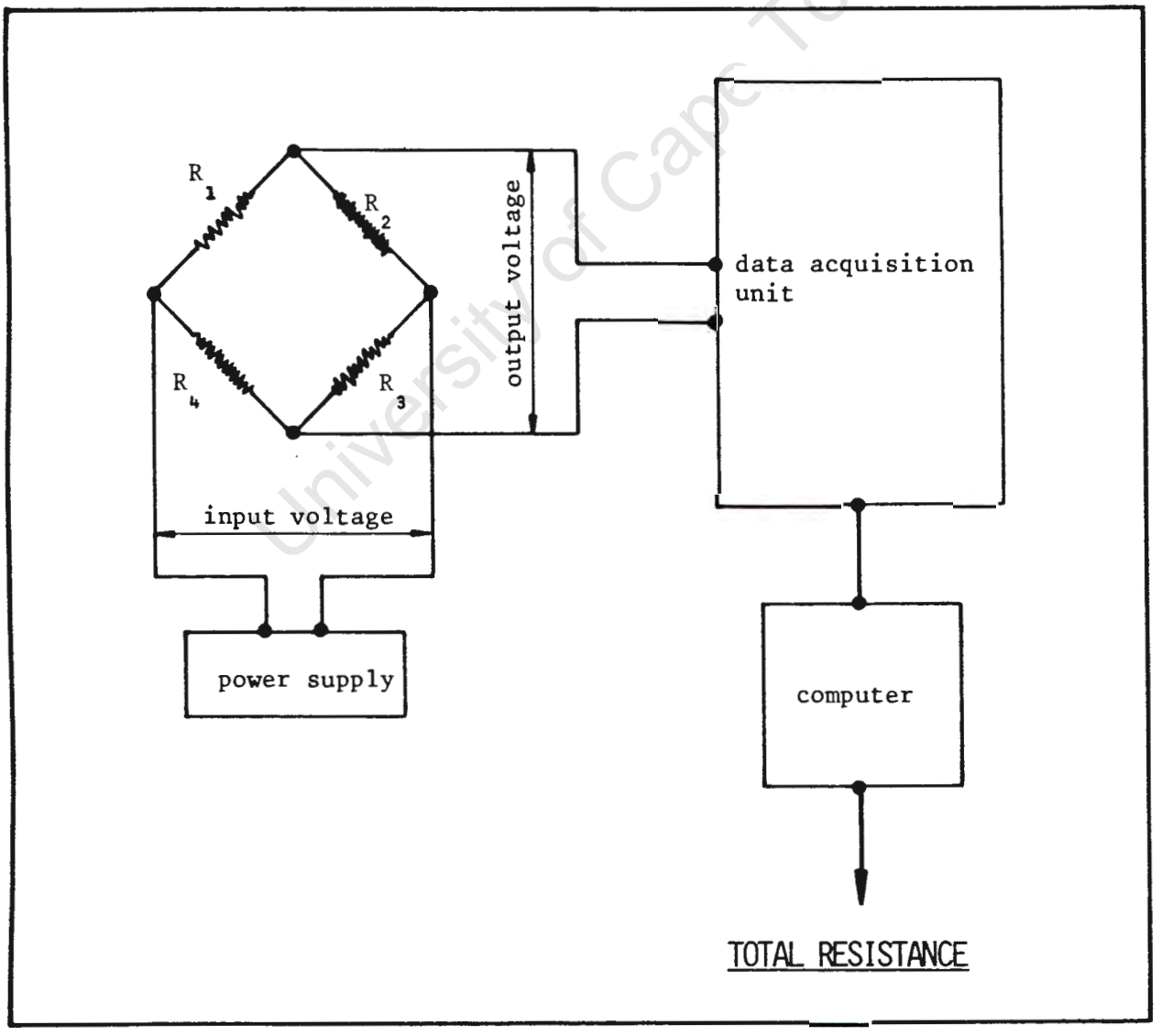

Figure 5.8 Strain gauge bridge connection diagram

University of Cape Town

5.4.5 Experimental procedure

5.4.5.1 Calibration of strain gauge bridge

1. The computer, data logger and power supply must be switched on at least 20 mins before the start of the calibration. This is to ensure that all the electrical components have stabilised before measurements are made. The strain gauge bridge also needs to reach an equilibrium temperature before readings are taken. Check that the output voltage of the power supply to the strain gauge bridge is approximately 5 volts.

2. A known force is applied to the cantilever and the output voltage read by the data logger and stored in the computer. This procedure is to be repeated from zero load building up to the maximum expected load, and then repeated again going down to zero load to check that there is no hysteresis in the strain gauge bridge. See Plates 5.6 and 5.7.

3. The ratio of the output voltage to the input voltage is plotted against the applied load. (See Figure 5.9). Using a least squares method the best fit line is found using the calibration program. The constants for the slope of the line and the y-intercept are then used later to calculate the total resistance of the model. Note that the slope is the most important constant since it does not change from the calibration location to the total resistance location. When calibrating under zero applied load there is still the self weight of the cantilever acting on the strain gauge bridge. Therefore, the y-intercept when measuring the total resistance will be different from the y-intercept when calibrating and this needs to be checked before the start of total resistance measurements.

University of Cape Town

Plate 5.6 Calibration of strain gauge bridge

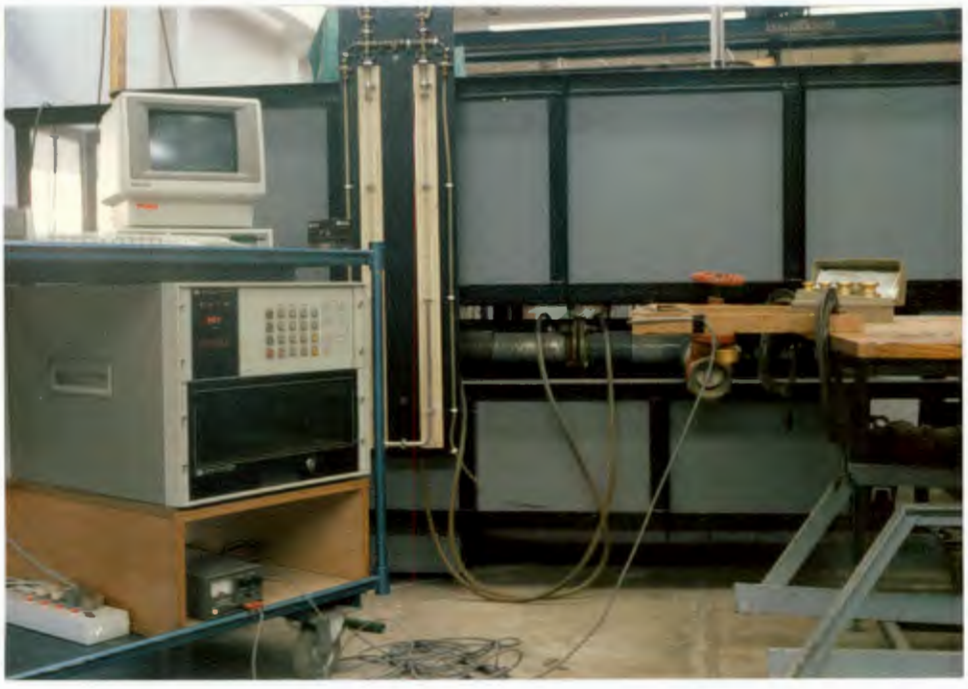

Plate 5.7 Calibration of the strain gauge bridge using the data logging facility

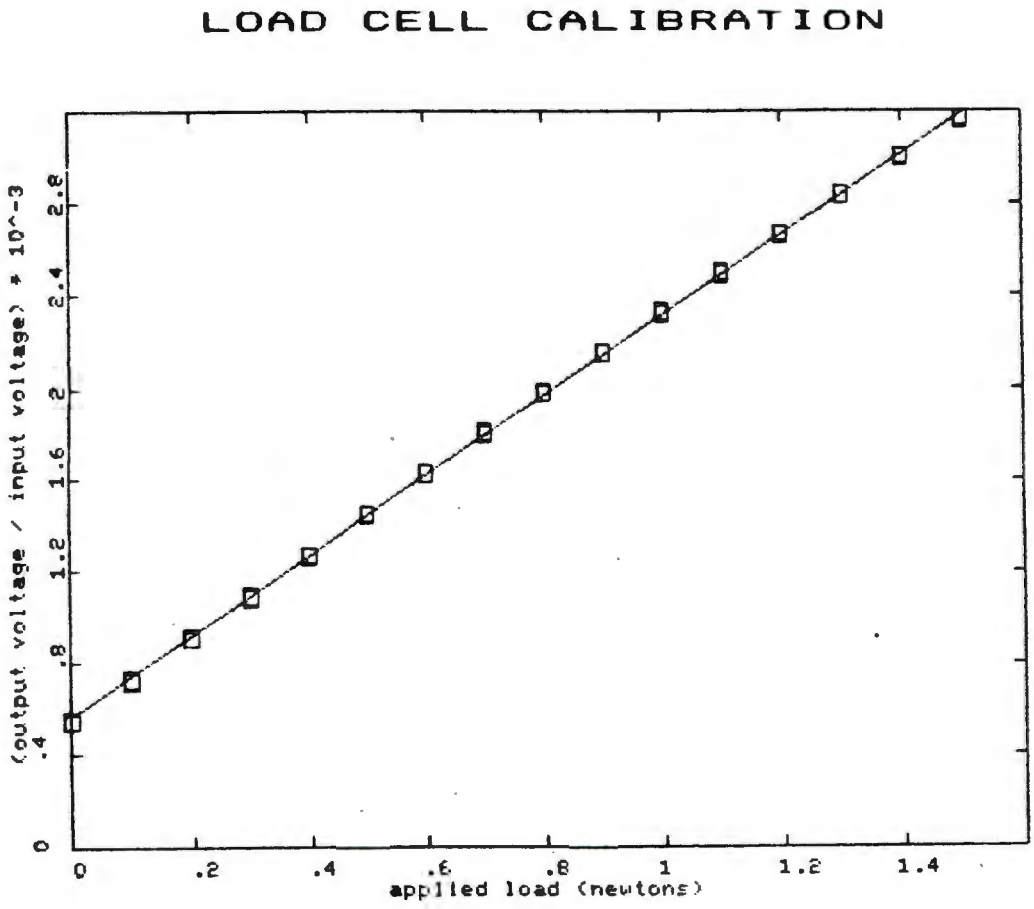

Figure 5.9 Typical strain gauge calibration graph

5.4.5.2 Total resistance measurement procedure

1. Switch on the compressor and check that the air tracks are parallel, correctly aligned and level. The air tracks are deemed to be level once the trolleys have no preferred direction of motion on the air tracks, with no water motion.

2. Place the model support and model onto the air track trolleys and check that the model is set to the specified draught.

3. Open the control valve to allow water to flow into the flume. By adjusting the tailgate and the control valve a range of water velocities at the same depth can be obtained. The water surface slope must be measured at the test section over the range of operating velocities to ensure that the water slope will not significantly affect the resistance measurement. If the slope of water surface is found to be too large the gradient of the flume must be changed using the motorised jack and the above procedure repeated.

4. A water depth is chosen for a series of tests (200 mm for deep water calibration). Tests are started at low velocities and increased up to the maximum testing speed (1 m/s).

5. After the selected water depth has been obtained by adjusting the tailgate and control valve the system is left to stabilise for 5 minutes.

6. Measure the output of the strain gauge bridge using the data logging system. The data logger takes readings every 2 seconds for 150 seconds and then plots the answers in the form shown in Figure 5.10.

7. While the data logger is reading the strain gauge bridge output voltage measure the dynamic head of the pitot tube on the manometer board, using a depth gauge, so that water velocity can be calculated. Record the water temperature.

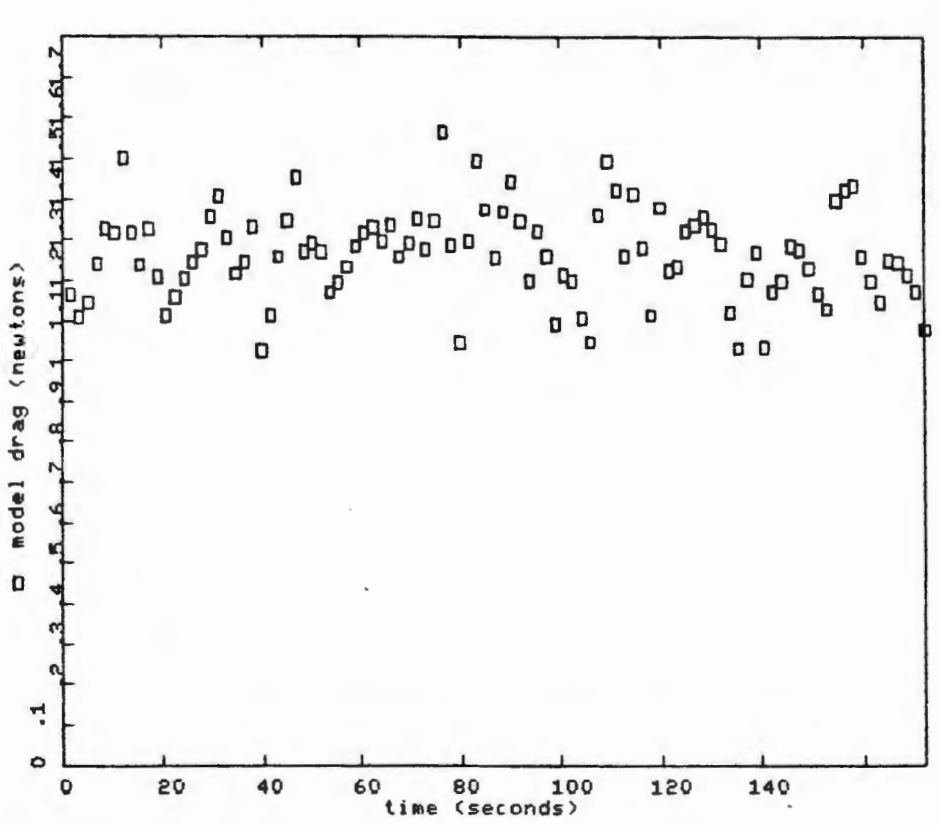

DATE : 03-07-1986 TIME : 19:53:31
WATER DEPTH = 200 mm
WATER TEMPERATURE : 25.2 °C
STRAIN GAUGE BRIDGE INPUT VOLTAGE = 5.0108 volts
SLOPE OF LOAD-VOLTAGE LINE = 1.75243
Y INTERCEPT OF LOAD-VOLTAGE = .5629295

The drag values are averaged between 10.42 and 149.41 seconds.
AVERAGE DRAG = 1.272 Newtons
VELOCITY = 1.022 m/s

Figure 5.10 Typical total resistance plot

8. Plot the average resistance obtained from the data logger against the velocity to check that the readings do not contain gross errors.

9. Increase the water velocity by adjusting the control valve. Re-set the water height using the tailgate and go back to step 5 until a complete curve of total resistance versus velocity is established.

5.5 Measurement of total pressure resistance

To calculate the total pressure resistance of the model the pressure distribution around the model hull must be established. To determine the pressure distribution of the model the pressure at each of the 40 pressure tappings must be measured.

5.5.1 Alternative methods of measuring pressure

Pressure transducers are commercially available which will read the low pressures (typically 500 Pa) acting on the model hull. The transducers basically consist of a diaphragm which has strain gauges mounted on it to form a bridge. Any deformation of the diaphragm due to an applied pressure causes a change in the resistance of the strain gauges and consequently a change in the output voltage. The pressure transducers have very fast response times typically 0,1 millisecond which allows reading times to be reduced considerably. The electrical output of the pressure transducers may also be measured using the data logging system discussed in Section 5.4. Pressure transducers are available that read either absolute pressures or differential pressures.

Another method of measuring pressure is to make use of the weight of a column of water. The water is lead from the pressure tapping into a container of water. To ensure equilibrium the water level in the container will adjust to match the pressure at the tapping. If the pressure fluctuates so will the water level in the container and hence so will its mass. Therefore, if the mass of the container is measured it can be interpreted as a pressure acting at the tapping by using a previous calibration. The method will have a slow response time to allow for the flow of water between the container and tapping, but it does have the advantage of an electrical output that can be measured using the data logging system.

The third method of measuring the pressures is the simplest. Tubes are led from the pressure tappings to a manometer board where the changes in water elevation are measured using a depth gauge. The accuracy that can be obtained by using the depth gauge to measure the water elevation is 0,1 mm. The pressure heads measured by this method are comparable to points on a hydraulic grade line and, therefore, a reference to the hull geometry must be made. The disadvantages of this method are the relatively slow response time and the lack of electrical output that could be measured using the data logging system.

5.5.2 Choice of pressure measurement method

Due to the high cost of the pressure transducers they were discarded as a choice for pressure measurement. A system could have been developed using say 2 pressure transducers and being connected to each tapping in turn, however, the extra time involved in connecting the hoses would have outweighed the advantages of the pressure transducers.

Of the other two alternatives it was felt that the manometer board represented the simplest and cheapest method of measuring the pressures. The manometer board does not need any calibration and, therefore, is a very pure pressure measurement. The weighing beaker method is more expensive to manufacture than the manometer board and the 0,1mm accuracy of the manometer board would have been difficult to surpass. Therefore, based on cost, ease of use and simplicity of construction, the manometer board was chosen as the pressure measurement method.

5.5.3 Fabrication of the manometer board

The manometer board consists of two sets of 22 glass tubes, each set mounted on the side of the flume (see Plates 5.8 and 5.9). A depth gauge is mounted above the tubes which can be moved along to any selected tube. 40 of the glass

University of Cape Town

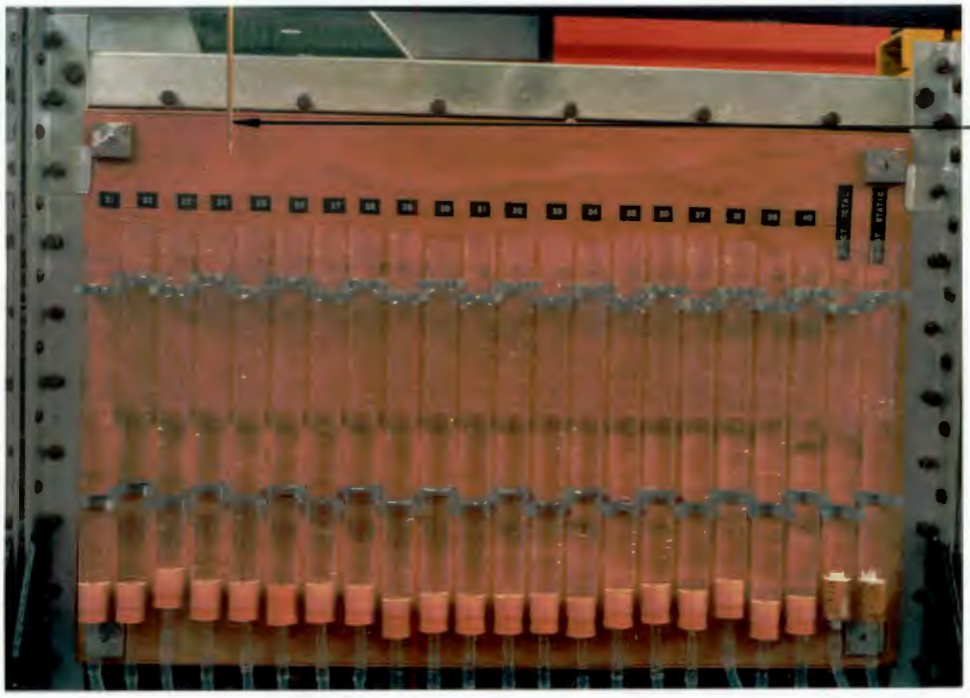

Plate 5.8 One set of 22 glass tubes mounted on the side of the flume

Plate 5.9 Connection of manometer board to model ship

tubes are used for the pressure tappings, 2 for the pitot tube, 1 for the upstream tapping and 1 for the downstream tapping. The upstream and downstream tappings are used to determine the slope of the water surface as discussed in Section 5.4.5.

The glass tubes have a 20 mm internal diameter with 1 mm thick wall. The tubes were chosen to have a fairly large diameter to minimise the effect of capillary rise in the tubes - see Appendix B.2. Connectors were manufactured to allow quick connection from the tubes leading from the hypodermic needles to 8 mm laboratory tubing. The 8 mm laboratory tubing connects to the glass tube by means of a rubber bung inserted into the bottom of the glass tube.

5.5.4 Experimental procedure

1. Connect the pressure tappings to their corresponding glass tubes.

2. By adjusting the tailgate and control valve bring the water level in the flume up to the specified level.

3. Prime all the pressure tappings and pitot tube hoses.

4. Leave the system to stabilise for 15 minutes.

5. Record the numbers of the tappings that are above the water surface. Read the water column heights in all the tappings, repeat again and check for discrepancies. If there are any discrepancies (i.e. difference in readings of greater than 0,5 mm) then re-prime the tapping, wait for 15 minutes and then re-check the water column height.

6. Take 3 photographs of the water surface profile along the hull. The one side of the hull has a 10 mm square grid drawn on a yellow background so that the profile

may be scaled from the photograph. Just before a photograph is taken a solution of potassium permanganate is introduced into the water upstream of the model to create a sharp colour contrast with the model hull - see Plate 5.10.

7. The water velocity is changed by adjusting the tailgate and control valve. The procedure (from step 4) is again repeated.

Plate 5.10 Typical test photograph to determine water surface profile

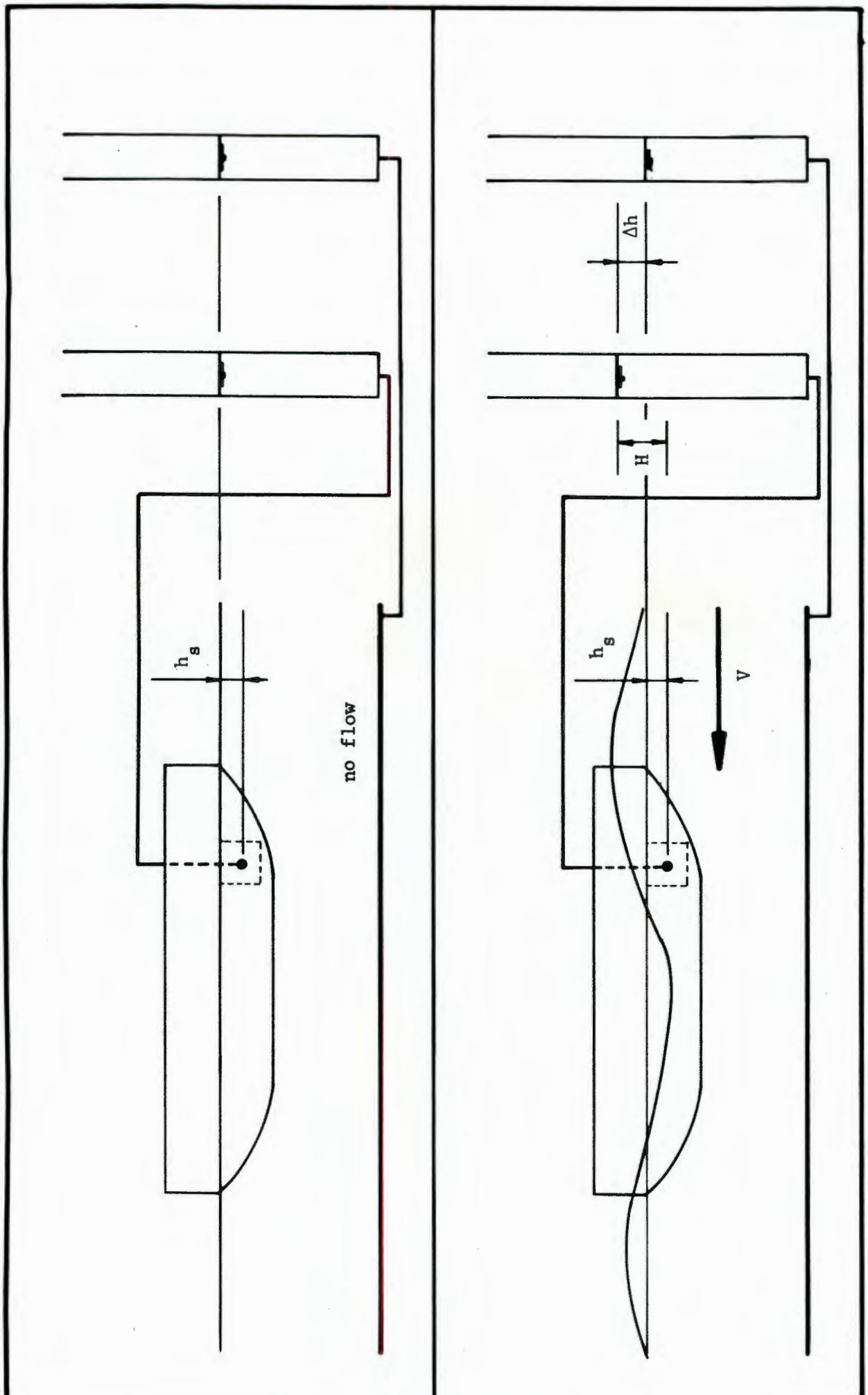

Figure 5.11 Model pressure tapping connection to manometer board

5.5.5 Calculation of total pressure resistance

Figure 5.11 illustrates the connection of one pressure tapping and the upstream tapping to the manometer board. Each tapping on the hull has a defined area dA as is shown in Figure 5.2 page 5.6.

Consider the first case of no flow in the flume shown in Figure 5.11. The water level in both the glass tubes will equal the still water level as shown. The pressure head in metres of water acting at the tapping will be the submergence of the tapping below the still water line (i.e. h_s). The value of h_s is fixed by the geometry of the pressure tapping locations.

In the second case where there is flow in the flume the level in the glass tube connected to the upstream tapping will remain at the still water level as the tapping has been chosen sufficiently far upstream to be unaffected by the presence of the model in the flume. However, the water level in the glass tube connected to the pressure tapping will either rise or fall depending on its location on the hull geometry. Therefore, by comparing the upstream tapping and pressure tapping readings the value of the change in water head Δh acting on the area dA can be found. By adding the submergence of the tapping below the still water level h_s the pressure head H can be calculated. The pressure ρgH is multiplied by the area dA to obtain the normal force acting on the element and then the component acting in the direction of motion calculated using the angle the hull surface makes with the direction of motion ϕ.

The wave profile along the hull of the model causes some of the superstructure above the still water level to be wetted and correspondingly, some areas below the still water line to be exposed. The effect of these changes must be taken into account when calculating the pressure resistance of the model. The pressure resistance of the model is calculated using the following procedure:

1. The water surface profile along the model is interpreted from the photograph taken of the water surface profile (see Plate 5.10 page 5.26). If any area dA has a portion of its area exposed, the exposed area is calculated and the area dA correspondingly reduced. If a pressure tapping is completely exposed, but its area dA still partially wetted, then the wetted area is calculated and added to an adjacent tapping (e.g. if tapping 10 was exposed, its wetted area would be added to tapping 11's area - see Figure 5.2 page 5.6).

2. The pressure heads H at each tapping are calculated using the geometry of the pressure tappings h_s and the measured changes in head Δh .

3. Pressure distributions around the hull are drawn using the water surface profile and the pressure heads H .

4. The resistance contribution below the still water level of each tapping is calculated using the following equation

$$R_p \text{ (below SWL)} - \rho g \, H \, dA \cos\phi \ .$$

These contributions are added to obtain the resistance contribution of the hull below the still water level - ΣR_p (below SWL).

5. The length of the superstructure is divided into segments. From the pressure distribution diagrams the average pressure in metres of water h_a and the area over which it acts is calculated for each segment. For each segment its contribution to the total pressure resistance is calculated

$$R_p \text{ (above SWL)} = \rho g \, h_a \, A \cos\phi$$

These contributions are addded to obtain the resistance contribution of the hull above the still water level - ΣR_p (above SWL).

CHAPTER 6

TOWING CHANNEL EXPERIMENT

6.1 Towing trolley and channel

The towing channel is constructed from reinforced concrete and located below ground level in U C T Civil Engineering laboratories. The channel is 92 m long, has a constant width of 1,5 m and a maximum water depth of 1,440 m. The channel has a wave generator at its northern end and a beach at the southern end to dampen out any wave action. An observation room is situated midway between the beach and wave generator which allows visual inspection of conditions in the flume. Opposite the observation window the floor level of the channel has been slightly raised.

Plate 6.1 View of towing trolley as seen from inside the channel

There are rail tracks on each side of the channel which carry the towing trolley. Plate 6.1 shows a view of the towing trolley as seen from inside the channel. The trolley may be operated in either direction, however, for this thesis measurements were only made on the south to north run. The trolley is powered by a three phase electrical motor and the power to the trolley is supplied through overhead electrical conductors. The trolley has four gears and in each of these gears the revolution rate of the motor may be varied from 100 to 2 400 r.p.m. This gives a speed range of up to 4,2 m/s although for practical reasons tests were only conducted up to 2,2 m/s.

6.2 Model

This set of experiments requires two models to be tested as discussed in Chapter 4 - a submerged model and a surface model. The submerged model is a body of revolution made to the form and dimensions given in Chapter 4. The surface model consists of one half of the body of revolution with a vertical sided superstructure. To prevent duplication of manufacture the submerged model was made in two halves which bolted together. To make up the surface model one half of the submerged model is bolted to the vertical sided superstructure. The frontal views of the two models are illustrated in Plates 6.2 and 6.3.

The models are all made from jelutong and then sealed with a two component epoxy paint. The bolt holes in the models are filled with glazing putty to about 5 mm from the surface of the model. The rest of the hole is filled with waterproof wood filter. Once the wood filter has dried the excess filter is sanded off using a fine water paper and then painted. This provides a finish that is flush with the model surface.

6.3 Measurement of trolley speed

The problem of measuring trolley is two fold: firstly the extent of the trolley's fluctuation about a pre-set speed is required and secondly, an accurate measurement of the actual mean speed over the test length is needed.

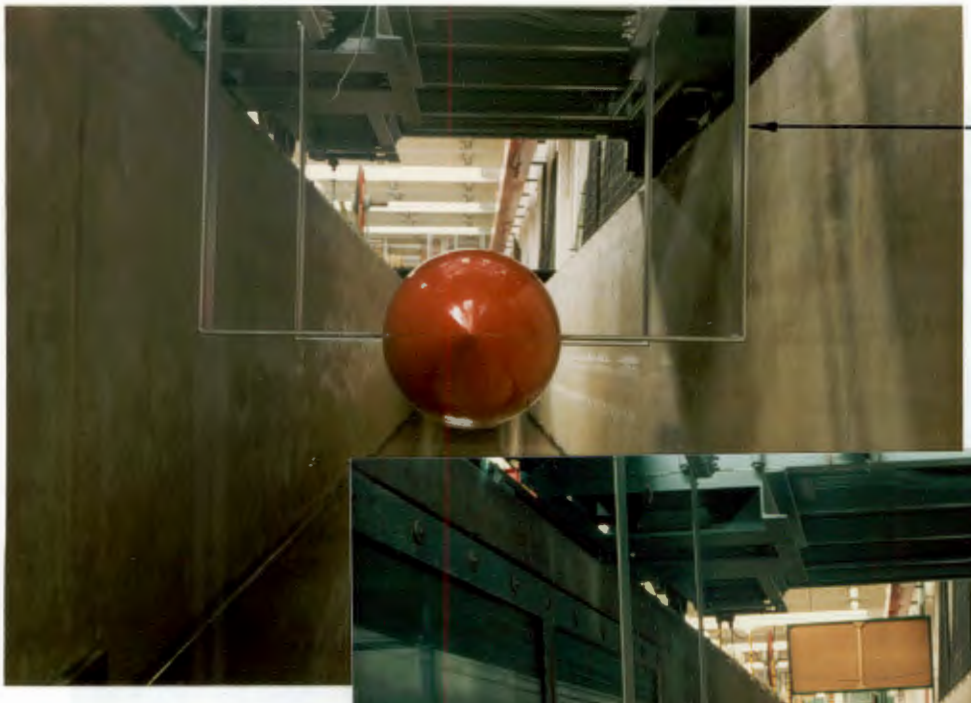

Plate 6.2 Frontal

Plate 6.3 Frontal view of surface model

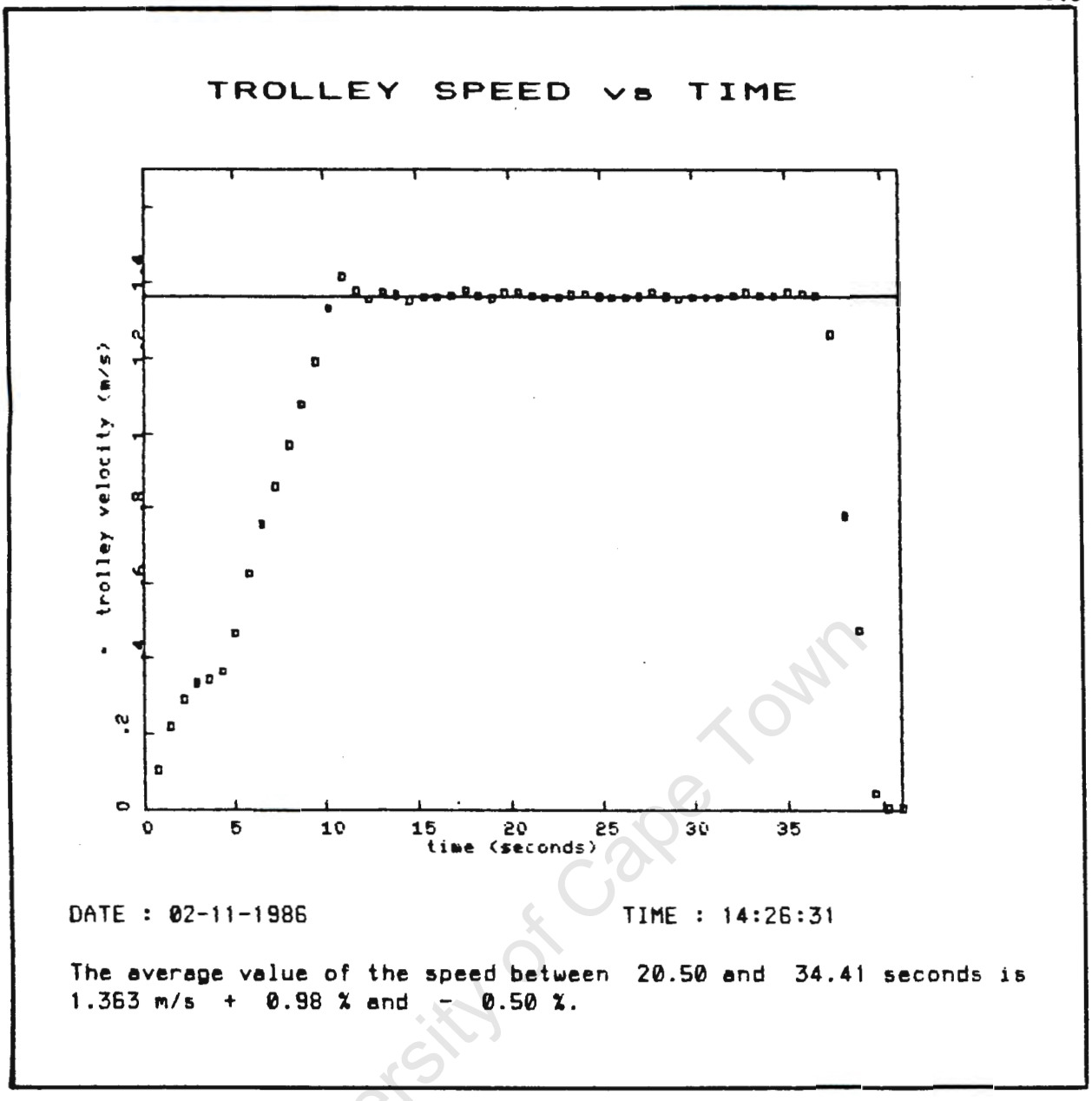

Figure 6.1 Typical variation of trolley speed with time

Figure 6.1 shows the output of one of the runs using the "frequency wheel". It was found that the variation of the trolley speed was generally within 2% of the pre-set speed. Since the fluctuation of the trolley about its mean speed is not great it was decided to measure the mean speed and correspondingly the mean total resistance. The frequency method of speed measurement was not, however, deemed to be accurate enough to use as an absolute measurement of the mean trolley speed.

University of Cape Town

To measure the mean speed accurately (to within 1%) an electronic timer capable of reading to 0,1 milliseconds is used. The timer is activated using a micro switch at the start of the test section and then again stopped by another micro switch at the end of the test section. The length of the test section is accurately measured using a steel tape. Thus, in this way, very accurate measurements of the mean speed of the trolley may be made.

6.4 Measurement of total resistance

6.4.1 Total resistance measurement system

The choices and problems for the measurement system are essentially the same as for the glass flume experiments. The only problem unique to the towing channel experiment is the measurement of the total resistance of the submerged model.

The submerged model must be supported in some way, and when the total resistance of the model is measured the resistance of the support structure must not be included in the measurement. One way to achieve this would be to place the load sensing device inside the model so that only the model resistance would be measured. The support structure would still, however, interfere with the flow around the model and this effect would be difficult to quantify. In addition, placing the load sensing devices under water introduces extra problems of waterproofing.

Consider the model shown in Figure 6.2 supported on either side by a strut. If the resistance of the model is measured with both struts in place the measured resistance would be the model resistance R_m plus two strut resistances $2R_{ST}$. If one of the sets of struts is now removed the measured resistance would be $R_m + R_{ST}$.

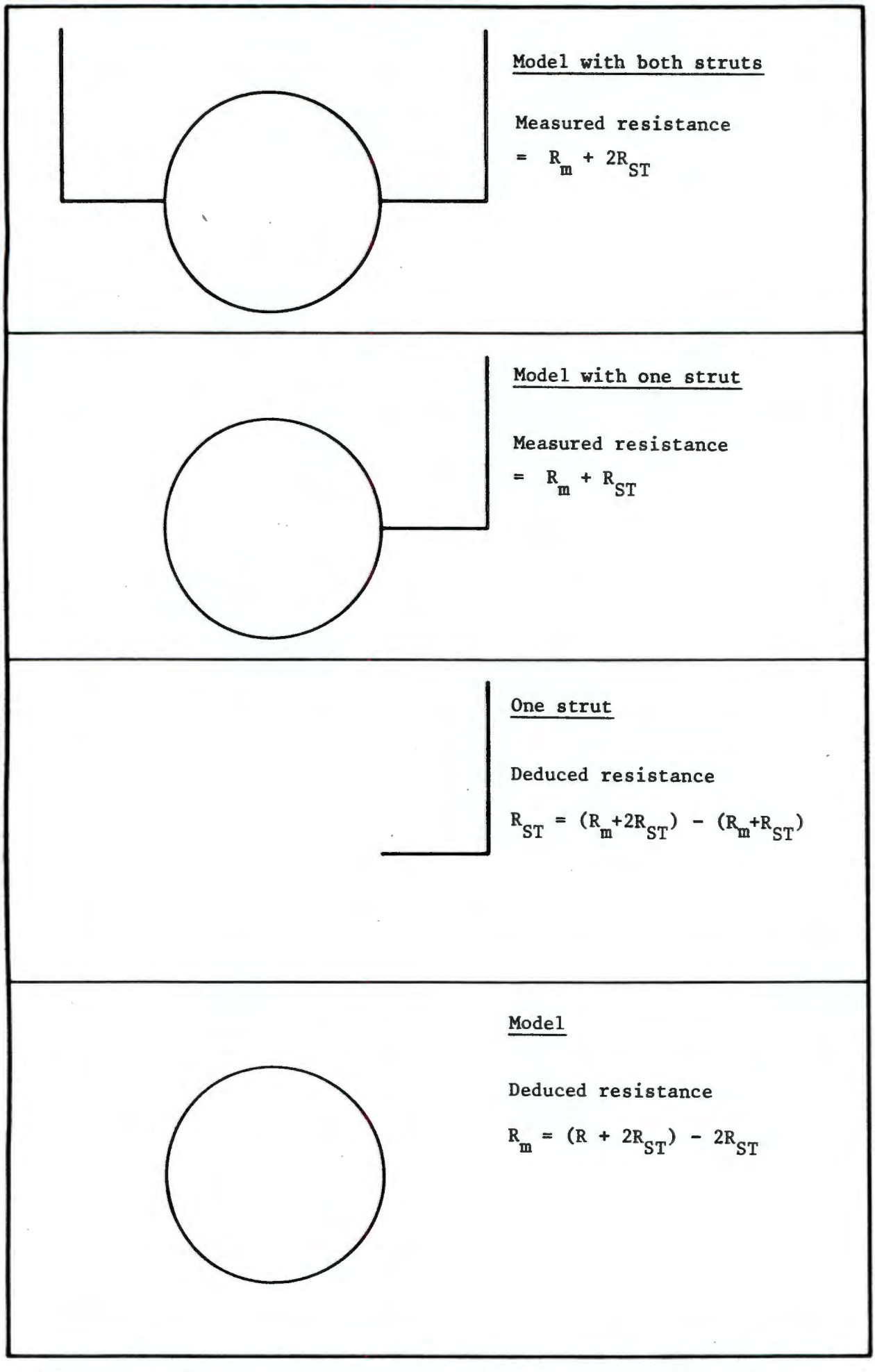

Figure 6.2 Method of obtaining total resistance of the submerged model

By subtracting the second measurement from the first measurement the resistance due to one strut, R_{ST} can be found. Now twice the strut resistance $2R_{ST}$ subtracted from the first measurement $(R_m + 2R_{ST})$ will give the resistance of the model R_m. This method provides an elegant and pure method of obtaining the submerged resistance of the model without positioning the load measuring device under water.

The use of an air track to support the model on the trolley would have required a relatively large air flow to lift the mass of the model. An air compressor would have to be mounted on the trolley to supply the required air flow. Since a compressor that could deliver the required air flow was not available the use of the air track as a support method was not possible.

Thus the rolling bearing support method was chosen to support the framework. The framework was designed bearing in mind that one set of struts would have to be removed later in the experimental work. To measure the resistance force acting on the model a strain gauge bridge is used.

6.4.2 Fabrication of total resistance measurement system

6.4.2.1 Support framework

Plate 6.5 shows the support framework on the trolley with the submerged model in position. The framework is made from 60 x 40 x 4 mm box sections and the struts from 80 x 8 mm flat sections. The struts below the water line are streamlined to the profile shown in Figure 6.3.

University of Cape Town

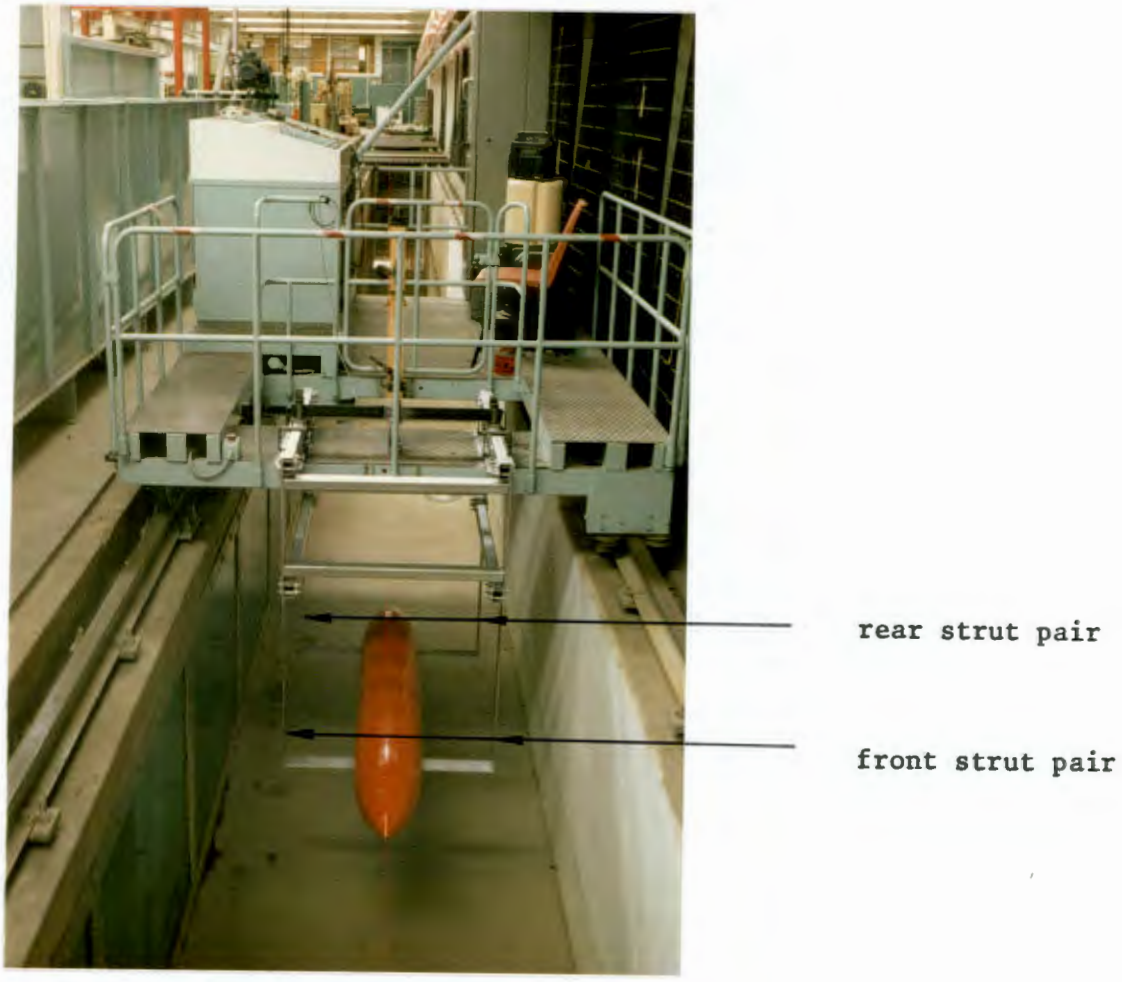

Plate 6.5 Model support framework

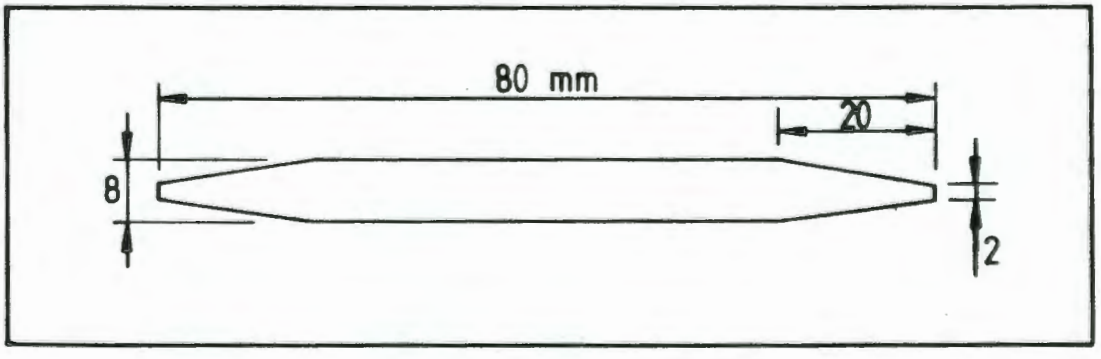

Figure 6.3 Support strut profile

The two halves of the submerged model are bolted with the struts running through the centre plane of the model. When the surface model is mounted on to the support system the whole support is raised by a height equal to the height of the superstructure. The struts are then bolted down on top of the superstructure. The reason that the support structure is raised for the surface model is to ensure that the under keel clearance remains the same for the submerged and surface models.

Plate 6.6 shows the machined surfaces on which the bearings roll. The vertically mounted bearings on the sides of the plates are to keep the alignment of the model parallel to the direction of motion. The four white hoops are a safety measure to ensure that the framework cannot come off the trolley. The white channel section between the plates is used as a central support for the load measuring device.

The two yellow box sections in Plate 6.7 house the bearings which permit the support structure to roll. The rest of the framework is mounted below onto the bolt holes that are visible. A bearing is shown in detail in Plate 6.8, while Plate 6.9 shows the machined surface against which one of the vertically mounted bearings runs.

6.4.2.2 Resistance measuring device

A plan view of the load sensing device is shown in red in Plate 6.10. The device is essentially a simply supported beam that is fixed to the trolley at its centre and fixed to the rolling framework at each of its ends. When the model experiences a resisting force this is transmitted to the beam.

Plate 6.6 Machined surfaces for bearings

Plate 6.7 Bearing housings

Plate 6.8 Detail of bearing

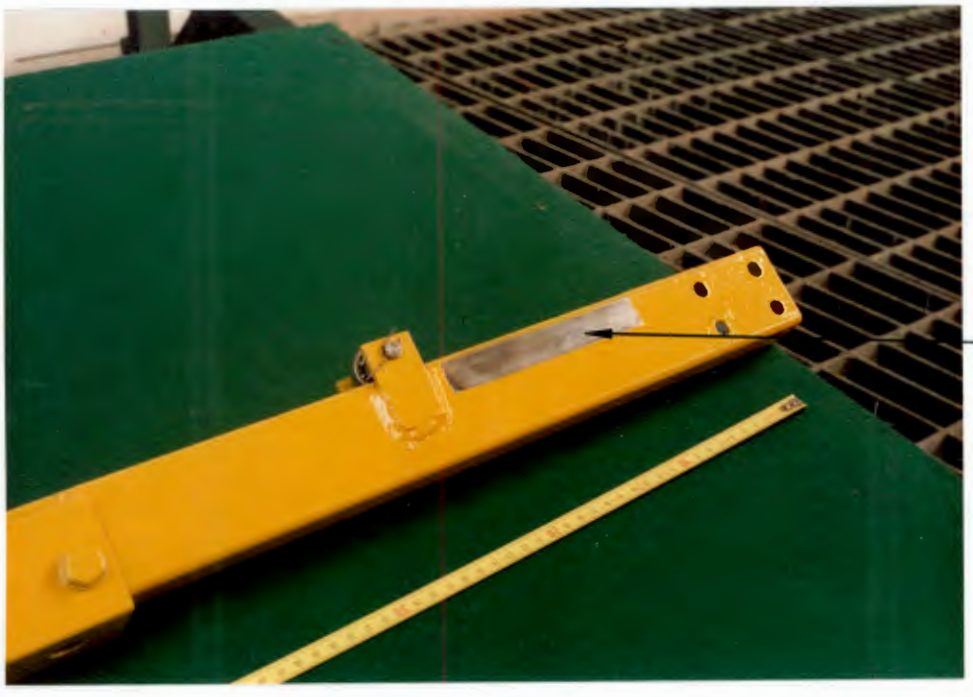

Plate 6.9 Bearing detail and machined surface for vertical bearing

The maximum bending occurs at the centre of the beam and for this reason the strain gauges are mounted on either side of the central support. On the left hand side of Plate 6.10 a hook is visible; this hook is used to calibrate the strain gauge bridge. Plate 6.11 illustrates how a known mass is applied to the framework through a cable from which the mass is suspended.

Once tests were started it was found that the output of the strain gauge bridge had an alternating voltage component. This was caused chiefly through the trolley not being able to maintain a completely uniform speed. Attempts to dampen the motion of the framework proved fruitless because of the relatively small resistance forces involved. Thus to solve the problem electrical damping was used. A simple first order low pass filter was made with a resistor value of 1 800 ohm and a capacitor value of 1 470 micro farad. The filter has a response time of about 4 seconds to reach 95% of the true value. Since all the run times were in excess of 10 seconds the delay was not significant. The theory behind the low pass filter is discussed in Appendix C.

The output voltage of the strain gauge bridge is read using a chart recorder and the resistance force interpreted using a previous calibration.

6.4.3 Experimental procedure

All runs are from the south end of channel to the north end and no readings are taken on the return run.

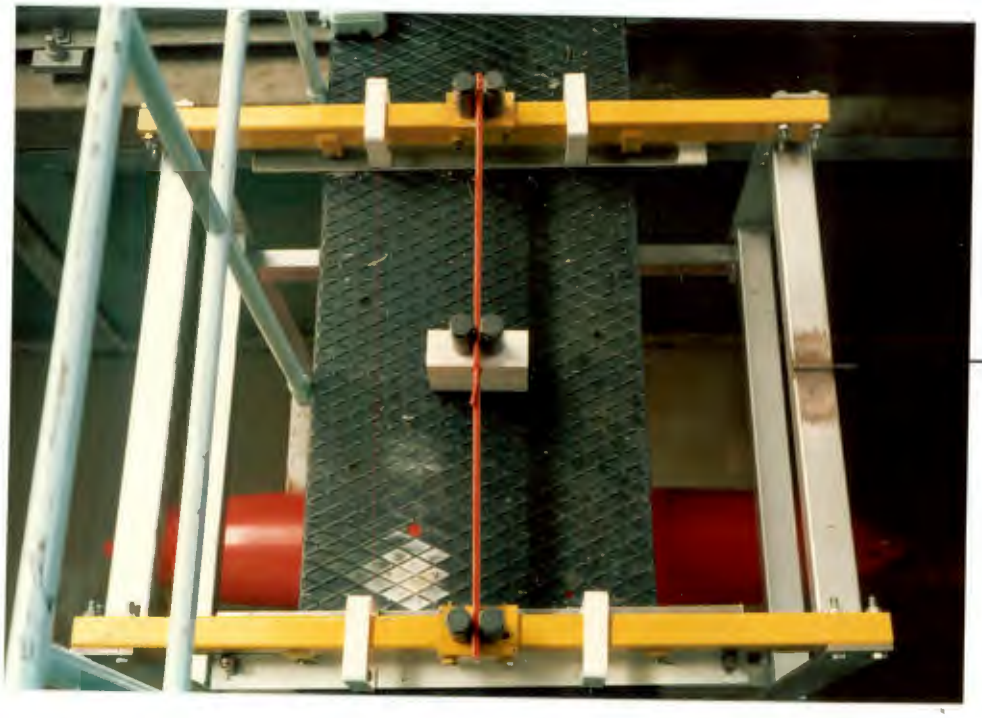

Plate 6.10 Plan view of resistance measuring beam

Plate 6.11 Calibration of strain gauge bridge

At the start of each run the strain gauge is calibrated on the chart recorder (see Figure 6.4). This sets the scale for the resistance time plot. Once the calibration is complete the run is started and the total resistance variation plotted using the chart recorder as shown in Figure 6.4. The time interval is recorded and the speed calculated.

The return run is done at approximately the same speed as the live run. About 5 to 20 minutes are required before the start of the next run to allow wave action and water currents to die down. This time period is dependent on the speed of the previous run. The water temperature is recorded every hour when tests are being conducted.

The total resistance is scaled from the resistance time plot and then plotted against speed.

To obtain the hull water surface profile for the surface model photographs are taken from the observation room (see Plate 6.12).

Plate 6.12 Photograph of hull water surface profile

At the start of each run the strain gauge is calibrated on the chart recorder (see Figure 6.4). This sets the scale for the resistance time plot. Once the calibration is complete the run is started and the total resistance variation plotted using the chart recorder as shown in Figure 6.4. The time interval is recorded and the speed calculated.

The return run is done at approximately the same speed as the live run. About 5 to 20 minutes are required before the start of the next run to allow wave action and water currents to die down. This time period is dependent on the speed of the previous run. The water temperature is recorded every hour when tests are being conducted.

The total resistance is scaled from the resistance time plot and then plotted against speed.

To obtain the hull water surface profile for the surface model photographs are taken from the observation room (see Plate 6.12).

University of Cape Town

Plate 6.12 Photograph of hull water surface profile

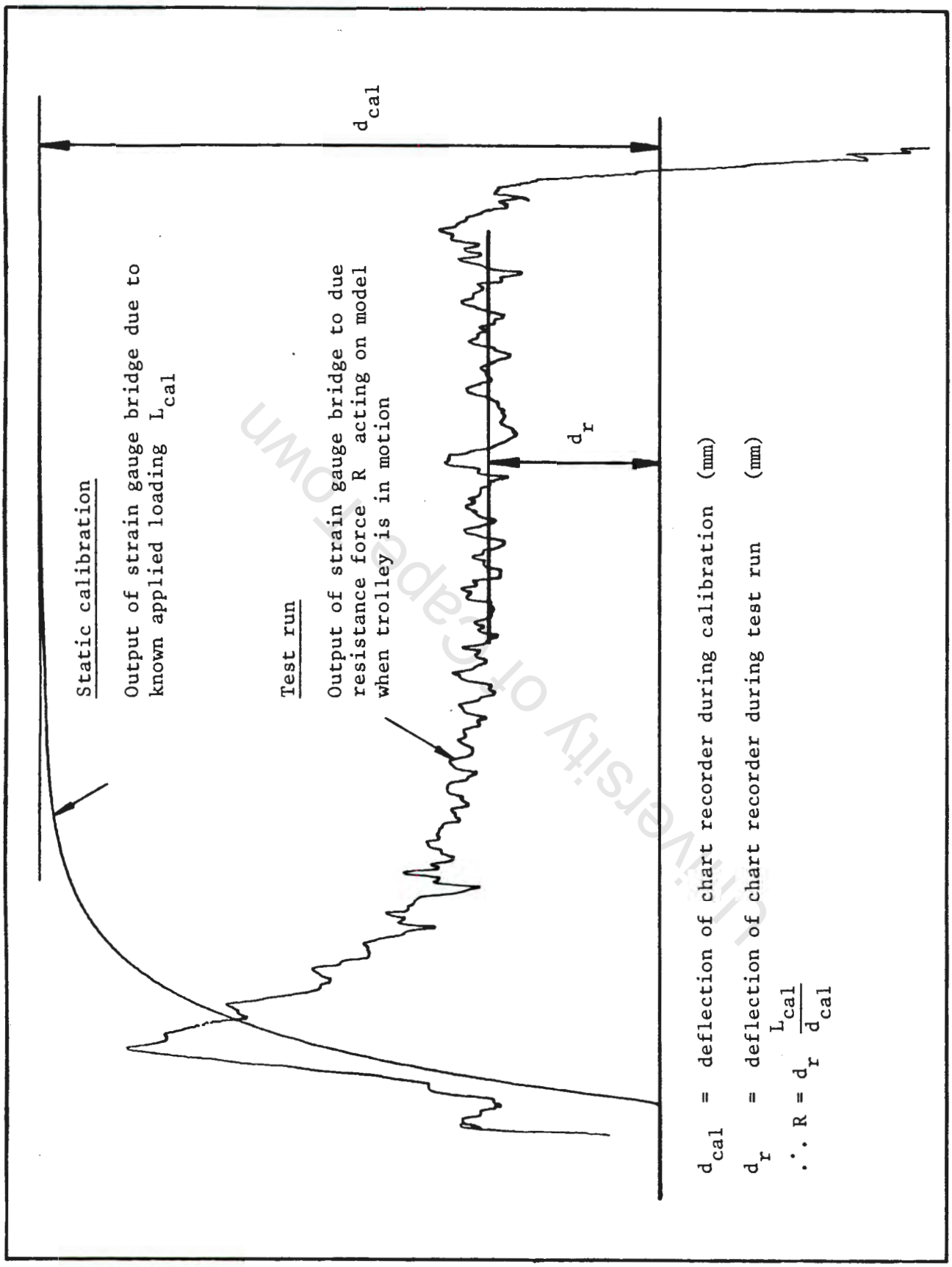

Figure 6.4 Typical measurement of total resistance

University of Tasmania

To ensure that the submerged model was deeply submerged, checks were made at higher speeds to ensure that the submerged model did not generate a set of waves at the water surface. This was done at speeds of up to 2,2 m/s and no evidence of waves due to the model were noted.

The sequence of testing was first the submerged model with both sets of support fins, then the surface model and, finally, the submerged model with one set of support fins removed.

Figure 6.5 shows a plan view of the submerged model and support fins. When testing the submerged model with one set of support fins removed, the ideal set to remove would be A and B, or C and D. To achieve this, however, the strength of the support fins would have to be increased leading to a larger fin cross-section. Therefore, fins A and D were removed which allowed the fin cross-section to remain relatively small. The two sets of fins (AC and BD) are relatively far apart and thus it is unlikely that the leading fin will influence the trailing fin, therefore, removing support fins A and D is hydraulically equivalent to removing A and B.

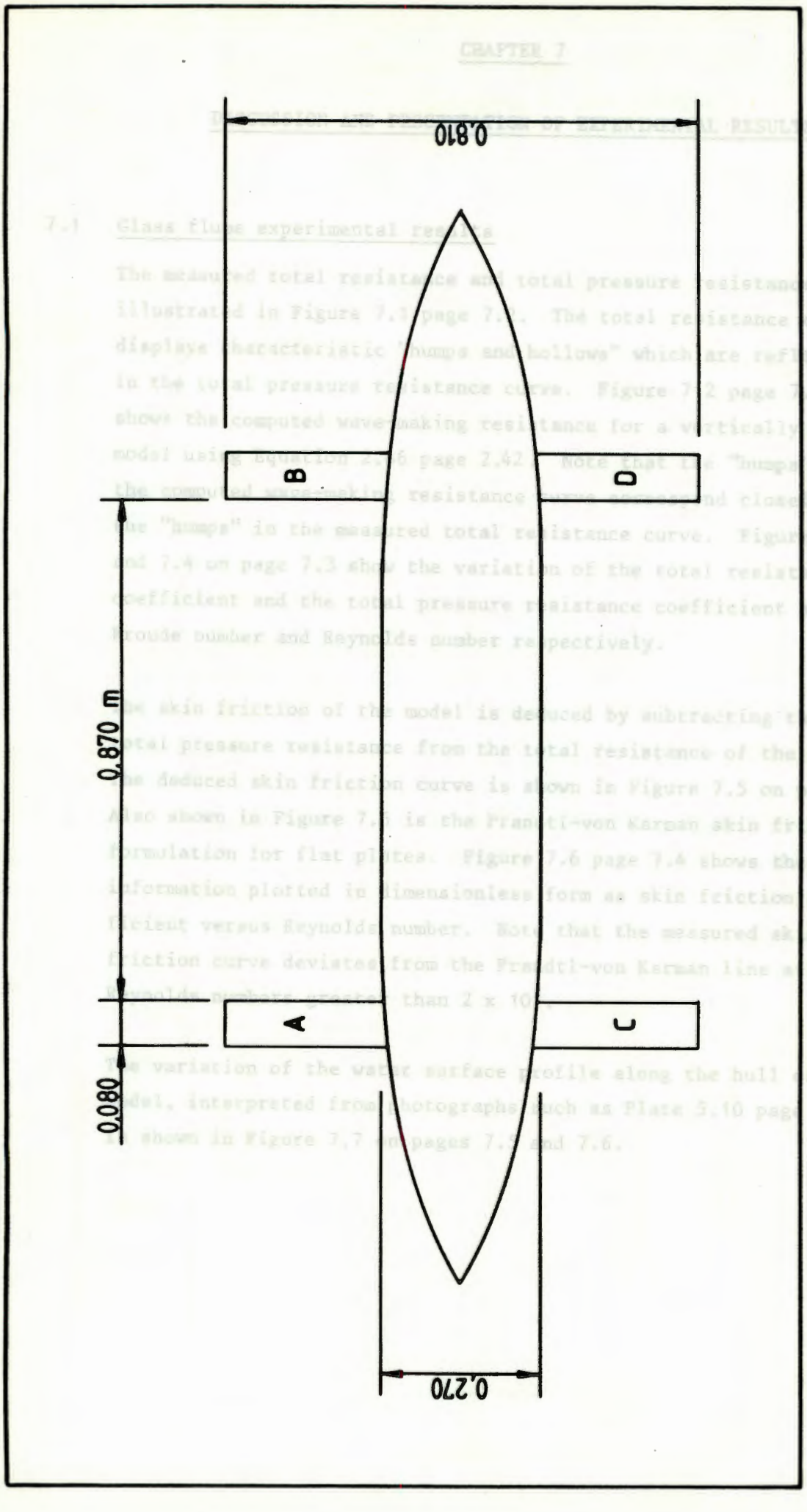

Figure 6.5 Plan view of submerged model and support fins

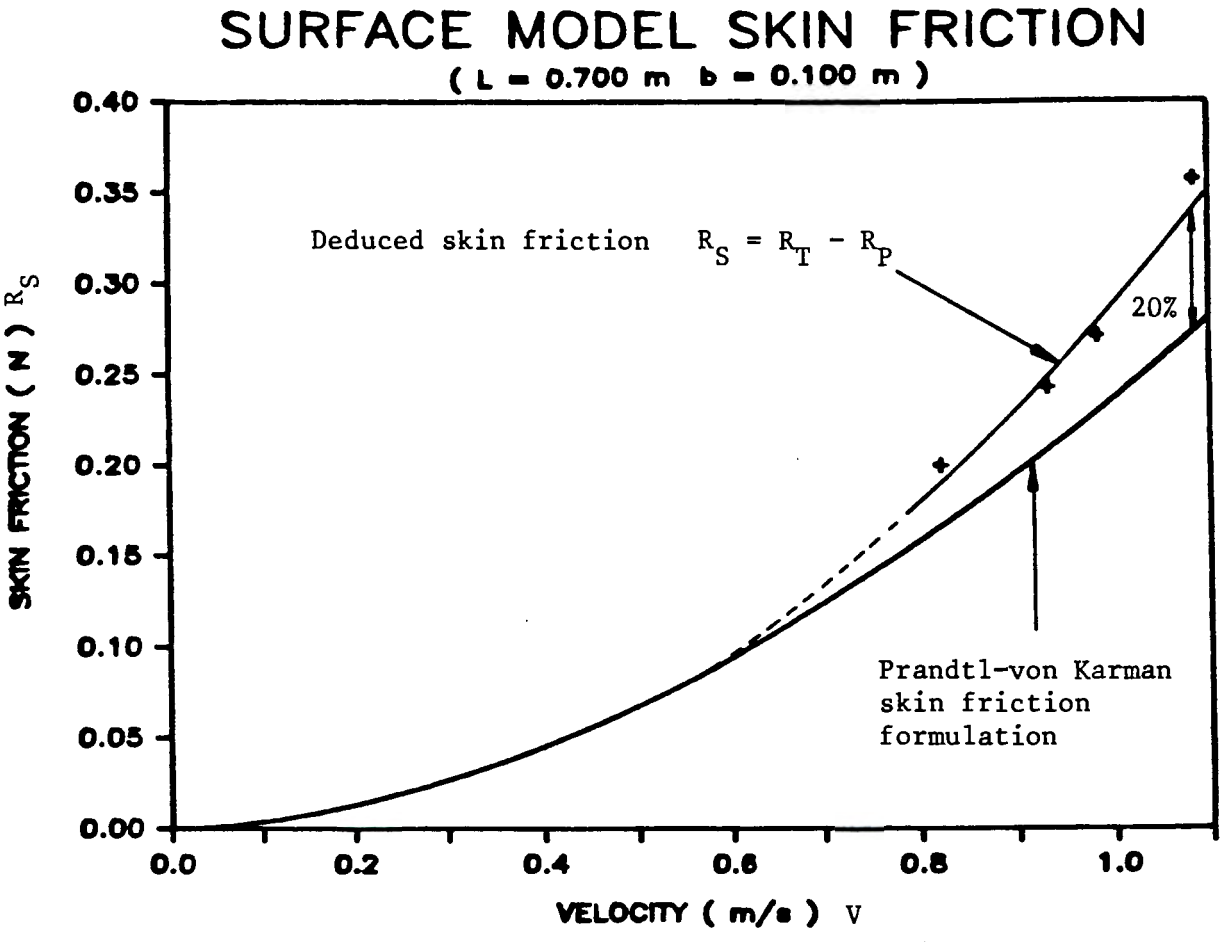

Figure 7.5 Skin friction versus model velocity

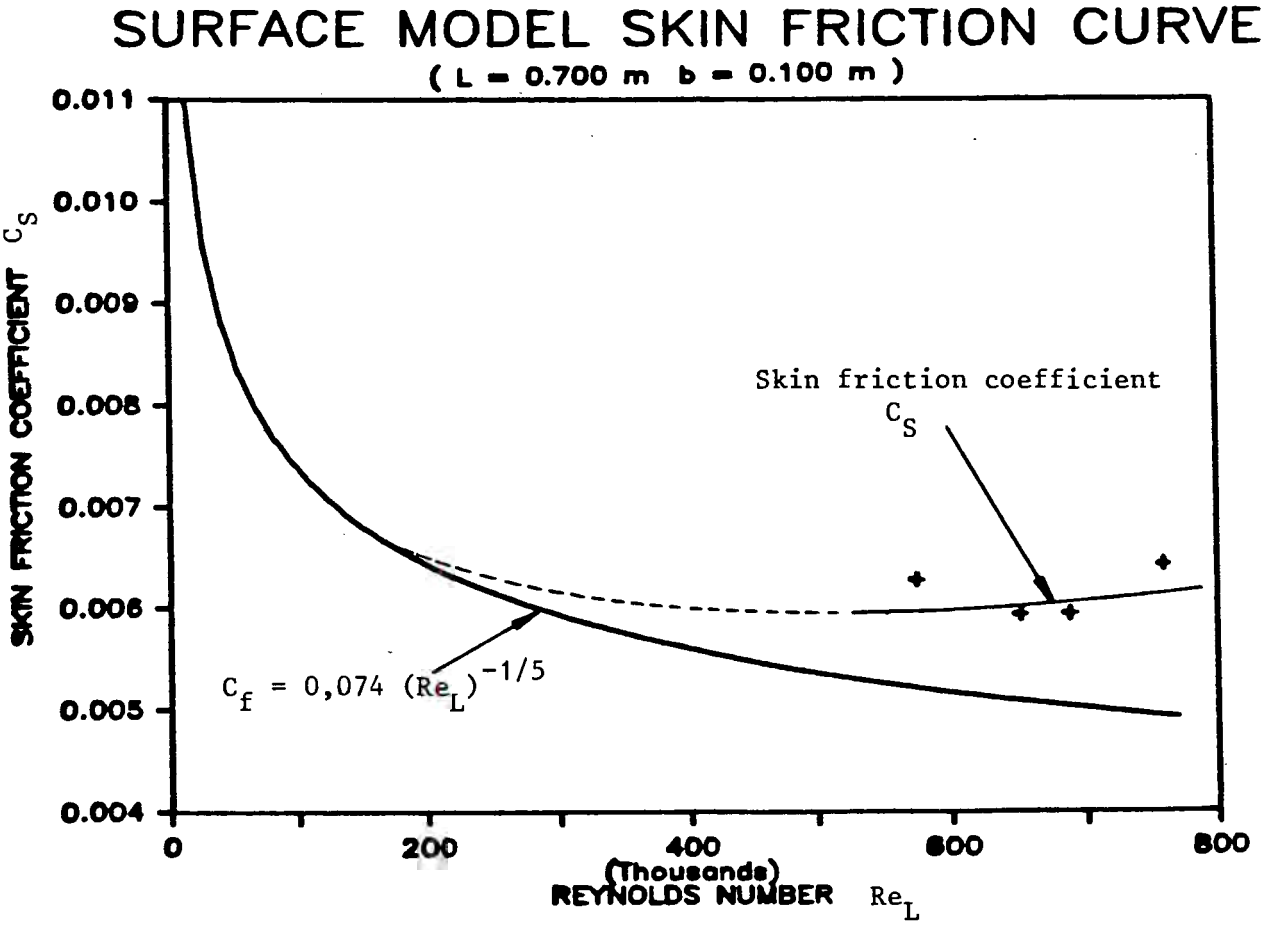

Figure 7.6 Skin friction coefficient versus Reynolds number

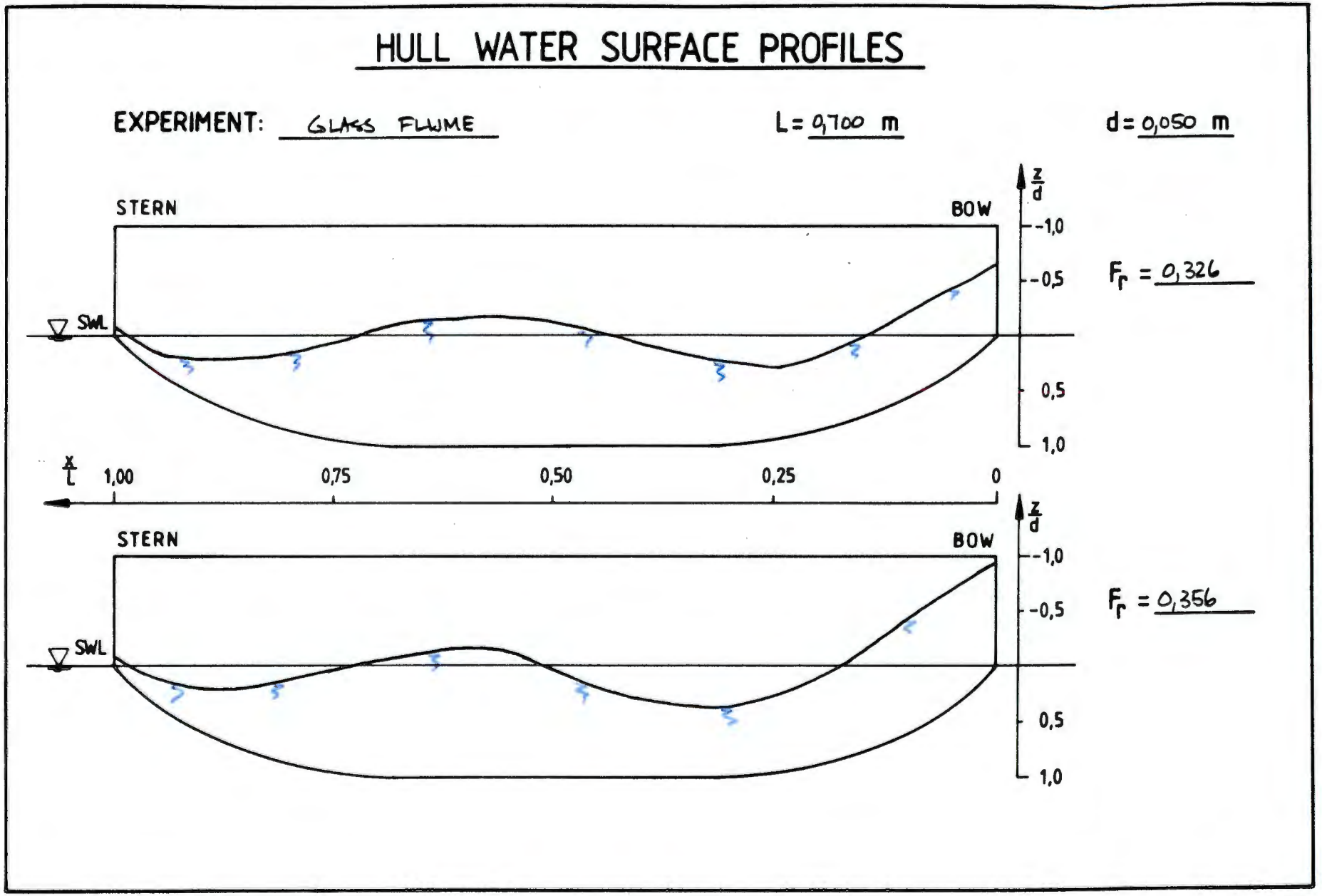

Figure 7.7 Water surface profiles along glass flume model

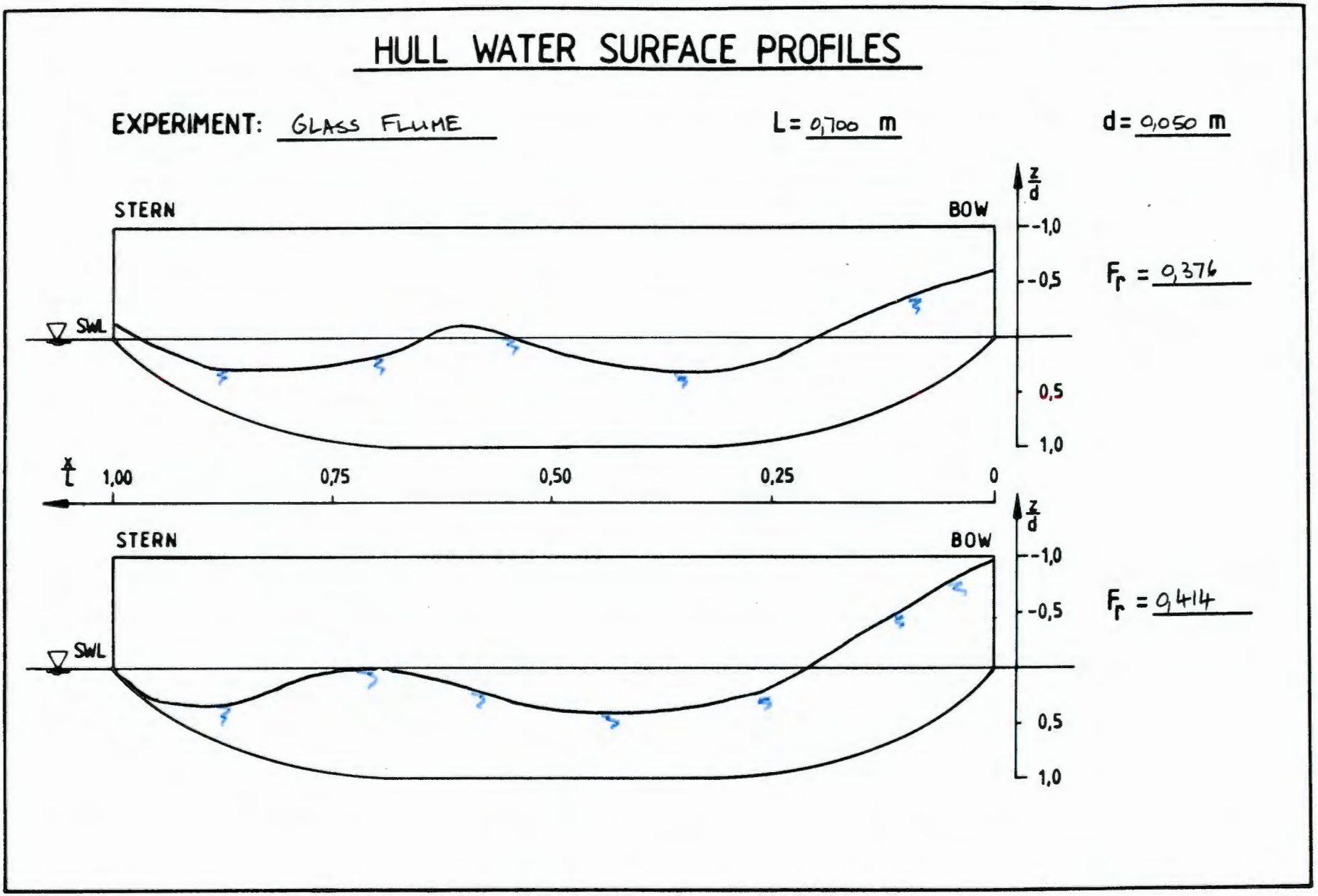

Figure 7.7 Water surface profiles along glass flume model (continued)

7.2 Towing channel experimental results

The total measured resistance of the submerged model with both sets of fins and with one set of fins is presented in Figure 7.8 page 7.10 Also shown is the deduced total resistance of the model without the support fins. The total resistance of the submerged model is equal to twice the total viscous resistance of the surface model as is shown in Figure 7.9 page 7.10. Note that the viscous resistance closely corresponds to the Prandtl-von Karman skin friction line for flat plates at lower speeds but sharply deviates away from the line at higher speeds. The results in Figure 7.9 are presented in dimensionless form against Reynolds number and Froude number in Figure 7.10 and 7.11 respectively (page 7.11). It can be seen that the deviation of the total viscous resistance curve from the Prandtl-von Karman line occurs at Reynolds number of 2×10^6 and Froude number of 0,25.

The total viscous resistance of submerged body of resolution may be calculated using the following equation (ref Blevins 1984)

$$C_V = C_F \left[1 + 1{,}5 \left(\frac{b}{L}\right)^{3/2} + 7 \left(\frac{b}{L}\right)^3\right]$$

valid for $Re_L > 10^5$ and $\frac{L}{b} > 2$

where C_F = resistance coefficient of a flat plate
b = beam at midships
L = total length.

Blevins states that the uncertainty of this equation can be as much as 20%. The measured results of the total resistance coefficient are plotted with the calculated values using the above equation in Figure 7.12 page 7.12. The measured resistance coefficient is lower than the calculated values up to Reynolds number of $2{,}5 \times 10^6$, but sharply increases away from the calculated values at higher Reynolds numbers.

Figure 7.13 page 7.13 shows the resistance coefficient of the model based on frontal area plotted against Reynolds number based on model diameter Re_D . Also shown are the resistance coefficient curves for a sphere and disc (from Vennard 1976), and the resistance coefficient of the submerged model calculated using Blevins' method. The variation in the resistance coefficient of the sphere is due to the size of the wake and the nature of the boundary layer. The resistance coefficient of the disc shows no variation with Reynolds number, as the separation point is fixed regardless of the nature of the boundary layer (i.e. the width of the wake remains constant and, therefore, the resistance coefficient remains constant). Therefore, it seems that the increase in the measured resistance coefficient of the model above Re_D of $2{,}5 \times 10^5$ is due to an increase in the size of the wake.

The measured total resistance of the surface model is shown in Figure 7.14 page 7.14. Also plotted is the total viscous resistance obtained from the submerged model. By subtracting the total viscous resistance from the total resistance, the wave-making resistance of the model can be deduced as shown in Figure 7.14. The deduced wave-making resistance is plotted with the calculated wave-making resistance in Figure 7.14 page 7.14. It is evident that the magnitude of the first few "humps" was too small to be measured. However, there is a fairly good correlation with the one peak shown although the magnitude of the measured value is greater than the calculated value.

Figure 7.16 page 7.15 shows the variation of the total resistance coefficient with Froude number, while Figure 7.17 page 7.15 shows the variation of the wave-making resistance coefficient with Froude number.

The hull water surface profiles for a range of Froude numbers are illustrated in Figure 7.18 on page 7.16 to 7.18, derived from photographs (e.g. Plate 6.12 page 6.15).

University of Cape Town

Consider the case of a body of revolution (such as submarine) rising from being deeply submerged to the surface of a fluid. When the body is deeply submerged it will have viscous resistance and no wave-making resistance, at the surface the body will generate waves and have viscous resistance although the surface area of the body in contact with the fluid has decreased. Figure 7.19 page 7.19 illustrates the resistance variation of the model as it rises through the surface. Notice that the maximum resistance occurs just before the model breaks the surface, i.e. when the model's surface area is still completely wetted and yet near enough to the surface to generate waves.

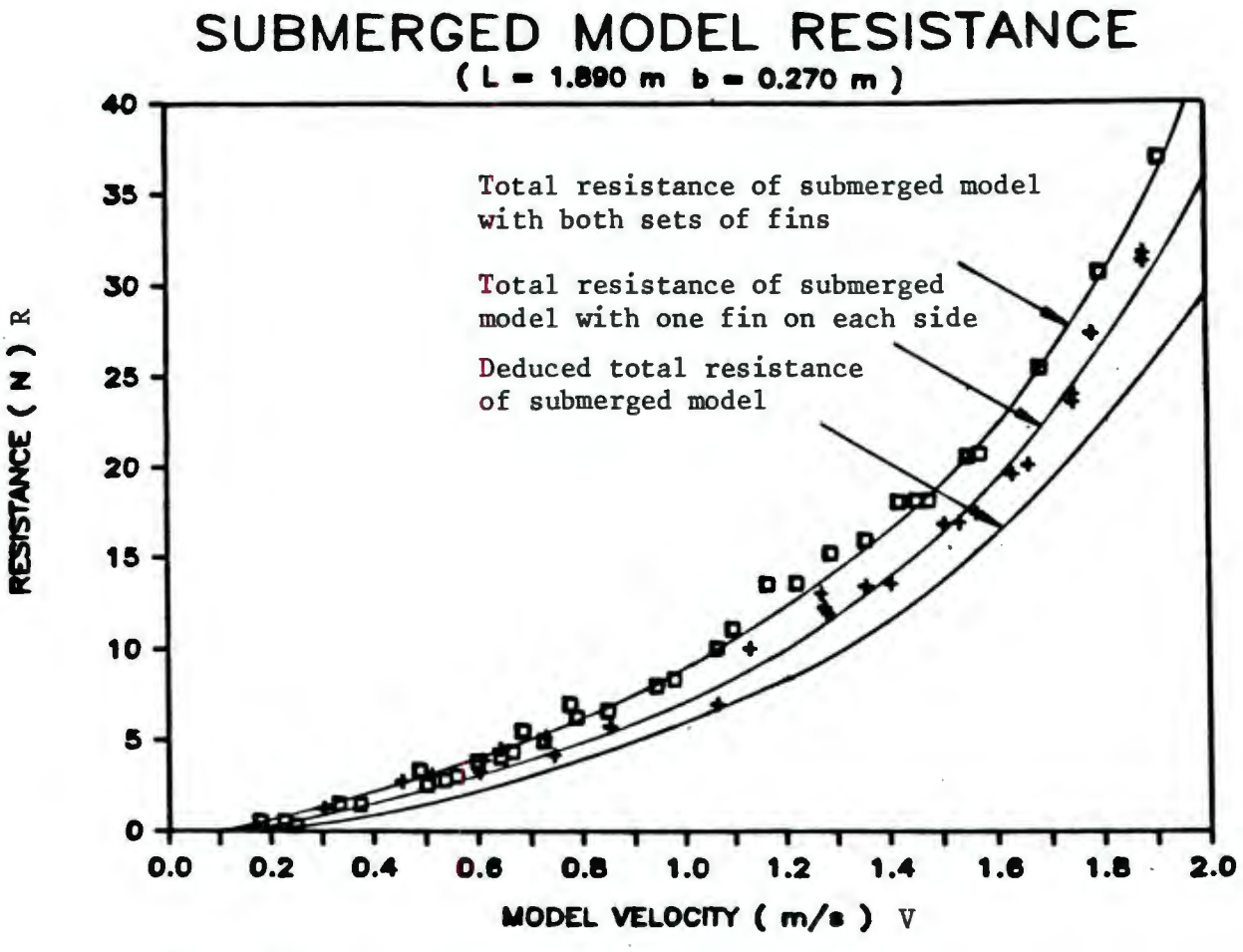

Figure 7.8 Total resistance of submerged model

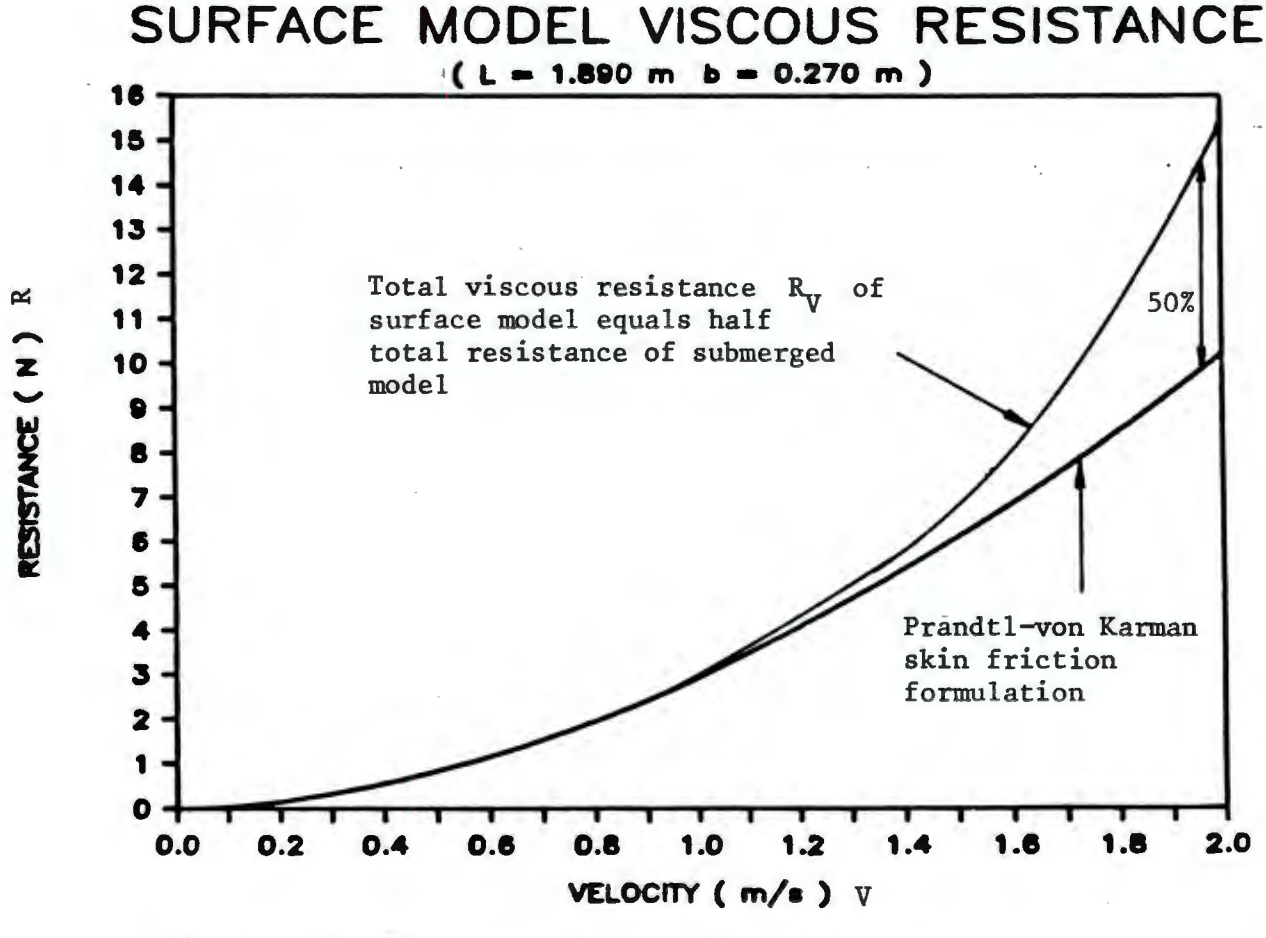

Figure 7.9 Viscous resistance of surface model

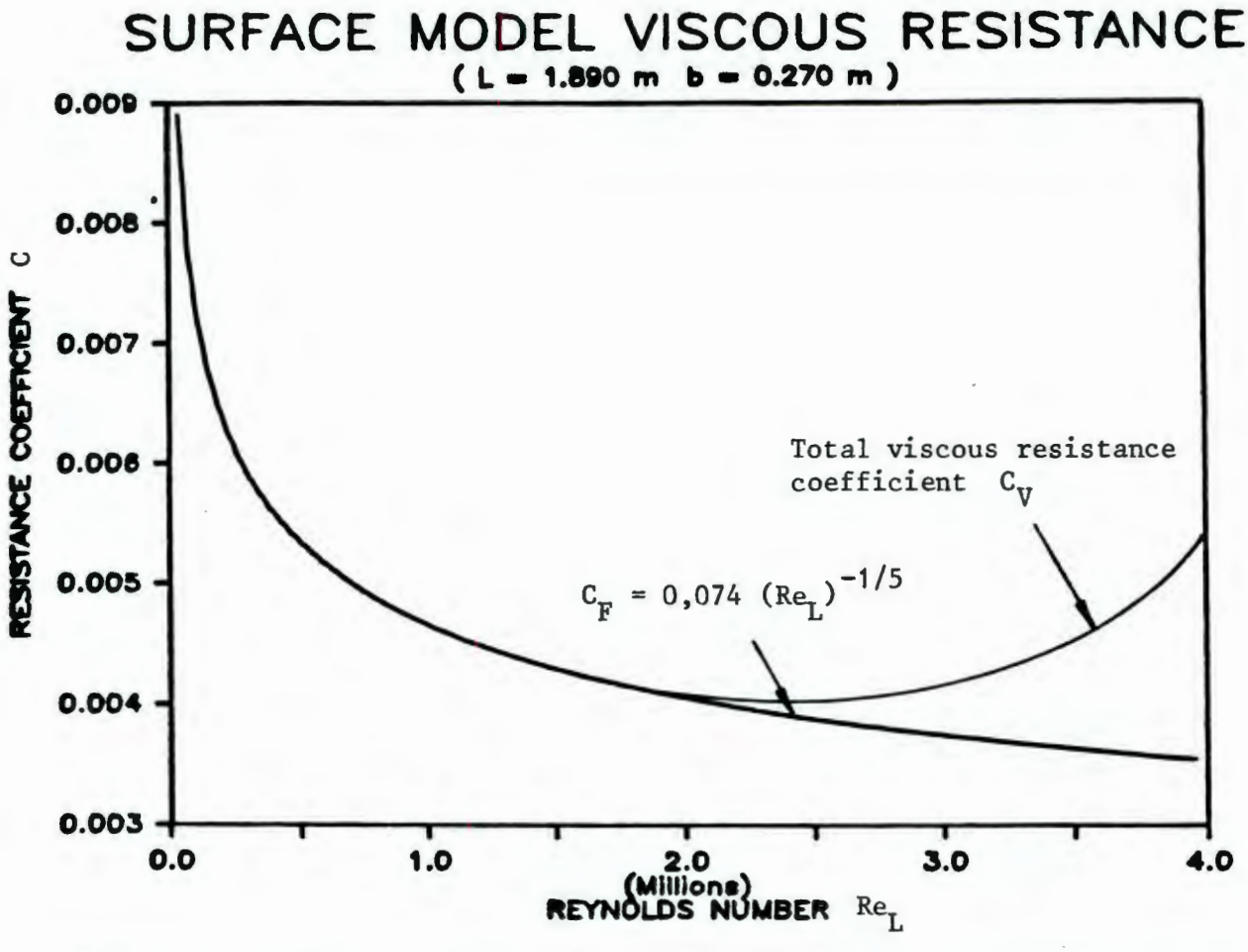

Figure 7.10 Total viscous resistance coefficient versus Reynolds number

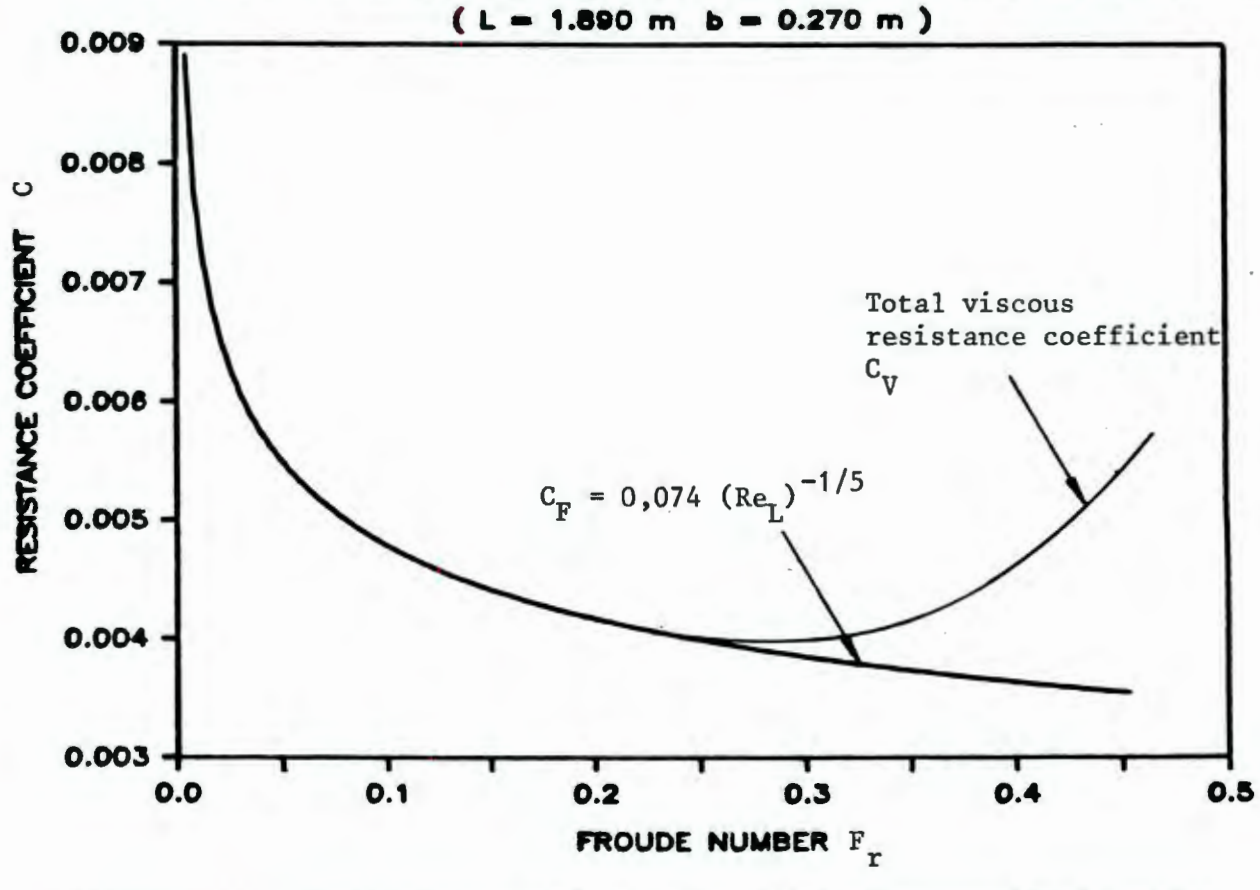

Figure 7.11 Total viscous resistance coefficient versus Froude number

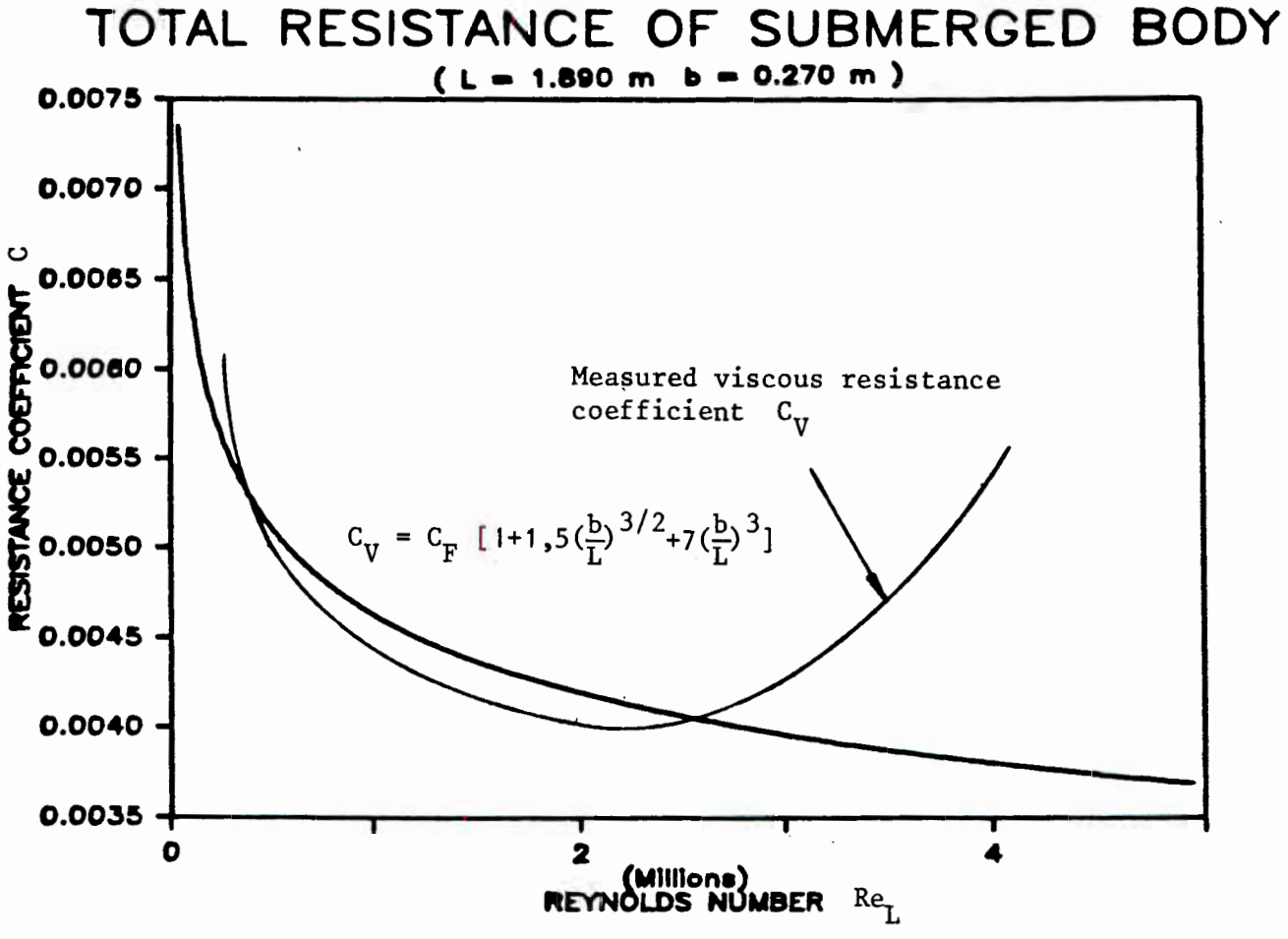

Figure 7.12 Measured C_V versus calculated C_V by Blevins method

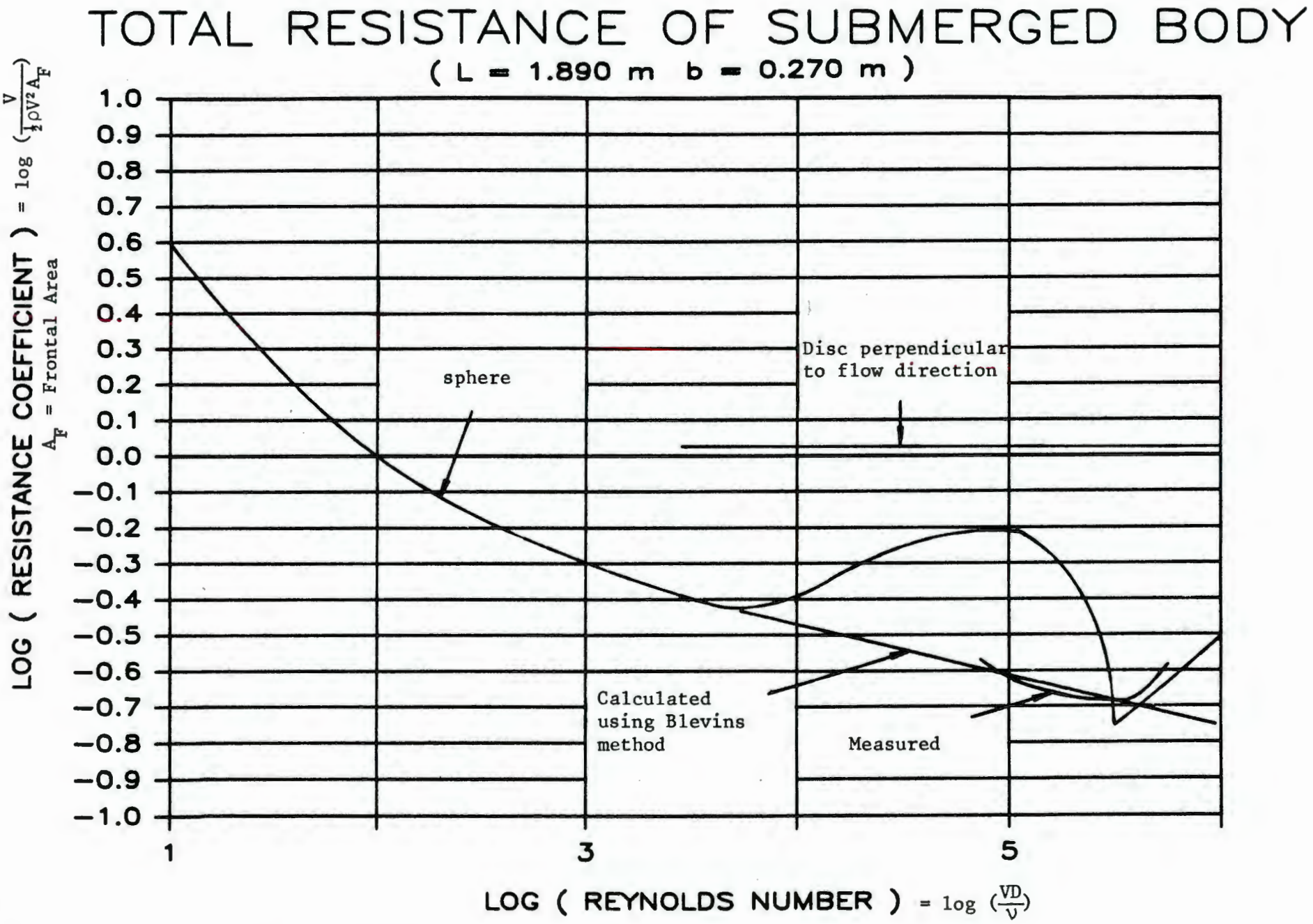

Figure 7.13 Comparison of resistance coefficients of various bodies

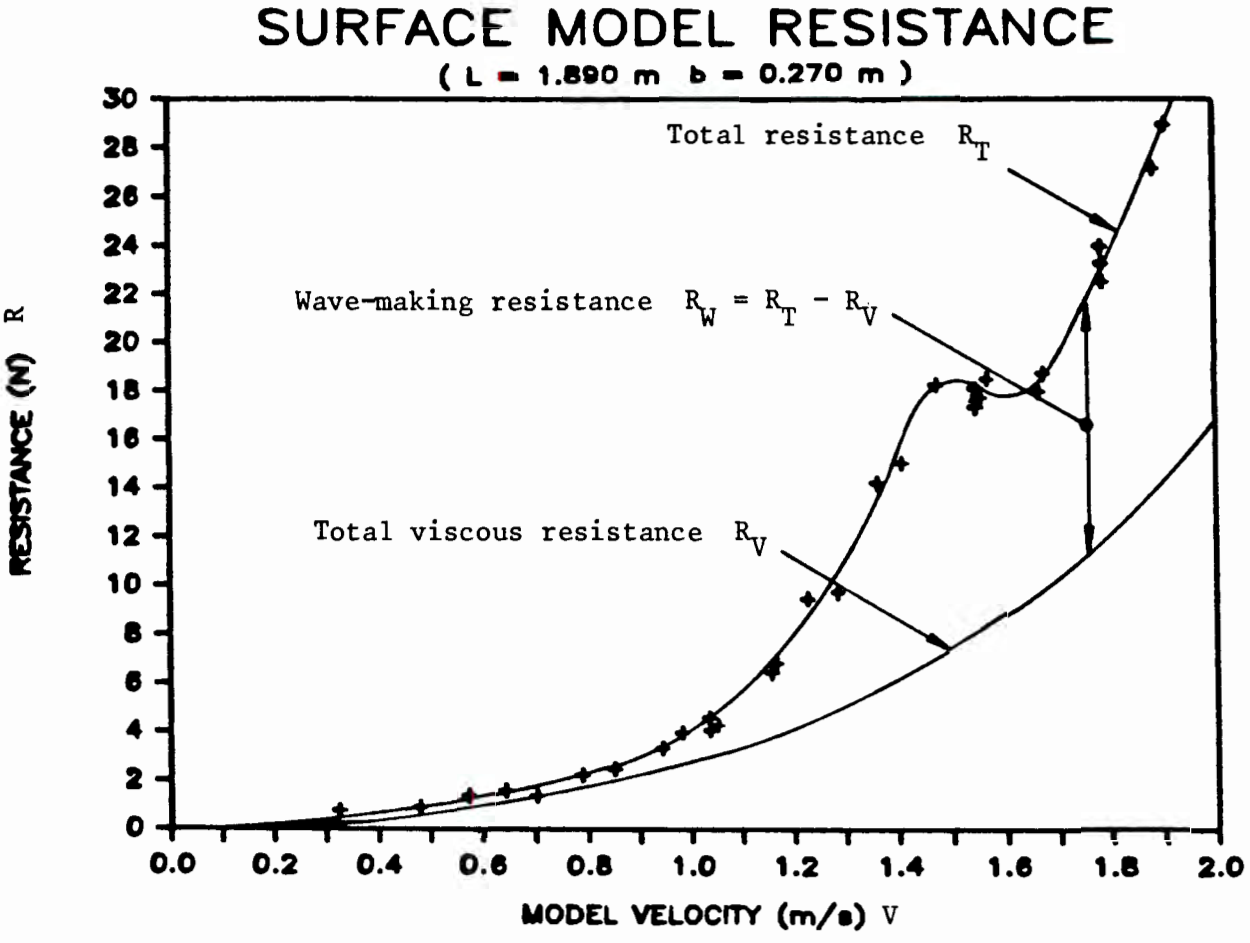

Figure 7.14 Resistance components of surface model

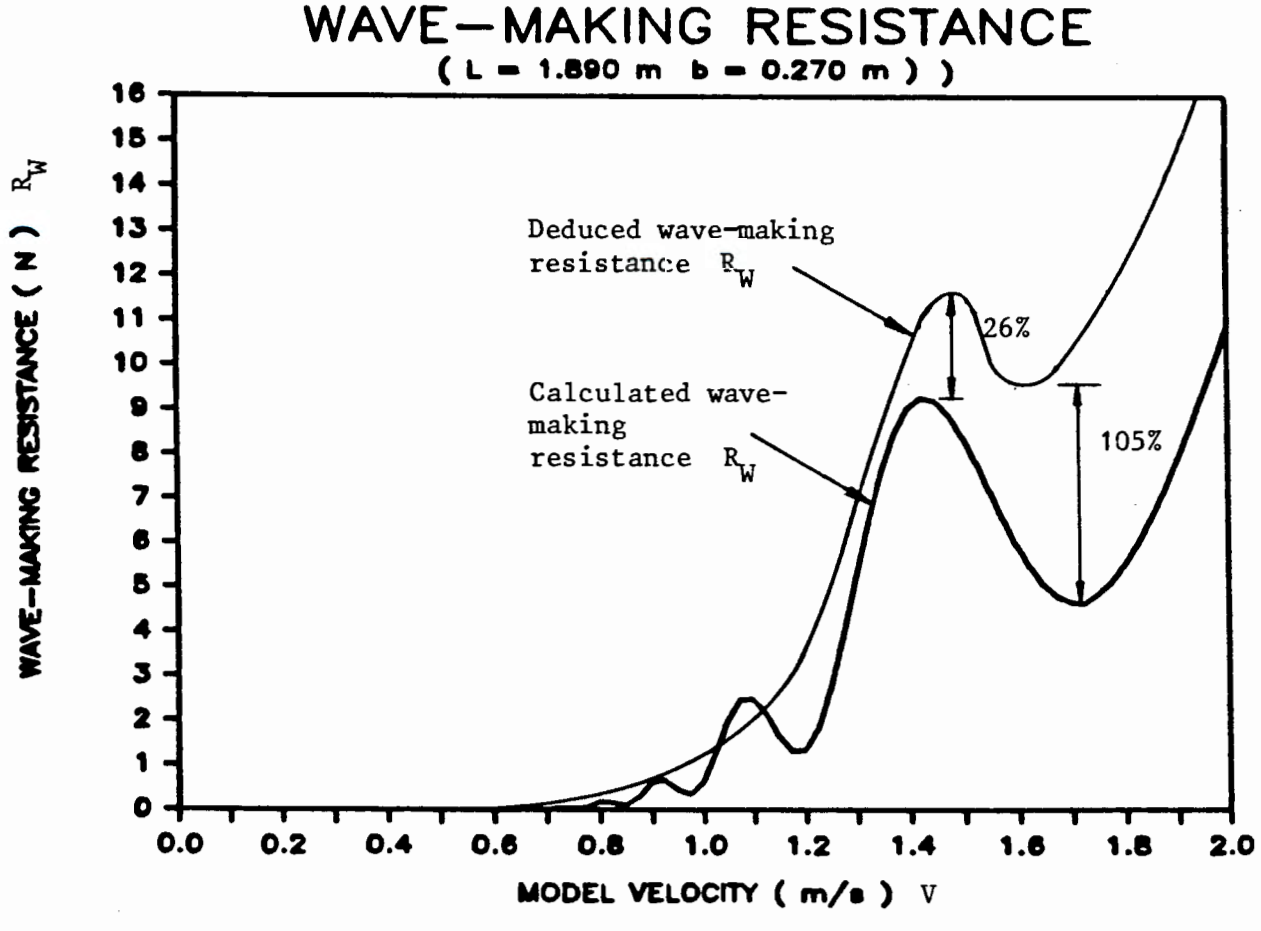

Figure 7.15 Deduced and calculated wave-making resistance

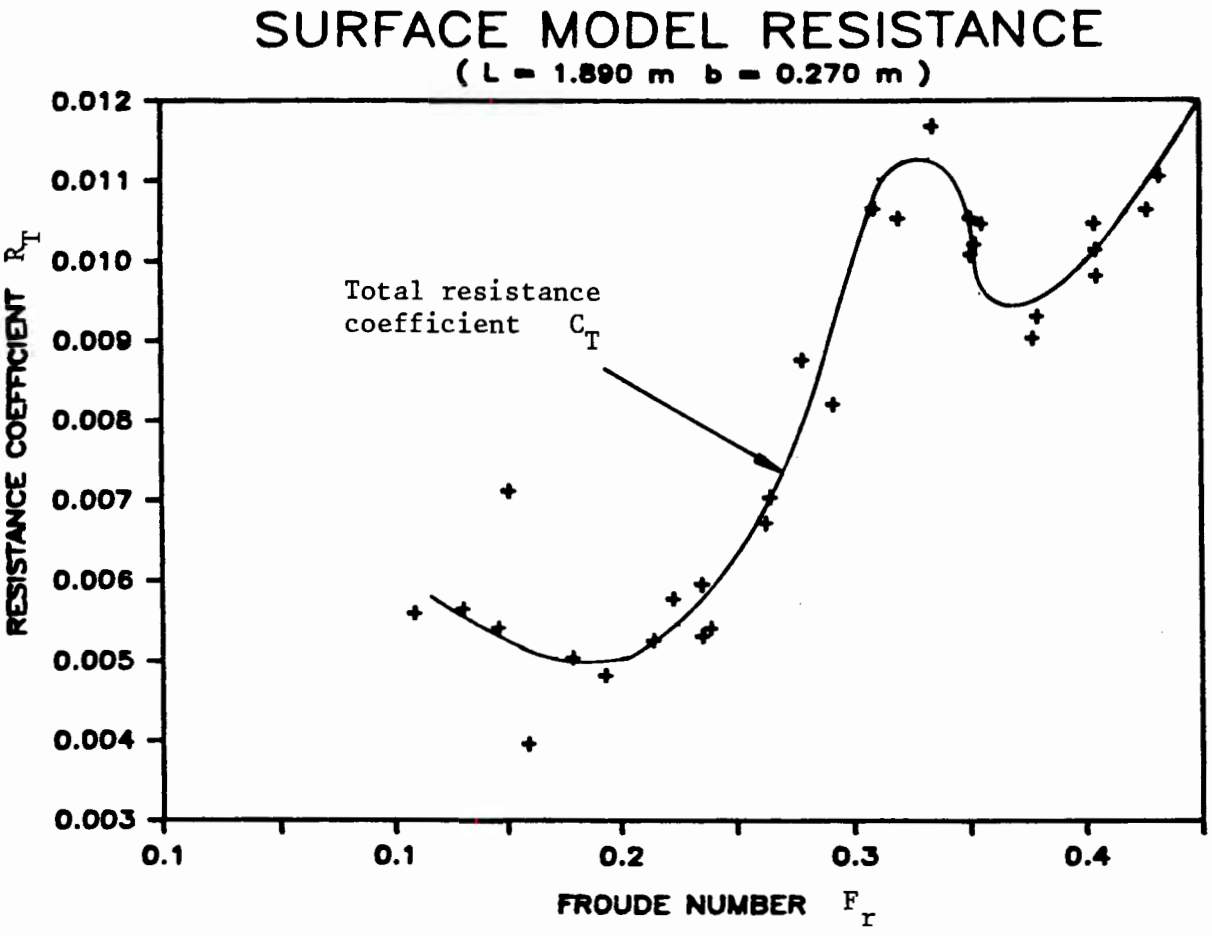

Figure 7.16 Total resistance coefficient curve

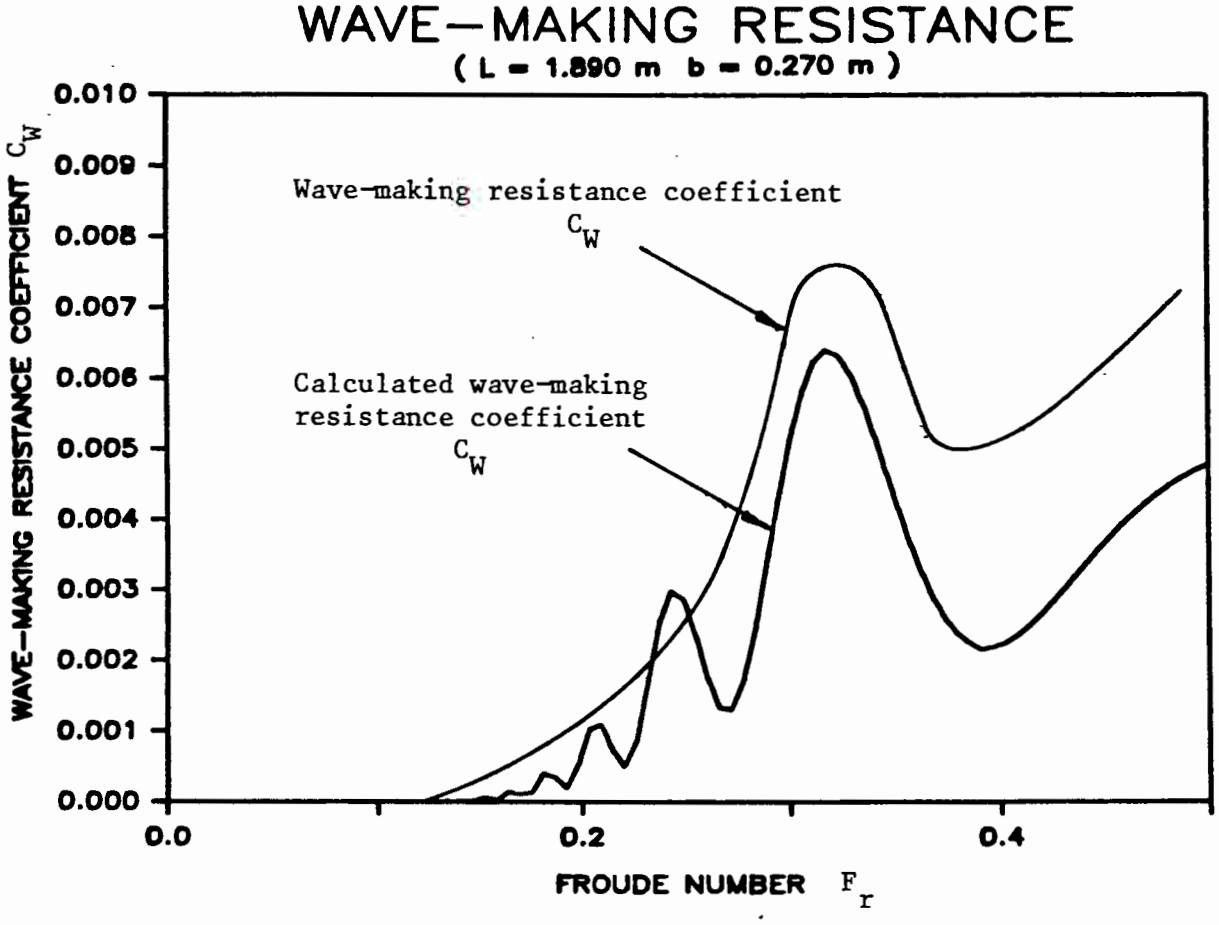

Figure 7.17 Wave-making resistance coefficient curve

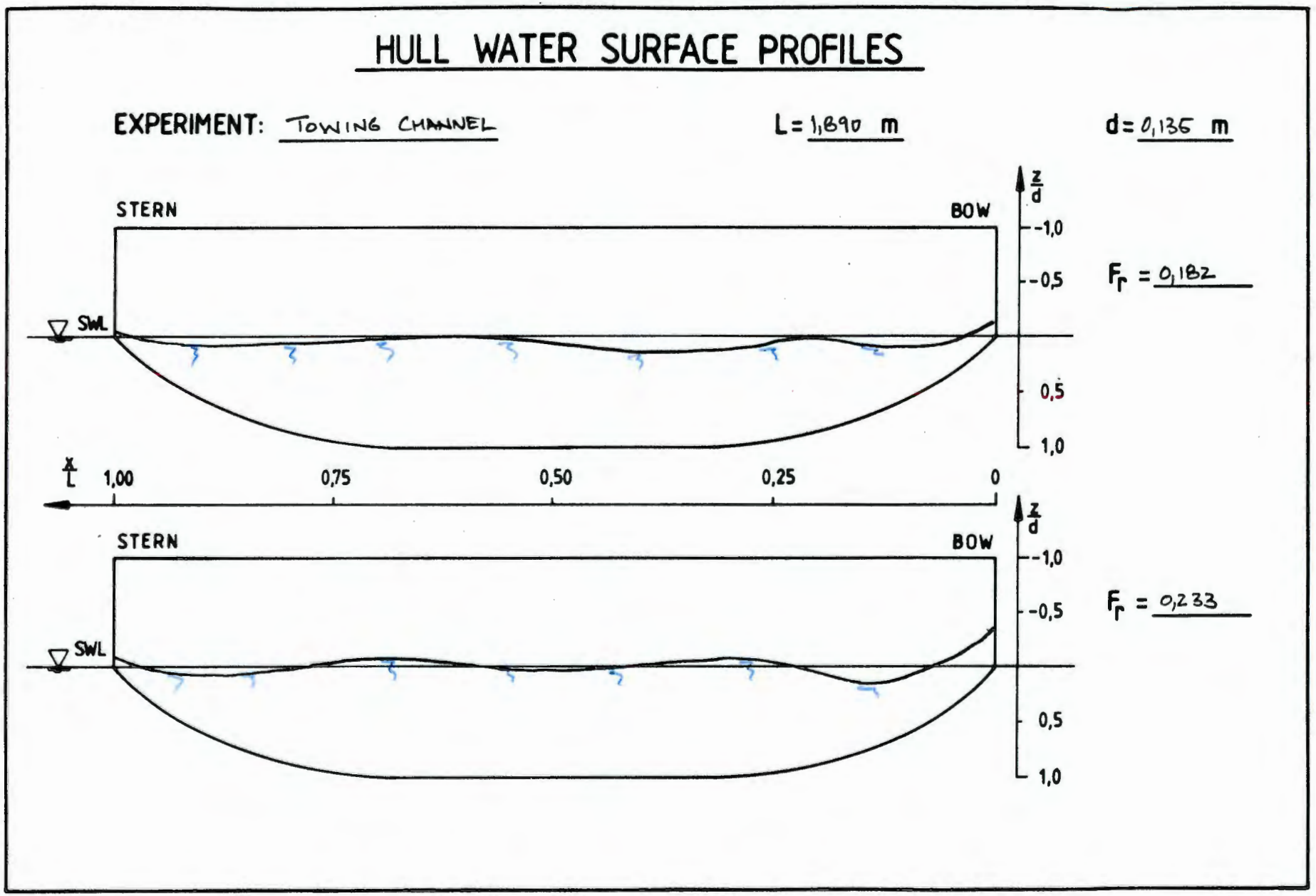

Figure 7.18 Water surface profiles along the hull of the towing channel model

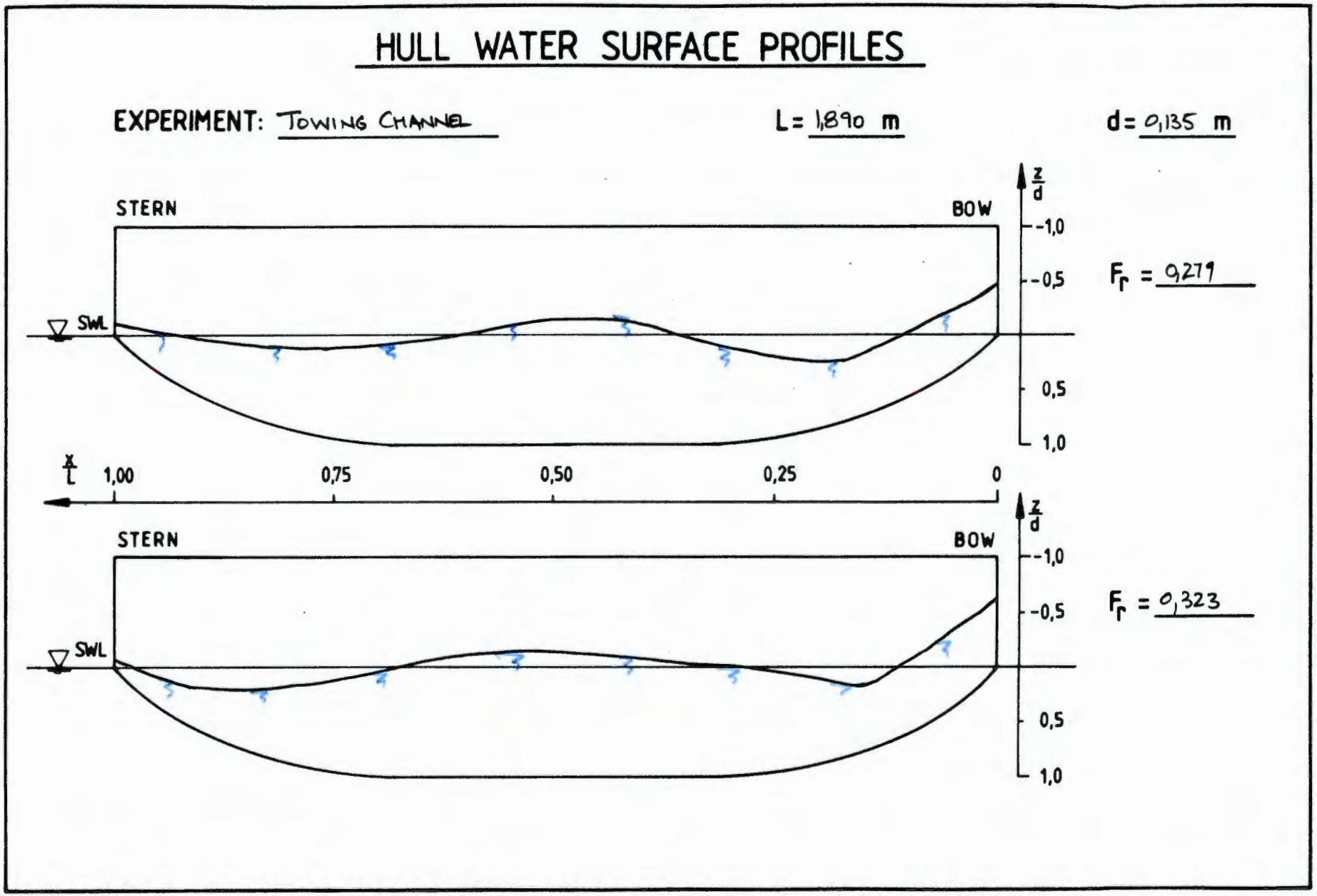

Figure 7.18 Water surface profiles along the hull of the towing channel model (continued)

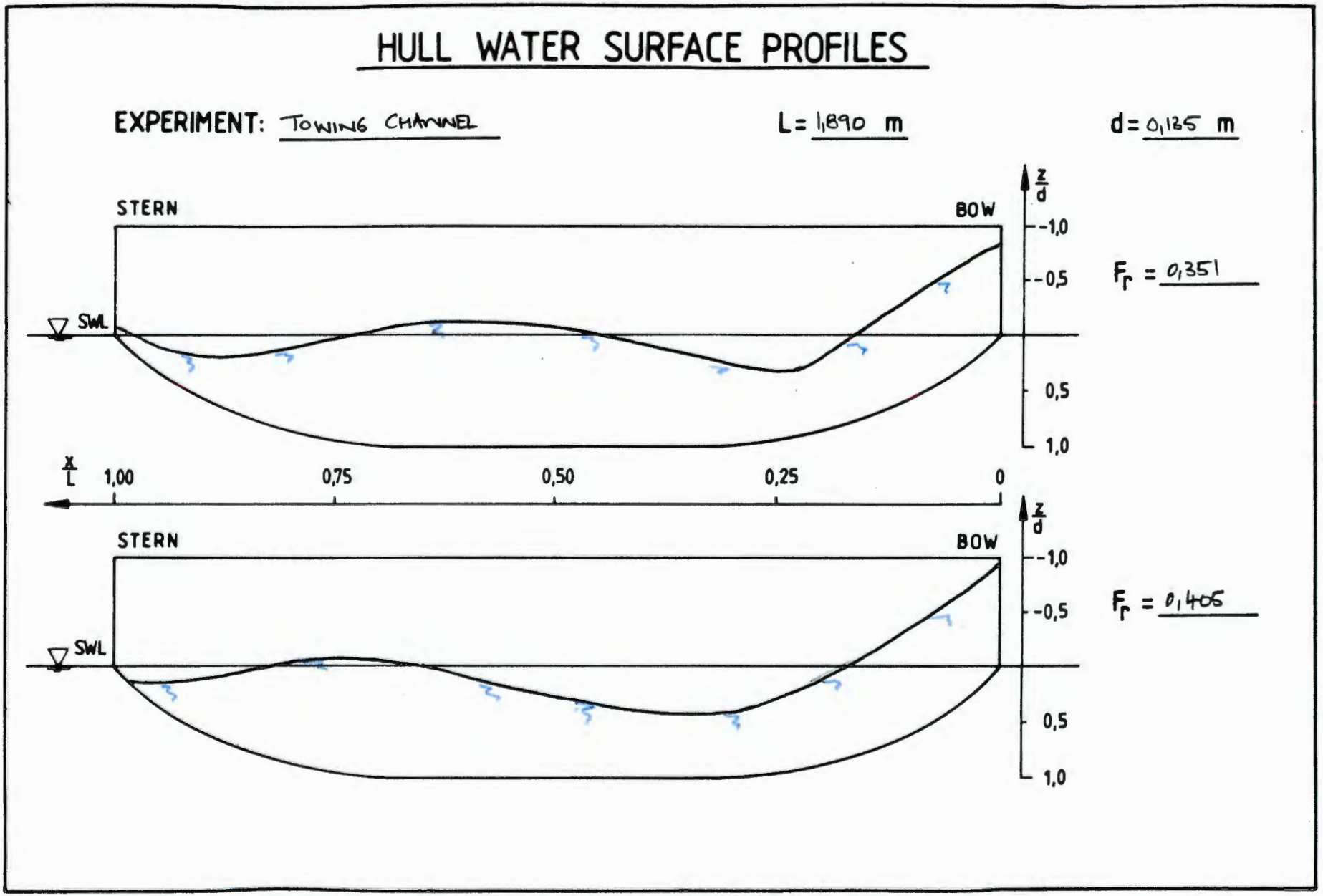

Figure 7.18 Water surface profiles along the hull of the towing channel model (continued)

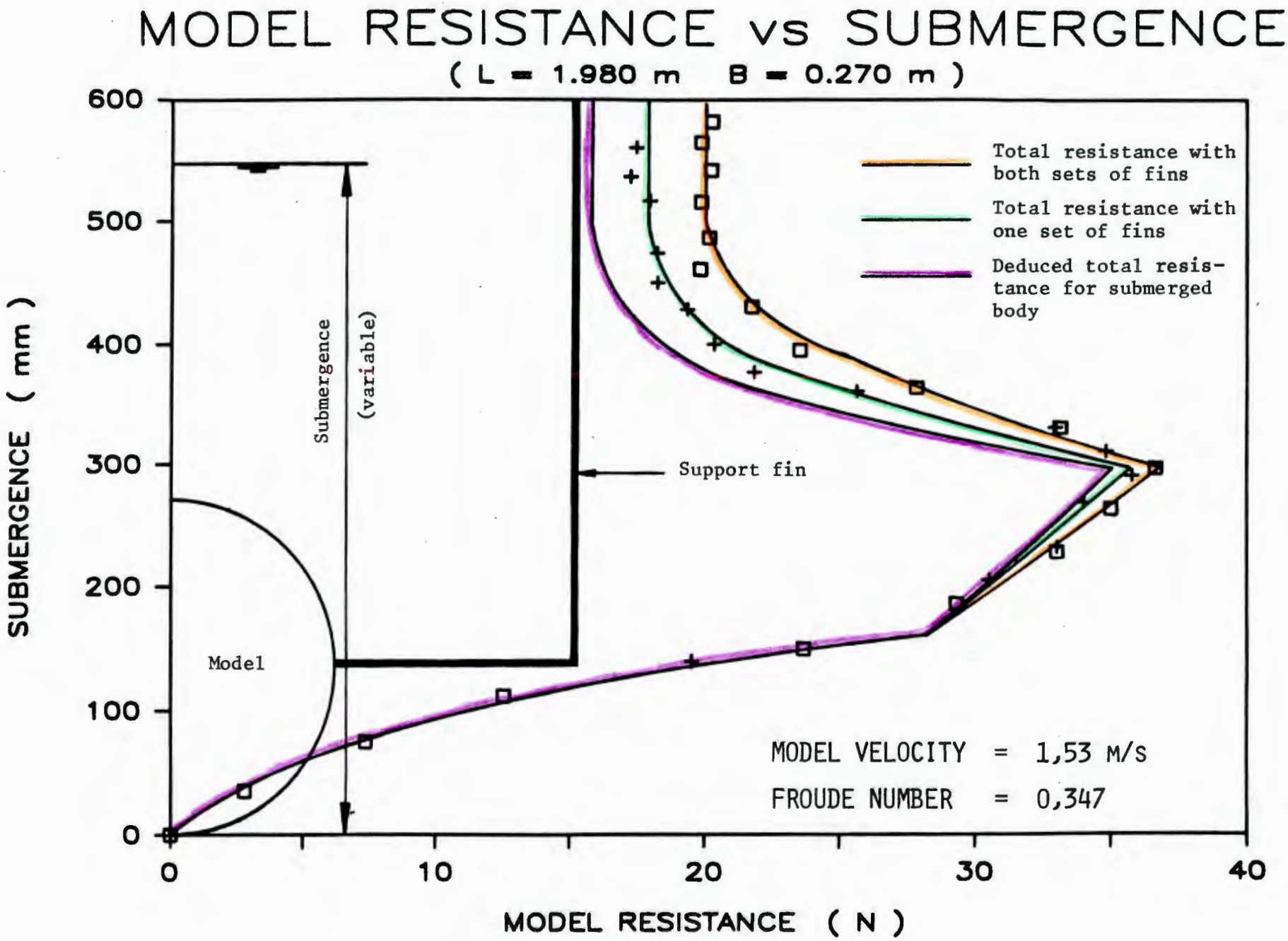

Figure 7.19 Variation of model resistance with submergence

7.2 Comparison between towing channel and glass flume experimental results

Figure 7.20 on page 7.22 shows the residuary resistance coefficient of the models versus Froude number. The residuary resistance has been calculated by subtracting the flat plate skin friction coefficient C_F from the total resistance coefficient C_T. The coefficient C_F has been calculated using the Prandtl-von Karman skin friction formulation. Obviously the agreement is not good, although the larger "hump" appears in both curves at the same Froude number (0,32).

Measurements on the glass flume model indicated that the underkeel clearance of the model only influenced the model's resistance when the clearance was less than the draught of the model. Since the underkeel clearance for both models is at least four times the draught (see Figure 4.3 page 4.5) the clearance cannot be the cause of the disparity in the residuary resistance coefficient curves. Similarly, the side blockage of the towing channel model is slightly greater than the glass flume model and, thus, cannot be the reason that the glass flume model's residuary resistance coefficient is greater than the towing channel model's residuary resistance coefficient. Therefore, the disparity between the two curves seems to be due to the scaling method.

Consider Figure 7.21 on page 7.23 which shows the skin friction coefficient C_S of the glass flume model and the total viscous resistance coefficient C_V of the towing channel model relative to the Prandtl-von Karman skin friction formulation. Since the form of the two models is the same the fact that the glass flume model's skin friction curve leaves the Prandtl-von Karman line much earlier than the towing channel's total viscous resistance curve is peculiar.

The skin friction coefficient curve of the glass flume model levels out at about 0,006. This coefficient corresponds to a roughness of 230 μm. The average surface roughness of the hull measured using a "Tallysurf" machine is 3,5 μm. Thus the deviation of the curve

cannot be due to hull roughness since the hull is "hydraulically" smooth. The effect of the change of wetted area due to the wave profile along the hull was checked at the higher velocities and found to be about 3%. The water surface slope in the flume was also measured and the error in total resistance measurement due to the slope could not be greater than 0,5%. Since the deviation is about 20% it does seem that the cause of the deviation is due to experimental error.

Inspection of Figures 7.5 and 7.8 on pages 7.4 and 7.10 respectively shows that for the glass flume model the deviation occurs at 0,6 m/s and for the towing channel model at 1 m/s. Since the geometric ratios of the models are 2,7 to 1 the ratio of these velocities would be expected to be in the ratio 2,7 to 1 if the effect was dependent on Reynolds number. The Froude number for each model for the above velocities is 0,23. Thus it appears that the break-away from the flat plate skin friction formulation is dependent on the wave profile along the model hull.

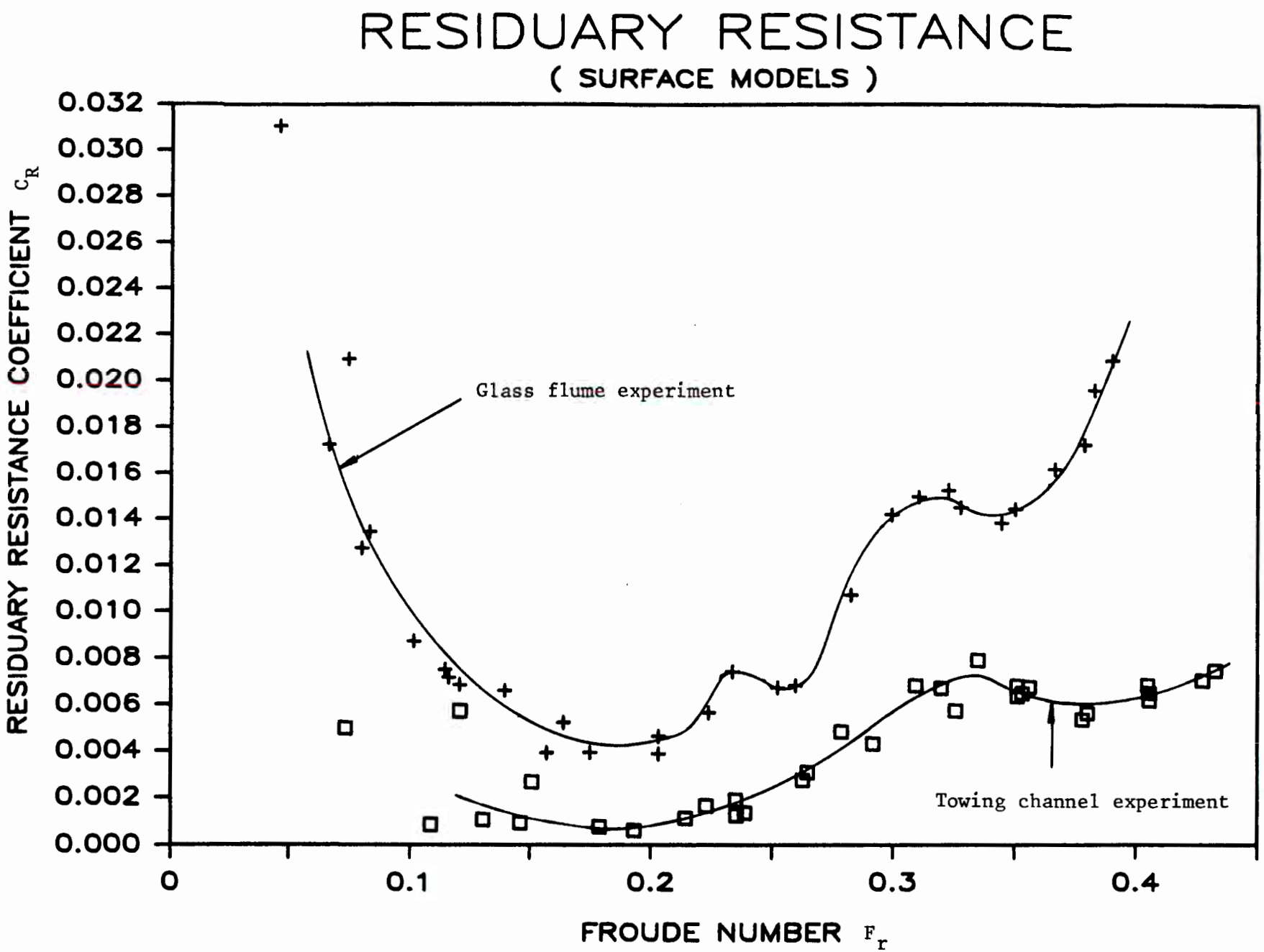

Figure 7.20 Residuary resistance of surface models versus Froude number

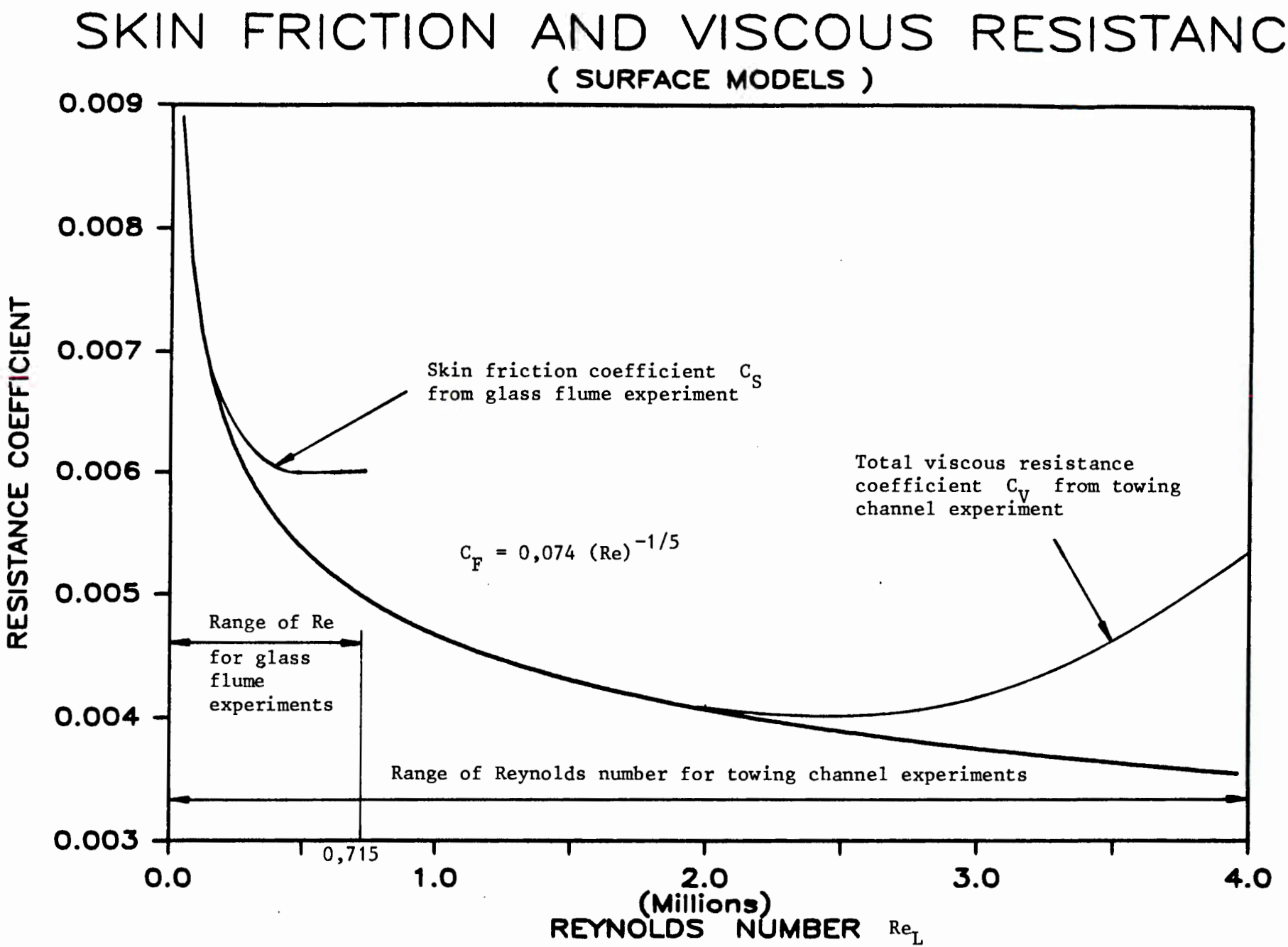

Figure 7.21 Skin friction and viscous resistance of surface models

CHAPTER 8

CONCLUSIONS

The deduced skin friction of the glass flume model deviated from the Prandtl-von Karman skin friction formulation for flat plates. This is probably due to the fact that the local fluid speeds around the hull are increased due to the form of the hull, resulting in a higher skin friction than would be measured on a flat plate. In the experimental work this deviation was found to occur at Froude number of 0,23 for both the models, indicating that the onset of the deviation from Prandtl-von Karman formulation is dependent on the wave-profile along the model hull.

The measured total viscous resistance of the towing channel model shows a marked increase in the viscous resistance coefficient at Reynolds numbers greater than 3×10^6. Thus the viscous pressure resistance seems to be significant and should, therefore, be included in the component of resistance that is scaled using Reynolds number scaling.

To circumvent the joint problems of obtaining the skin friction and viscous pressure resistance (i.e. the total viscous resistance) of a model, the total viscous resistance of reflex model could be measured. This would entail additional expense during model testing as two models would have to be made, but the rewards of predicting the power requirement of a ship more accurately should justify the additional cost.

BIBLIOGRAPHY

Allan, J.F., Conn, J.F.C., 1950
"Effect of laminar flow on ship models"
Royal Institution of Naval Architects, Vol 92

Batchelor, G.K., 1977
"An introduction to fluid dynamics"
Cambridge: Cambridge University Press

Betts, P.L., Binnie, A.M., 1966
"Some experiments on ship models held in a small open water-channel with slotted walls"
Royal Institution of Naval Architects, Vol 108

Bellhouse, B.J., Shultz, D.L., 1966
"Determination of mean and dynamic skin friction, separation and transition in low speed flow with a thin film heated element"
Journal of Fluid Mechanics, Vol 24, part II

Blevins, R.D., 1984
"Applied fluid dynamics handbook"
New York: Van Nostrand Reinhold

Cole, A.J., Millward, A., 1977
"The measurement of skin friction on a planning hull using a miniature Preston tube"
Royal Institution of Naval Architects, Vol 119

Comstock, J.P., 1980
"Principles of naval architecture"
New York: Society of Naval Architects and Marine Engineers

University of Cape Town

Daugherty, R.L., Franzini, J.B., 1977
"Fluid mechanics with engineering applications", 7th edition
Tokyo: McGraw-Hill

Davies, P.O.A.L., Kimber, G.R., 1976
"Skin friction measurement with a heated film"
Sixth thermodynamics and fluid mechanics convention
London: Institution of Mechanical Engineering Conference Publications

Emrich, R.J., 1981
"Methods of experimental physics: fluid dynamics"
New York: Academic Press

Francis, J.R.D., 1975
"Fluid mechanics for engineering students", 4th edition
London: Edward Arnold

Froude, W., 1872
"Experiments on the surface friction experienced by a plane moving through water"
British Association for the Advancement of Science

Froude, W., 1874
"On experiments with H.M.S. Greyhound"
Institution of Naval Architects, Vol 16

Froude, W., 1874
"Experiments for the determination of the frictional resistance of water on a surface under various conditions"
British Association for the Advancement of Science

University of Cape Town

Froude, W., 1874
"Experiments in relation to the pressure-log, with a description of the apparatus employed"
British Association for the Advancement of Science

Froude, W., 1877
"Experiments upon the effect produced on the wave-making resistance of ships by length of parallel midbody"
Institution of Naval Architects, Vol 19

Froude, R.E., 1881
"On the leading phenomena of the wave-making resistance of ships"
Institution of Naval Architects, Vol 23

Froude, R.E., 1888
"On the 'constant' system of notation of results of experiments on models used at the Admiralty experiment works"
Institution of Naval Architects, Vol 30

Gillmer, T.C., 1975
"Modern ship design", 2nd edition
Annapolis: Naval Institution Press

Goldstein, R.J., 1983
"Fluid mechanics measurements"
New York: Hemisphere

Havelock, T.H., 1924
"Wave patterns and wave resistance"
Royal Institution of Naval Architects, Vol 66

Head, M.R., Rechenberg, I., 1962
"The Preston tube as a means of measuring skin friction"
Journal of Fluid Mechanics, Vol 14, Part 1

Hughes, G., 1966
"An analysis of ship model resistance into viscous and wave components"
Parts I and II
Royal Institution of Naval Architects, Vol 108

Hughes, G., 1967
"An analysis of ship model resistance into viscous and wave components"
Part III
Royal Institution of Naval Architects, Vol 109

Hughes, W.F., Brighton, J.A., 1967
"Theory and problems of fluid dynamics"
New York: Schaum

Inui, T., 1962
"Wave-making resistance of ships"
Society of Naval Architects and Marine Engineers

Keith, H.D., 1957
"Simplified theory of ship waves"
American Journal of Physics, Vol 25

Kent, J.L., 1958
"Ships in rough water"
London: Thoman Nelson

University of Cape Town

Kilner, F.A., 1983
"Boundary layers on plates"
CE 540 course notes, Department of Civil Engineering, U.C.T.

Kwang, J.B., McCarthy, J.H., 1979
"Ship wave-resistance computations"
Maryland: David Taylor Naval Ship Research and Development Centre

Lackenby, H., 1962
"Resistance of ships with special reference to skin friction and hull surface condition"
Institution of Mechanical Engineers

Lackenby, H., 1965
"An investigation into the nature and interdependence of the components of ship resistance"
Royal Institution of Naval Architects, Vol 107

Landweber, L., Patel, V.C., 1979
"Ship boundary layers"
Annual Review of Fluid Mechanics

Larson, L., 1977
"An experimental investigation of the three-dimensional turbulent boundary layer on a ship model"
Institution of Mechanical Engineers

Manning, G.C., 1930
"Manual of Naval Architecture"
New York: Van Nostrand

University of Cape Town

Matheson, N., Joubert, D.N., 1973
"Experimental determination of the components of resistance of a small 0,80 C_B tanker model"
Journal of Ship Research, Vol 17

Matheson, N., Joubert, P.N., 1974
"A note on the resistance of bodies of revolution and ship forms"
Journal of Ship Research, Vol 18

McCarthy, J.H., Power, J.L., Huang, T.T., 1977
"The roles of transition, laminar separation and turbulence stimulation in the analysis of axisymmetric body drag"
Institution of Mechanical Engineers

Millward, A., 1981
"The effect of shallow water of the resistance of a ship at high sub-critical and super-critical speeds"
Royal Institution of Naval Architects, Vol 123

Millward, A., 1982
"Shallow water and channel effects on ship wave resistance at high sub-critical and super-critical speeds"
Royal Institution of Naval Architects, Vol 124

Miyata, H., Inui, T., 1984
"Non-linear ship waves"
Advances in Applied Mechanics, Vol 24

Muckle, W., 1975
"Naval Architecture for Marine Engineers"
London: Newnes-Butterworths

Patel, V.C., 1965
"Calibration of the Preston tube and limitations on its use in pressure gradients"
Journal of Fluid Mechanics, Vol 23, part I

Paterson, A.J.C., 1986
"The analysis of ship wave resistance using close range photogrammetry"
MSc Dissertation, U.C.T.

Pope, R.J., Bellhouse, B.J., 1971
"Measurement of local skin friction on ship models using thin film probes"
Royal Institution of Naval Architects, Vol 113

Potter, C.P., Foss, J.F., 1975
"Fluid Mechanics"
New York: John Wiley

Preston, J.H., 1958
"The minimum Reynolds number for a turbulent boundary layer and the selection of a transition device"
Journal of Fluid Mechanics, Vol 3, Part IV

Rabl, S.S., 1942
"Practical principles of naval architecture"
New York: Cornell Maritime Press

Rosenhead, L., 1963
"Laminar boundary layers"
Oxford: Clarendon Press

University of Cape Town

Rossel, H.E., Chapman, L.B., 1941
"Principles of Naval Architecture"
New York: Society of Naval Architects and Marine Engineers

Saunders, H.E., 1972
"Hydrodynamics in ship design" Vol 1 and 2
New York: Society of Naval Architects and Marine Engineers

Schlichting, H., 1968
"Boundary layer theory" 7th edition
New York: McGraw-Hill

Shearer, J.R., Cross, J.J., 1965
"The experimental determination of the components of ship resistance for a mathematical model"
Royal Institution of Naval Architecture, Vol 107

Shearer, J.R., Steele, B.N., 1970
"Some aspects of the resistance of full form ships"
Royal Institution of Naval Architecture, Vol 112

Sorensen, R.M., 1973
"Ship generated waves"
Advances in Hydroscience, Vol 9

Steele, B.N., Pearce, G.B., 1968
"Experimental determination of the distribution of skin friction on a model of a high speed liner"
Royal Institution of Naval Architecture, Vol 110

Streeter, V.L., 1961
"Handbook of fluid dynamics"
New York: McGraw-Hill

Todd, F.H., 1966
"Viscous resistance of ships"
Advances in Hydroscience, Vol 3

Townsin, R.L., 1971
"The viscous drag of a 'Victory' model - results from wake and wave pattern measurements"
Royal Institution of Naval Architects, Vol 113

Tulin, M.P., 1951
"The separation of viscous drag and wave drag by means of the wake survey"
Washington: David Taylor Model Basin report 772

Vennard, J.K., Street, R.L., 1976
"Elementary fluid mechanics"
New York: John Wiley

Wehansen, J.V., 1973
"The wave resistance of ships"
Advances in Applied Mechanics, Vol 13

APPENDIX A

EXAMINATIONS WRITTEN BY THE AUTHOR TO COMPLETE THE REQUIREMENTS OF THE DEGREE

Examination		Credit rating
CE5B17	Finite Element Analysis (July 1985)	4
P.O.1a	Physical Oceanography 1a (July 1985)	5
P.O.1b	Physical Oceanography 1b (November 1985)	5
CIV519X	Advanced Hydraulic Structures (November 1985)	5
CIV516F	Coastal Hydraulics (July 1986)	5
Thesis:	"An experimental investigation into the components of ship resistance"	20
	TOTAL	44
	Credit requirements for degree	40

UNIVERSITY OF CAPE TOWN

DEPARTMENT OF CIVIL ENGINEERING

FINAL EXAM. MONDAY, 24 JUNE 1985

CE 5B17 : FINITE ELEMENT ANALYSIS

TIME : 3 hours

Note:

The student may refer to class notes and assignments.

1. The diagram shows half a plane symmetric frame structure, which is to be modelled using 5 elements.

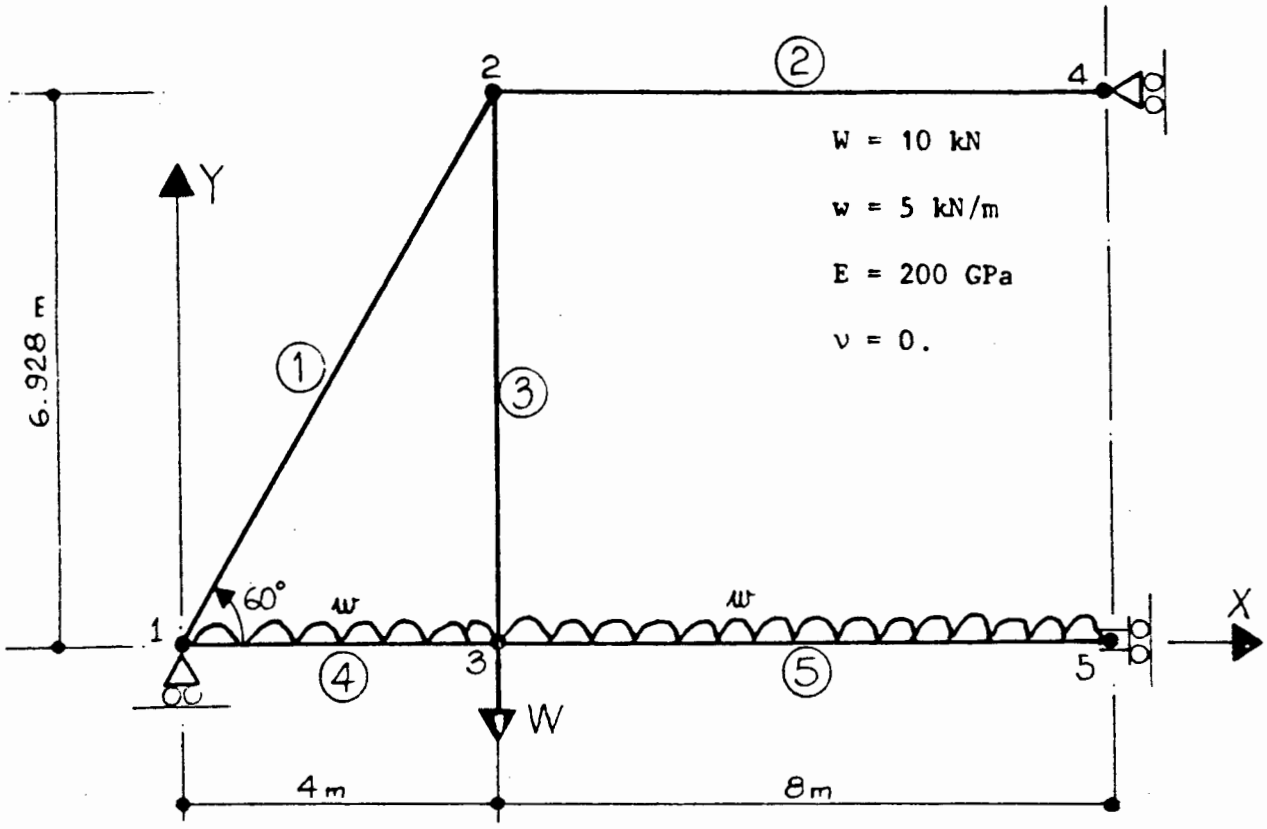

Element 1,2 : linear bar ; $A = 5000\ mm^2$

3 : Bernoulli-Euler beam ; $A = 30000\ mm^2$

$I = 50 \times 10^6\ mm^4$

4,5 : linear Timoshenko beam ; $A = 125000\ mm^2$

$I = 2600 \times 10^6\ mm^4$

$\alpha = 1.2$

(i) Compute the <u>global</u> element stiffness matrices for elements 1, 3 and 4 .

(20)

(ii) Comment <u>briefly</u> on the relative stiffnesses contained in these element matrices.

(3)

(iii) Assemble elements 1 and 4 <u>only</u> into the global system stiffness matrix; show only what is necessary, i.e. nodes 1, 2 and 3 .

(5)

(iv) Compute the global system load vector.

(5)

(v) Assume the following displacement solution (mm and rads) :

Node	u	v	θ
1	0.010	0.	-1.0×10^{-6}
3	0.012	-0.001	-0.5×10^{-6}

Using this solution compute the shear force and bending diagrams for element 4 .

(12)

2. A 5-noded quadrilateral plane stress element is shown below. Side 2-5-3 is curved.

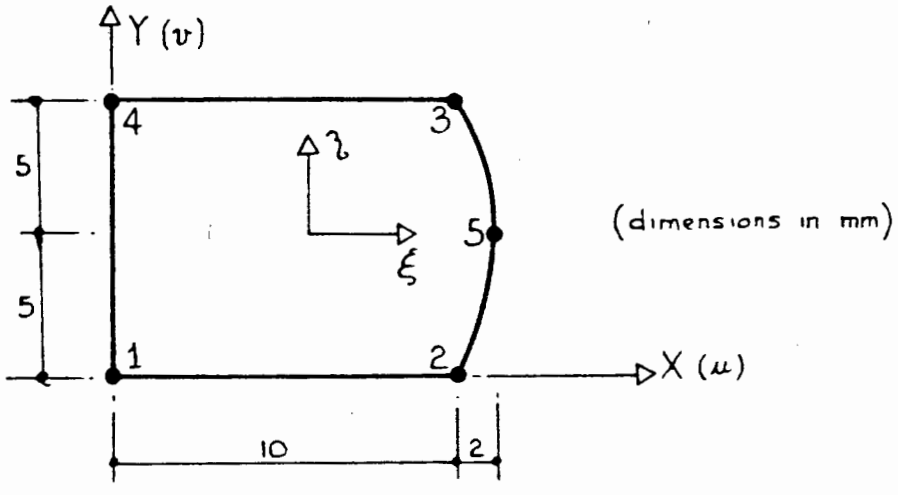

(i) Show that the Jacobian matrix for this element is :

$$J_{11} = 6 - \eta^2 \qquad J_{12} = 0$$

$$J_{21} = -2\eta(1 + \xi) \qquad J_{22} = 5$$

(10)

(ii) For a thickness $t = 1$ mm , compute the volume of the element using exact numerical integration.

(5)

(iii) Show that the normal strain along the side 3-4 is a constant with magnitude

$$\varepsilon_{xx} = 0.1\ (u_3 - u_4)$$

(10)

Note: You may request the element shape functions if you do not have them in your notes.

3. A parabolic shear load is applied across the edges of two 8-node quadrilateral elements as shown in the diagram.

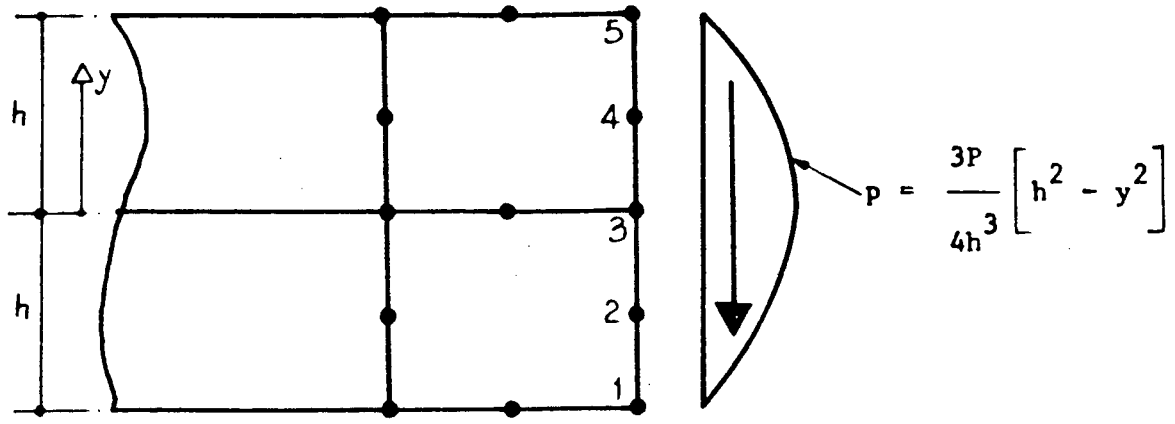

Show that the equivalent nodal load at node 3 is (11/40)P .

(15)

4. A 4-node quadrilateral element and a 2-node bar element together support a point load P = 6000N . Nodes 1, 3 and 4 are fully restrained, and node 2 can only move horizontally.

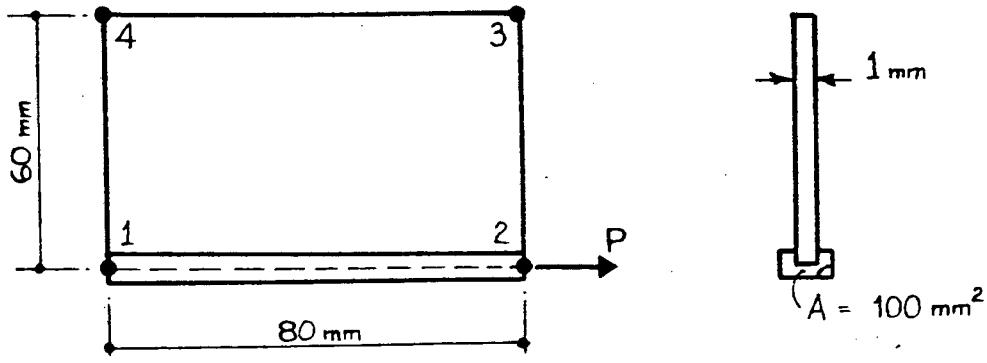

The following additional information is given :

$$\frac{\partial N_2}{\partial x} = \frac{1}{16}(1-\eta) \quad ; \quad \frac{\partial N_2}{\partial y} = -\frac{1}{12}(1+\xi)$$

$$\underset{\sim}{J} = \begin{bmatrix} 4 & 0 \\ 0 & 3 \end{bmatrix} \quad ; \quad E = 300 \text{ GPa} \; ; \quad \nu = 0.3$$

Compute the horizontal displacement at node 2.

(15)

UNIVERSITY OF CAPE TOWN

DEPARTMENT OF PHYSICAL OCEANOGRAPHY

Physical Oceanography 1b
November 1985

Time : 3 Hours
Answer ALL questions in Section A (40 marks)
and THREE whole questions from Section B

Total : 100 marks

SECTION A

Short questions. Answer ALL questions in this section.

1. Discuss the concept of a level surface and its relation to the local vertical, explaining the nature of the various contributing phenomena.

2. Explain the quasi-static approximation in the vertical balance of forces in ocean dynamics.

3. What quantity provides a contrast between the following curved currents; the South Atlantic gyre, inertial oscillations, and whirls in river flows.

4. Discuss the horizontal divergence of a geostrophic flow with particular emphasis on the relevance of the beta effect.

5. Explain what is meant by a dispersive wave. Is the Kelvin wave dispersive?

6. What is an amphidromic point?

7. Explain how wave energy can be concentrated at particular points on a coastline.

8. Explain how stratification can restrict the transfer of turbulence down the water column.

9. Discuss how the large scale wind field over the South Atlantic gyre can give rise to a deep central thermocline.

10. Explain how the Agulhas current can be "topographically steered" down the south east coast of South Africa.

(40 marks)

SECTION B

Long questions. Answer THREE whole questions only.

Question 1

The continuity equation can be interpreted as a balance between horizontal divergence and the vertical variation of vertical velocity.

Hence explain

(a) The deepening of a well-mixed layer
(b) The vertical velocity structure in a geostrophic flow
(c) The vertical velocity structure in a planetary scale geostrophic flow.

(20 marks)

Question 2

Many of the large scale surface currents of the ocean are confined to the upper layers of the ocean. Give a full explanation of the sense of the sea surface isobaric surface and the sense of the subsurface isopycnal surfaces associated with such a surface-confined geostrophic current in the Southern Hemisphere.

(20 marks)

Question 3

(a) For surface gravity waves on the ocean, the general geophysical fluid dynamic equations can be simplified considerably. By introducing two appropriate length scales and a time scale, show how the equations can be simplified to give:

$$\frac{\partial u}{\partial t} = -\frac{1}{\rho_0}\frac{\partial p}{\partial x}$$

$$\frac{\partial w}{\partial t} = -\frac{1}{\rho_0}\frac{\partial p}{\partial z} - g$$

$$\frac{\partial u}{\partial x} + \frac{\partial w}{\partial z} = 0$$

Simplify these equations further by splitting the pressure into dynamic and static contributions. Show that these two contributions to the pressure operate at vastly different scales. (You can consider typical waves to have amplitudes of 1 metre, wavelengths of 100 m, and periods of 10 seconds).

(b) Wave energy travels at the "group velocity $C_g = \frac{d\sigma}{dk}$. By considering special simplifications of the dispersion relation

$$\sigma^2 = gk \tanh(kh)$$

find the group velocity in "deep" and "shallow" water in terms of the phase velocity.

(20 marks)

Question 4

(a) In order to determine the tidal attraction due to the moon, we have to consider the variations in the angle γ which is subtended between the sublunar point M and a position P on the earth's surface. With the use of spherical trignometry, the term $(\cos^2\gamma - \frac{1}{3})$ in the tidal potential can be written as

$$\frac{3}{2}\left(\frac{1}{6} + \frac{1}{2}\cos 2\Delta\right)\left(\cos^2\theta - \frac{1}{3}\right)$$

$$+ \frac{1}{2}\sin 2\Delta \cos\alpha \sin 2\theta$$

$$+ \frac{1}{2}\left(\frac{1}{2} - \frac{1}{2}\cos 2\Delta\right)\cos 2\alpha \sin^2\theta$$

where θ is the co-latitude of P
Δ is the declination of moon
α is the transit angle (see accompanying diagram)

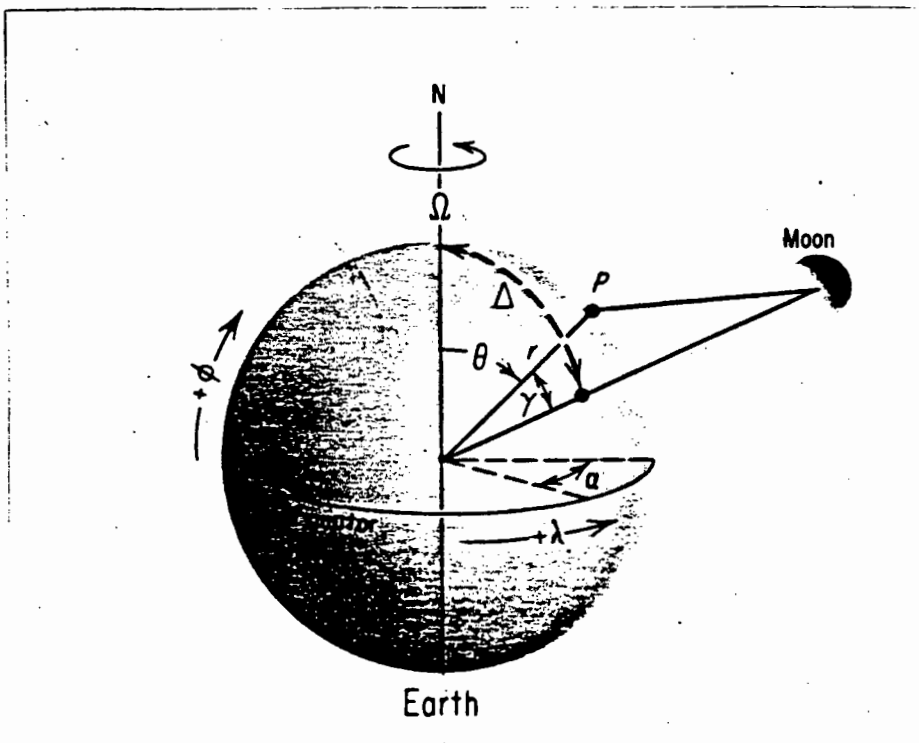

In the light of this equation, discuss the contribution to tides at long periods, diurnal periods and semidiurnal periods. Show also at which latitudes the long period, diurnal, and semidiurnal tides will be weak or absent.

(b) What will the speed of propagation of the tide be if the M_2 component has a wave length of 920 km and period of 12.42 hours? If the tide is considered as a shallow water wave, what would the the appropriate depth be to give the speed found above?

(20 marks)

Question 5

What is the cause of the surface layer phenomenon known as "ice-edge upwelling"? Provide the mechanism and give an opinion as to its frequency of occurrence in the Antarctic.

(20 marks)

Question 6

The full form of the conservation of potential vorticity of a wind forced surface layer of constant density is

$$\frac{d}{dt}\left(\frac{J+f}{h}\right) = \frac{1}{h^2 \rho_0}\left(\frac{\partial s^y}{\partial x} - \frac{\partial s^x}{\partial y}\right)$$

where J is the relative vorticity and h the thickness of the layer, f is the planetary vorticity and ρ_0 the density. The wind stress is (s^x, s^y) and the total time derivative follows the current. This conservation law is to be applied to an ocean gyre and western boundary current in the southern hemisphere.

Estimate the size of the right hand side and show that it is only important for time scales which are very long compared with $\frac{1}{f}$.

Explain how the fast western boundary current responds to its poleward flow along the boundary, and how the slow return gyre current supplies the "lost" vorticity.

(20 marks)

UNIVERSITY OF CAPE TOWN - JUNE EXAMINATION 1985

PHYSICAL OCEANOGRAPHY 1a

TIME: 3 HOURS TOTAL MARKS: 150

Answer ALL questions in SECTION A

Answer TWO questions EACH from SECTION B and SECTION C

Use separate books for Sections B and C.

Section A

Answer ALL questions in this section.

1. Define a barotropic current. (2)

2. Briefly explain the Coriolis force. (2)

3. Sketch a reversing thermometer and explain how it is used. (2)

4. Describe three different instruments used to determine temperature at different depths. (3)

5. Define the terms: potential temperature, salinity, sigma-t, specific volume anomaly, standard ocean. (5)

6. What is the solar constant? (1)

7. What is black body radiation? (1)

8. What are the units of pressure? geopotential? (2)

9. Give examples (with sketches) of fronts in the atmosphere and ocean. (2)

10. What is a Kelvin wave? (1)

11. What three factors are required in order for waves to be present. (3)

12. What is a wave spectrum? (2)

13. What do you understand by "dispersion of water waves" (1)

14. What is the diurnal inequality of the tide - when does it vanish? (1)

15. What are typical oxygen concentrations in the sea? (1)

16. What is the temperature and salinity of Antarctic Bottom Water? (1)

Section B

Answer TWO questions ONLY from this section.

(i) Describe briefly, with sketches where necessary, the surface wind systems around southern Africa. Distinguish between winter and summer circulation patterns and draw surface pressure maps typical of winter and summer. (30)

(ii) Describe briefly the major surface currents around southern Africa. Draw a map of the surface currents and indicate the major topographic features in relation to the currents. (30)

(iii) Given that there is no global gain or loss of heat in the ocean, write down the heat balance equation for the ocean. Describe the various terms and give the magnitude. Pay particular attention to the detail of how the solar radiation reaches the sea surface. (30)

(iv) Describe the circulation and water masses in a section from pole to pole through the Atlantic ocean. Describe the circulation in a vertical section from pole to pole through the atmosphere. What is the jet stream and where can it be found? (30)

Section C

Answer TWO questions ONLY from this section.

(a) Small amplitude gravity waves can be found as a solution to the relevant equations, provided that the dispersion relation holds:

$$\sigma^2 = gk \tanh(kd)$$

where $\sigma = \frac{2\pi}{T}$, T the period of the waves

$k = \frac{2\pi}{L}$, L the wavelength of the waves

g = 10 m/s, d is the depth of water.

Define the terms for "deep" and "shallow" water waves and give the approximate relations for the speed of deep and shallow water waves. (12)

Given that the period T of the waves is independent of the water depth, discuss what happens when gravity waves approach the beach. (12)

If there is a long wave with a wavelength of 1000 km, what will its speed be in water of 4 km depth? (6)

(b) Assuming simple tidal theory, discuss how the tides are generated in principle by the sun and moon. Which tide producing force dominates?

Consider the following tidal record for Simons Bay carefully and discuss various features of the tide there. Expand your discussion to include details of tides around the south African coast. (30)

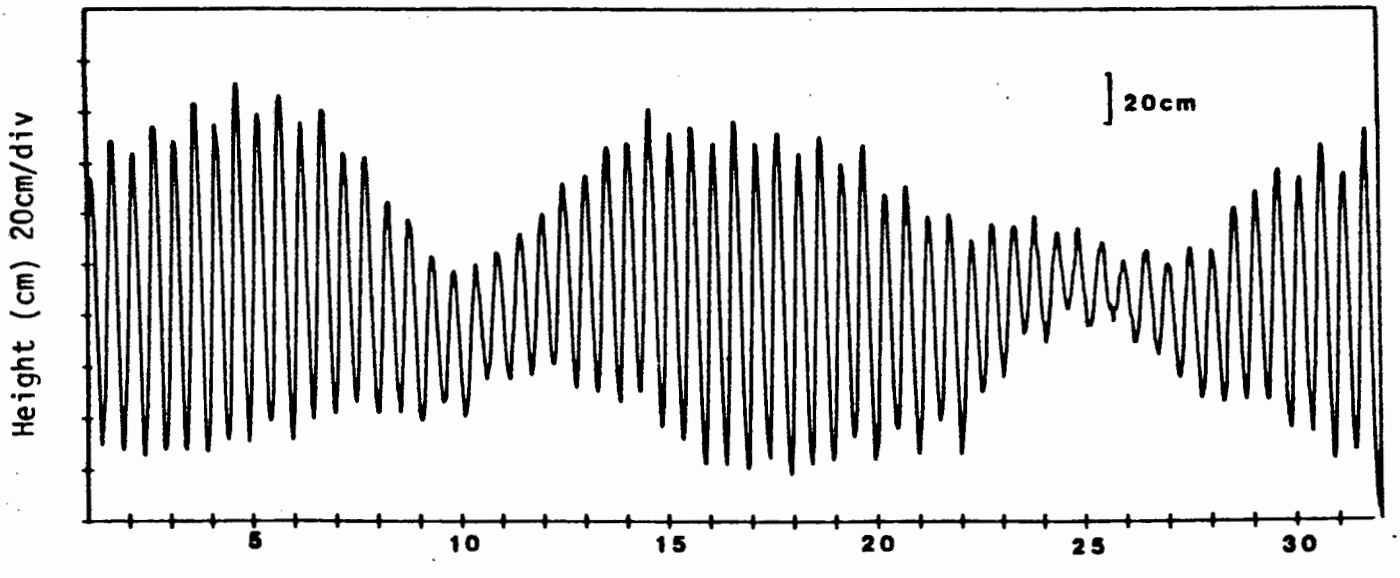

Simons bay sea level October 1982

(c) Starting with the equations of motion for fluids as a rotating earth, make appropriate assumptions so that you can derive the geostrophic velocity equation. (15)

Calculate the geostrophic, barotropic current at 30^{o}S latitude if the sea surface slopes up away from the coast by 1 metre in 100 km. If this current is on the east coast of Australia, in which direction does it flow? (15)

NOTES:

$$\frac{Du}{Dt} = -\frac{1}{\rho}\frac{\partial p}{\partial x} + fv + T_x$$

$$\frac{Dv}{Dt} = -\frac{1}{\rho}\frac{\partial p}{\partial y} - fu + T_y$$

$$\frac{Dw}{Dt} = g - \frac{1}{\rho}\frac{\partial p}{\partial z} + T_z$$

$f = 2\,\Omega \sin \phi$ rad/s

$\rho = 1000$ kg/m^3, $g = 10$m/s^2

(d) Discuss briefly the irregular phenomenon of El Nino in the Pacific Ocean giving some details of the Walker circulation and the southern oscillation. (30)

(e) Discuss the classical ideas of Ekman relating the vertical two dimensional current structure with depth to the wind stress at the surface.

By considering a lateral boundary and an equatorward wind stress, extend these ideas to give a simple model of coastal upwelling. (30)

(f) Write short notes on:
The Pnillips-Miles theories of wind wave generation.
Wave spectra.
Sampling temperature and salinity in the sea.
The origin of the most dense water mass in the sea. (30)

UNIVERSITY OF CAPE TOWN

DEPARTMENT OF CIVIL ENGINEERING

COURSE CE 5D5 : ADVANCED HYDRAULIC STRUCTURES

There is no written examination for this course.

The result will be assessed from two equal value projects.

Project 1 : Analysis of side channel spillway.

Project 2 : Analysis of side weir overflow.

September 1985.

(4 PAGES)

UNIVERSITY OF CAPE TOWN

DEPARTMENT OF CIVIL ENGINEERING

M.Sc. in CIVIL ENGINEERING

UNIVERSITY EXAMINATION : JULY 1986

CIV 516F : COASTAL HYDRAULICS

ALL questions may be attempted. Time: 4 hours

Constants

Sea water density = 1025 kg/m^3
Sea water height = 10 kN/m^3

QUESTION 1

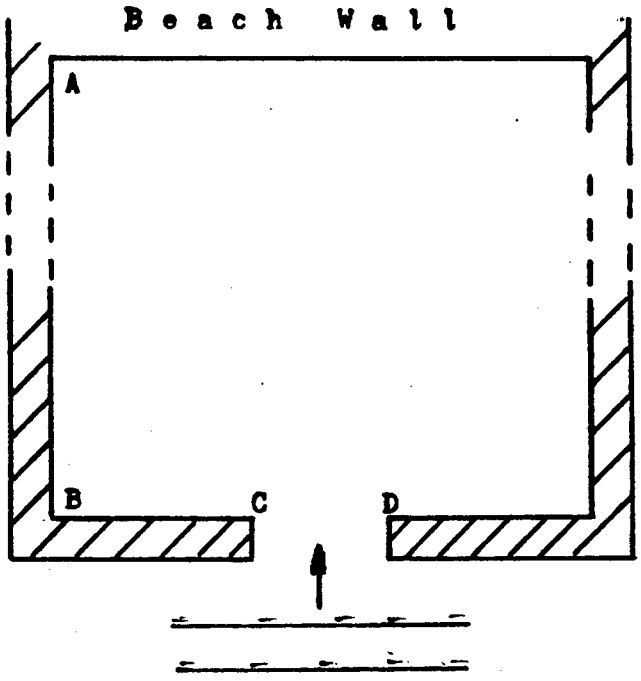

The diagram shows a rectangular shaped harbour with an entrance width of 174 m (CD) and side arm lengths of 261 m (BC). The harbour dimension to the beach wall is about 1,65 km (AB). If wave crests are approaching parallel to BC with a period of 10 seconds and a deep water wave height, H_o , of 4 metres, estimate the wave heights at 5 selected points along the wall AB and also at the harbour centre point. Give the angularity of the wave at the mid point of AB. Ignore refraction and reflection within the harbour, and take the water depth in the vicinity of the breakwater ends as 8,7 m. A selection of diffraction charts are available, ask for the one you need.

QUESTION 2

The standard alignment chart is attached, and a new blank line has been inserted at the bottom of the page. This line is to be used for determining values of u_{max} , the maximum horizontal orbital velocity at the bed, according to the Airy theory. If

$$u^*_{max} = \frac{u_{max}}{\pi H/_T}$$

is to be the dimensionless form of the variable on this line, mark off the positions of the u^*_{max} values given in the following list :

u^*_{max} =			
	0,01	1,00	5,00
	0,10	2,00	6,00
	0,20	3,00	8,00
	0,50	4,00	10,00

Note that H is the local wave height throughout. Suggest a small change in the line label which would permit the scale to be used for maximum horizontal acceleration values. Use the line to solve the following problem.

QUESTION 2 (continued)

A swell of 10 second period with a deep water wave height H_o = 3,2 m approaches a beach with the wave crests parallel to the shore. Plot the value of u_{max} at the bed versus depth from deep water beachwards. Suggested values for depth are:

73m 56m 31m 16m 5m

If the beach sediment is mobile when the bed velocity exceeds 1 m/s, find the depth when this first occurs and check whether this is outside the breaker zone.

(1 diagram attached)

QUESTION 3

(a) The attached diagram shows a wave height record, metres versus seconds. Use the diagram to find the following :-

i. significant wave height by definition
ii. significant wave height by CERC method
iii. significant wave height by the Draper method.

(1 diagram attached)

(b) A wave rider buoy is a type of accelerometer device used for wave height measurements. If such an instrument requires calibration in a laboratory, for a range of typical sea wave periods and wave heights up to 10 m, suggest a way of doing this.

(c)

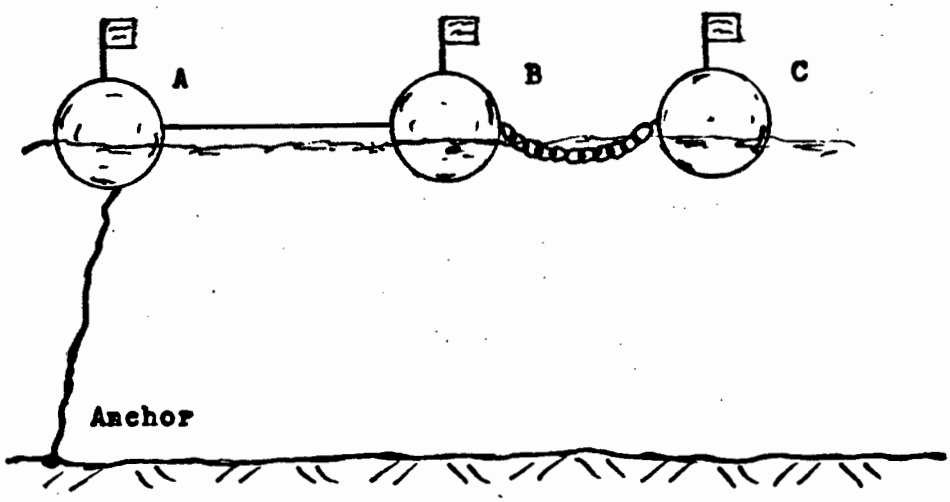

The diagram shows a device anchored to the sea bed outside the surf zone, where A, B and C are identical spherical buoys with visible flags on the top. A is joined to B with a nylon (lightweight) cord

QUESTION 3(c) (continued)

B is joined to C with a fairly heavy catenary chain. Suggest how an observer on the beach could use this device to take a coastal measurement, outline the detailed procedure and specify any beach instrument needed. State whether the device would need calibration.

QUESTION 4

A sea platform consists of a square concrete slab positioned horizontally on four cylindrical vertical piles, each placed at a corner, the slab side being parallel to the local wave crest. The pile diameter is 1 m, the total pile height above the sea bed is 6,4 m, and the slab dimensions are sides of 5 m with a thickness of 200 mm. The local wave characteristics are height 2 m, length 100 m, and period 12 s, the local water depth being 8 m.

(a) Considering the central 1 m high slice of any pile, calculate the horizontal forces per metre due to velocity and acceleration and by plotting these throughout one wave period identify the maximum force and the timing of its occurrence. Check that the velocity and acceleration distributions over the height of the pile are reasonably constant and thus estimate the total force on one pile.

Take $C_D = 1,2$ and $C_M = 2,0$.

(b) Estimate the maximum vertical force on the slab due to wave action.

Take $C_D = 1,0$ and $C_M = 1,8$.

QUESTION 5

In a study of wave penetration into a bay, the 9 m, 8 m and 7 m sea bed contours are approximated by three straight lines with contained angles of 12 degrees as shown on the attached page. An incoming wave orthogonal, 10 second period, impinges on the 9 m contour at an angle of 50 degrees as shown. With the usual approximations obtain by trial the angle at which the emerging orthogonal cuts the 7 m contour. Take the step lines on the 8,5 m and 7,5 m lines.

(1 diagram attached).

- - - - - -

APPENDIX B

GLASS FLUME EXPERIMENT

B.1 Pressure tapping locations

B.2 Capillary rise in tubes

B.3 Calculation method for total pressure resistance

APPENDIX B.1

PRESSURE TAPPING LOCATIONS

Each tapping is defined at a specific section x. (x is 0 at midships and +350 and -350 mm at the bow and stern respectively). At each section the tapping is specified in terms of x, y and z.

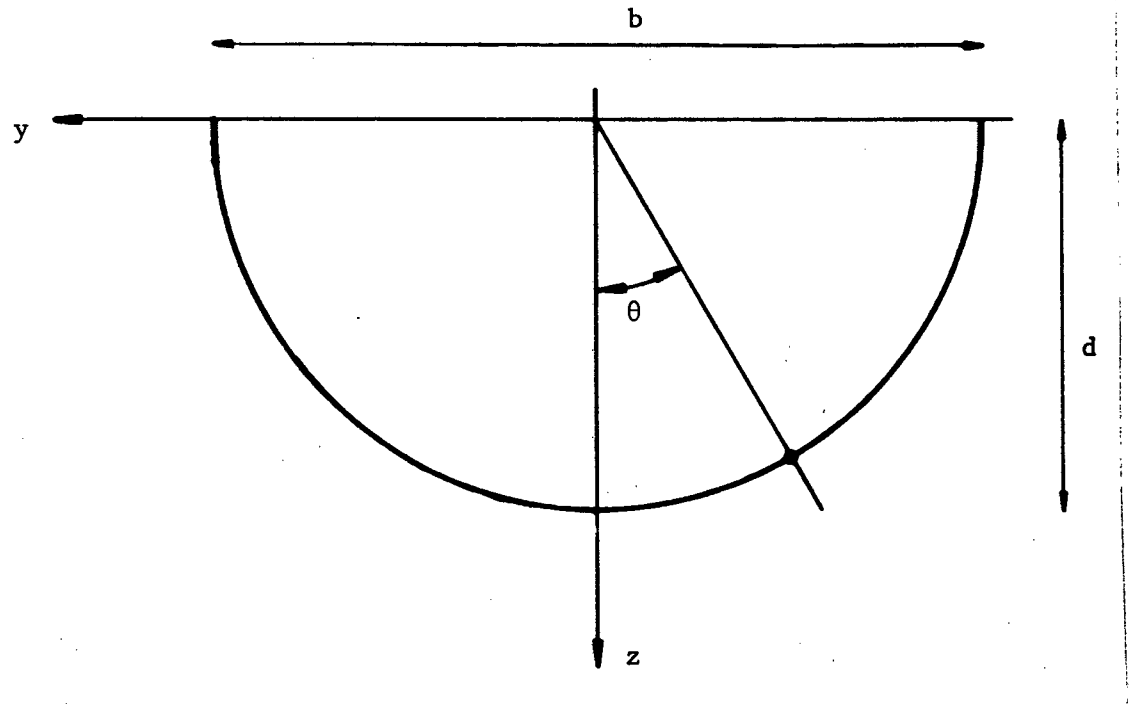

Only the coordinates for the tappings on the bow half of the model are given here (numbers 1 to 20). The coordinates of the tappings on the stern are same except the sign of the x value changes (numbers 21 to 40).

Tapping Number	x (mm)	y (mm)	z (mm)
1	340	-5,6	5,6
2	326	2,9	14,5
3	324	-17,9	4,5
4	309	-9,7	24,4
5	309	23,9	11,0
6	306	-27,5	1,7
7	290	9,8	32,4
8	290	-26,2	21,4
9	290	33,2	6,5
10	271	-9,7	38,0
11	271	26,9	28,6
12	271	-37,7	10,9
13	241	19,4	40,3
14	241	-42,2	14,8
15	201	-19,4	44,1
16	201	44,9	17,5
17	161	19,4	45,5
18	161	-45,9	18,4
19	121	-19,5	46,0
20	121	31,2	18,7

APPENDIX B.2

CAPILLARY RISE IN TUBES

The capillary rise may be approximated by assuming that the meniscus is spherical and by equating the lifting force created by surface tension to the gravity force.

$$2 \pi r \sigma \cos\theta = \pi r^2 h \gamma$$

$$\therefore \quad h = \frac{2 \sigma \cos\theta}{\gamma r}$$

where σ = surface tension (N/m)

γ = specific weight of liquid (N/m^3)

r = radius of tube (m)

h = capillary rise (m)

θ = angle between glass and meniscus slope.

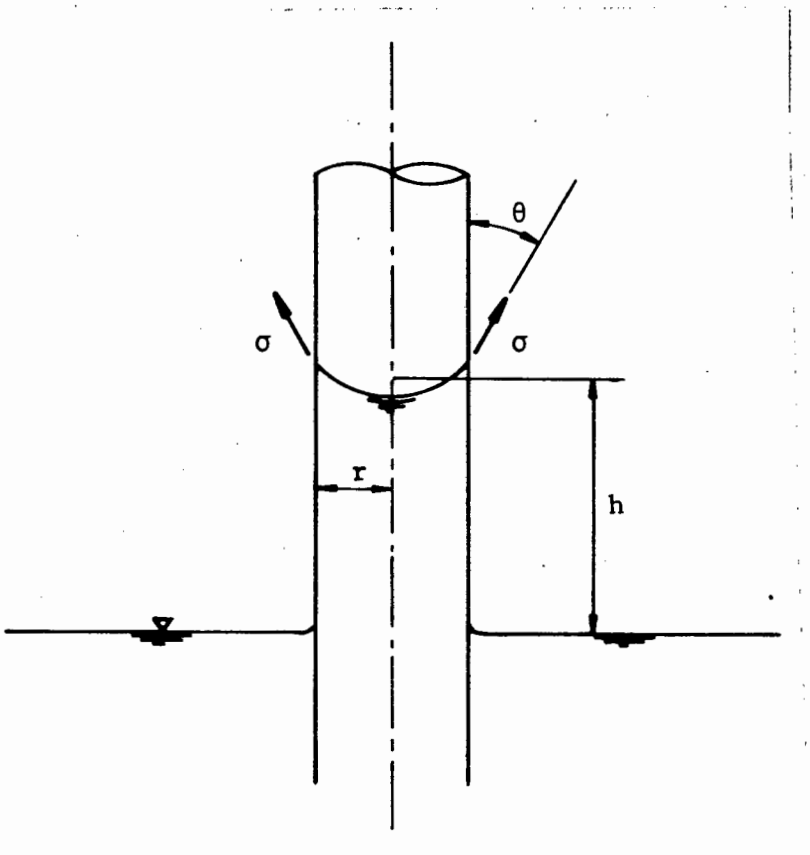

σ = 0,0728 N/m at 20°C

γ = 9,81 x 10^3 N/m^3

r = 10 x 10^{-3} m

θ = 0° for a clean glass tube

$\therefore$ h = 1,484 mm

This rise in the tube is relatively small. However, it will not affect the pressure measurements since it will occur in all the glass tubes.

APPENDIX B.3

CALCULATION METHOD FOR TOTAL PRESSURE RESISTANCE

An example of the calculation method is shown on pages B.7 to B.12.

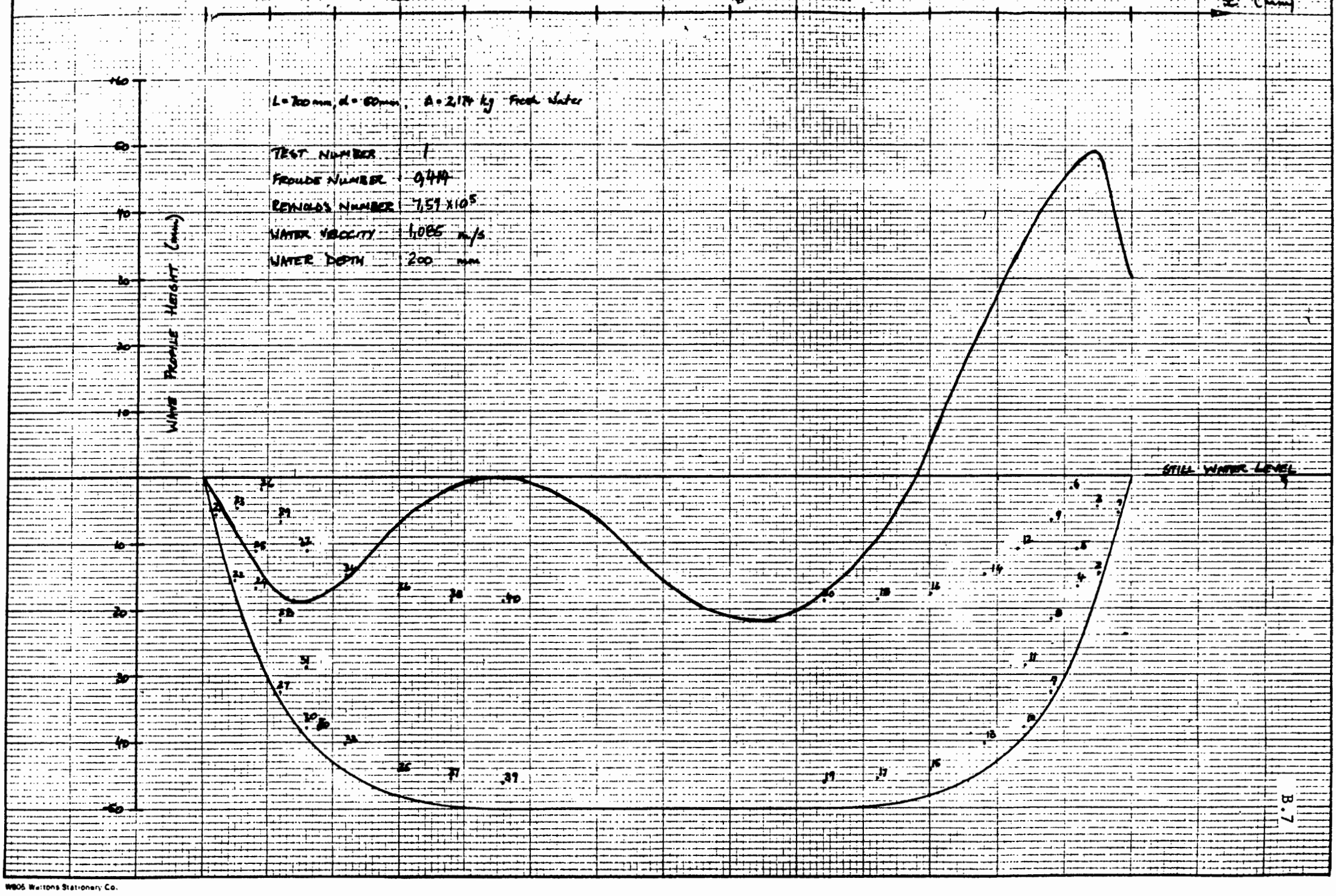

W806 Waltons Stationery Co.

TEST 1

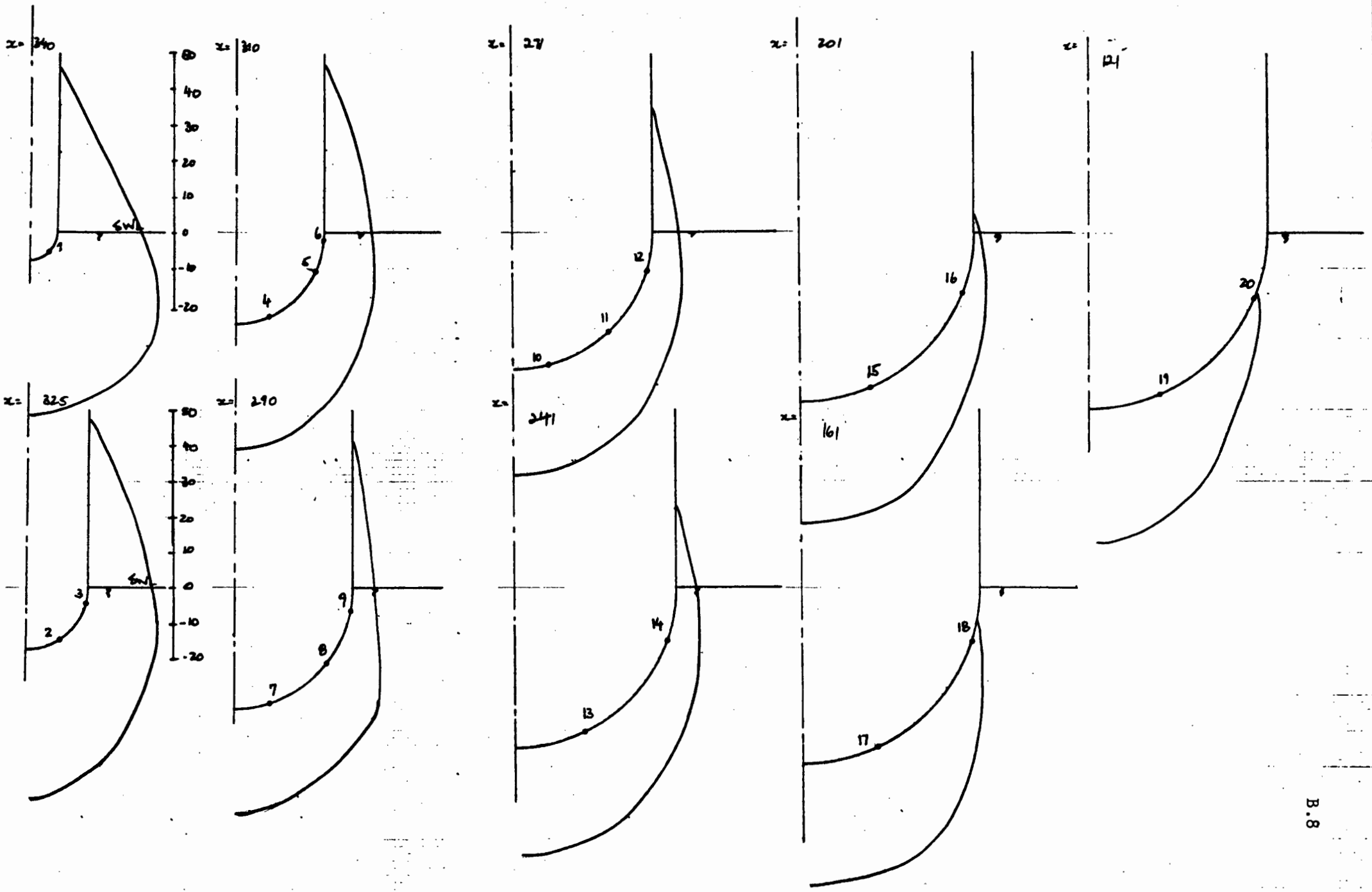
x= 340
x= 310
x= 27
x= 201
x= 121
x= 325
x= 290
x= 241
x= 161
SWL
SWL
80
40
30
20
10
0
-10
-20
1
2
3
4
5
6
7
8
9
10
11
12
13
14
15
16
17
18
19
20

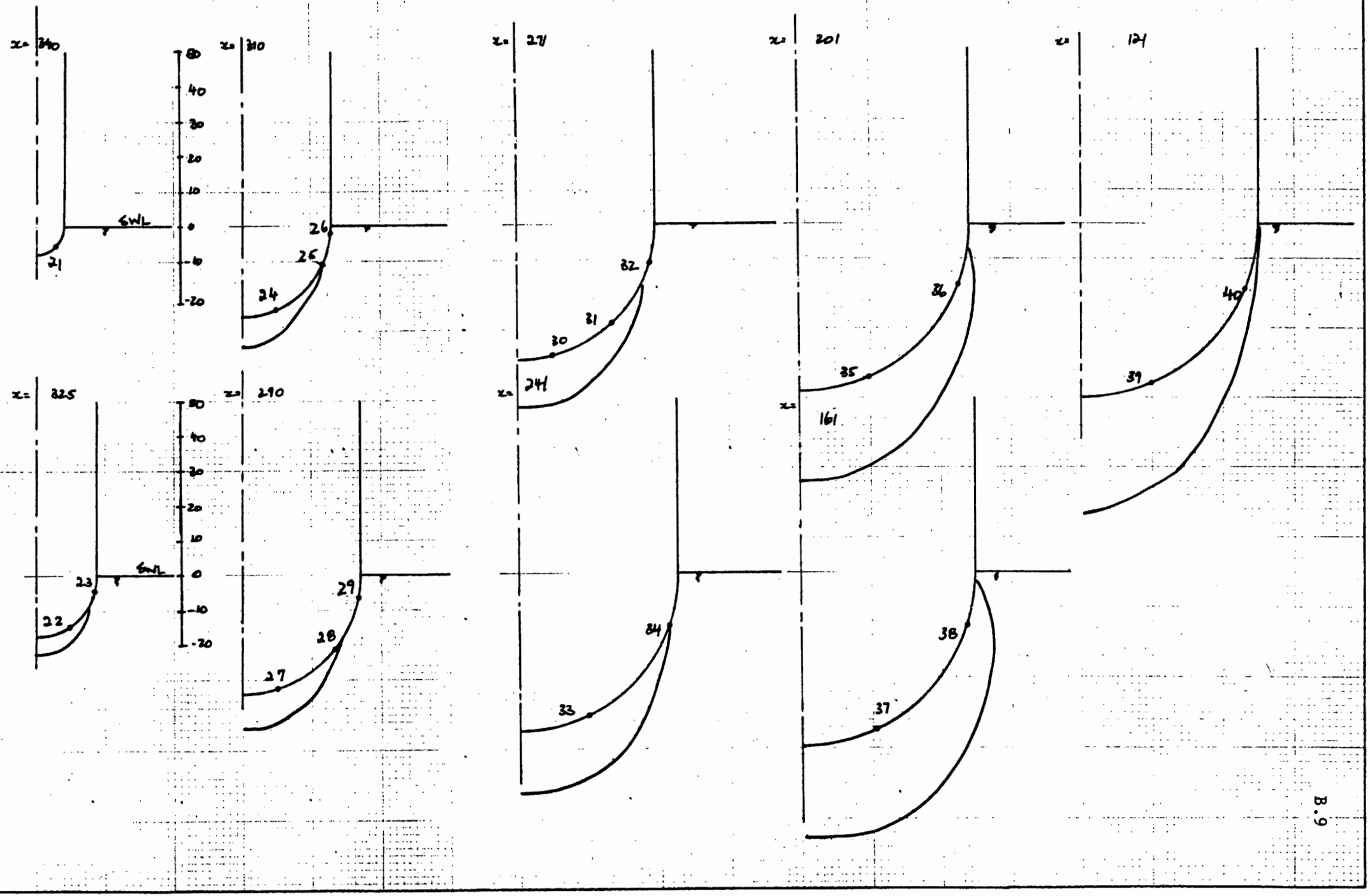
x= 340
80
40
30
20
10
SWL
0
-10
-20
21
x= 330
26
25
24
x= 271
32
31
30
x= 201
36
35
x= 161
x= 121
40
39
x= 325
23
22
x= 290
29
28
27
x= 241
34
33
38
37

WATER TEMP: 20 °C WATER DENSITY: 1000 kg/m³

TAPPING NUMBER	Δh MEASURED CHANGE IN HEAD (mm)	h_s SUBMERGENCE OF TAPPING (mm)	H (mm) PRESSURE HEAD	AREA dA (mm²)	AREA CORRECTION (mm²)	CORRECTED AREA (mm²)	$\theta = 90 - \phi$ (degrees)	NORMAL FORCE (N)	DRAG COMPONENT (N)
1	33,9	5.6	39,5	141.1023			86,5567	0,0547	0,0326
2	18,7	14.6	33,2	331.8987			31,0016	0,1081	0,0667
3	17,1	4.5	21,6	120.4026			80,2290	0,255	0,0128
4	6	24.4	30,4	358.6292			24.6898	0,1070	0,0447
5	6,4	11.0	17,4	358.6292			24.6898	0,0612	0,0256
6	8,8	1.7	10,5	24.1876			23.6460	0,0025	0,0010
7	-4,8	32.4	27,6	377.1319			18.5073	0,1021	0,0324
8	-2,5	21.4	18,9	377.1319			18.5073	0,0699	0,0222
9	1,5	6.5	8,0	247.5033			18.5073	0,0194	0,0062
10	-10,1	38.0	27,9	394.4656			13.4166	0,1080	0,0251
11	-8	28.6	20,6	394.4656			13.4166	0,0797	0,0185
12	-9,6	10.9	10,3	441.0832			13.4166	0,0446	0,0103
13	-13,4	40.3	26,9	1593.2476			7.5577	0,4204	0,0553
14	-4,5	14.8	10,3	1201.9220			7.5577	0,1214	0,0160
15	-13,7	44.1	30,4	1596.8976			3.0648	0,4762	0,0255
16	-10,5	17.5	7,0	1426.3845	-15	1411,3845	3.0648	0,0969	0,0052
17	-14,1	45.5	31,4	1698.9103	+ 1170,6002	2 769,5105	1.0114	0,8581	0,0151
18	-	18.4		1510.6002			1.0114		
19	-17,1	46.0	28,9	1599.7241	+ 895,7602	2 495,4843	0.2425	0,7075	0,0030
20	-	18.7		1535.7602			0.2425		

TOTAL FORCE ACTING ON BOW 0,4072 N

TEST NUMBER: 1 WATER VELOCITY: 1,085 m/s

WATER TEMP: 20 °C WATER DENSITY: 1000 kg/m³

TAPPING NUMBER	Δh MEASURED CHANGE IN HEAD (mm)	h_s SUBMERGENCE OF TAPPING (mm)	H (mm) PRESSURE HEAD	AREA dA (mm²)	AREA CORRECTION (mm²)	CORRECTED AREA (mm²)	$\theta = 90 - \phi$ (degrees)	NORMAL FORCE (N)	DRAG COMPONENT (N)
21	–	6.6		141.1023			36,5567		
22	-16	14.6	-1,5	331.8987	+142,505	474,4036	31.0016	-0,0049	-0,0025
23	–	4.5		120.4026			20.2290		
24	-19,1	24.4	5,3	358.6292	+ 148,8168	507,4460	24.6898	0,0264	0,0110
25	–	11.0		358.6292			24.6898		
26	–	1.7		24.1876			23.6460		
27	-23,6	32.4	8,8	377.1319	+ 292,1352	669,2671	18.5073	0,0578	0,0183
28	–	21.4		377.1319			18.5073		
29	–	6.5		247.5033			18.5073		
30	-25,0	38.0	13	394.4656			13.4166	0,0503	0,0117
31	-25,7	28.6	2,9	394.4656	+ 71,0832	465,5488	13.4166	0,0132	0,0031
32	–	10.9		441.0832			13.4166		
33	-26,2	40.3	14,1	1593.2476	+ 621,9230	2215,1706	7.5577	0,3064	0,0403
34	–	14.8		1201.9220			7.5577		
35	-23,3	44.1	20,8	1596.8976	+ 1 126,3845	2 723,2821	3.0648	0,5567	0,0297
36	–	17.5		1426.3845			3.0648		
37	-20,2	45.5	25,3	1598.9103			1.0114	0,3968	0,0070
38	-18,4	18.4	0	1510.6002	-80	1430,6002	1.0114	0	0
39	-19,7	46.0	26,3	1599.7241			0.2425	0,4127	0,0017
40	-17,4	18.7	1,3	1535.7602			0.2425	0,0196	0,0001
							TOTAL FORCE ACTING ON STEM		0,1204 N

APPENDIX C

LOW PASS FILTER

APPENDIX C

LOW PASS FILTER

The low pass filter can remove an unwanted alternating component on a direct voltage, or an unwanted high frequency noise that is superimposed on a low frequency alternating voltage.

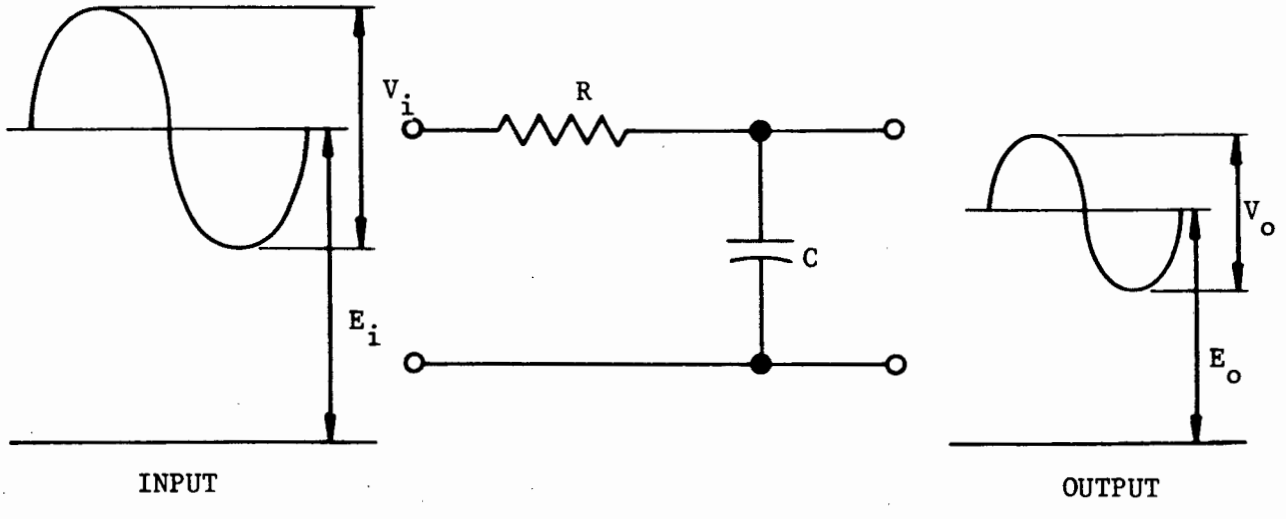

The circuit above shows a simple low-pass filter. The input is a direct voltage with an a_c waveform superimposed, and the output is a direct voltage and an attenuated alternating waveform. Apart from a voltage drop across R due to any direct current flow, the presence of C and R have no significant effect upon the d_c input voltage. However, the capacitor offers a definite impedance X_c to alternating input voltages, and this impedance decreases as input frequency increases. The higher the a_c frequency, the lower the capacitive impedance, and consequently the greater the attenuation.

$$X_c = \frac{1}{\omega C}$$

where $\omega = 2\pi f$

f = frequency of a.c. waveform

The equivalent circuit with the impedance is shown below:

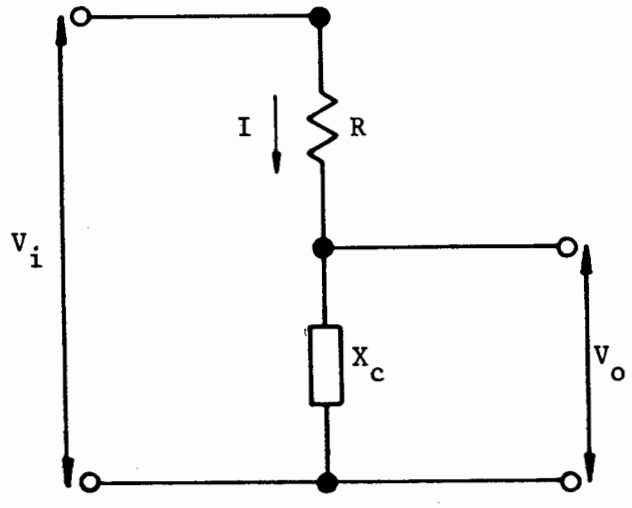

The filter attenuation is given by the following formula:

$$\frac{V_o}{V_i} = \frac{X_c}{\sqrt{R^2 + X_c^2}}$$

APPENDIX D

STRAIN GAUGE BRIDGE THEORY

APPENDIX D

STRAIN GAUGE BRIDGE THEORY

For a strain gauge the following relationship defines the gauge factor of the strain gauge in terms of the strain imposed on the gauge, the initial resistance and the change in resistance.

$$\frac{\Delta R}{R_o} = K \varepsilon \qquad (D.1)$$

where ΔR = change in resistance

R_o = initial value of the strain gauge resistance

K = gauge factor

ε = strain imposed on strain gauge.

Strain gauge bridge

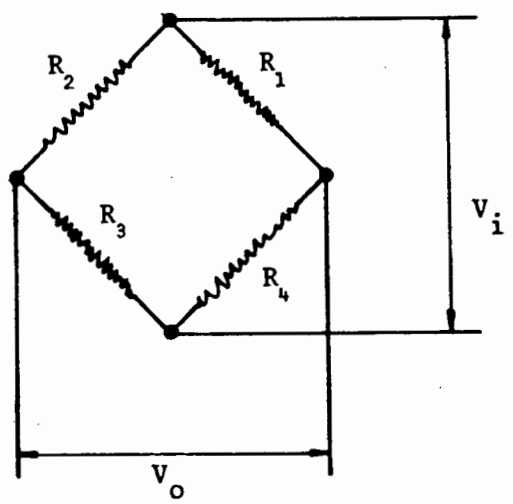

V_i = input voltage

V_o = output voltage

Generally we have

$$\frac{V_o}{V_i} = \frac{R_1}{R_1+R_2} - \frac{R_4}{R_3+R_4}$$

$$\therefore \quad \frac{V_o}{V_i} = \frac{R_1 R_3 - R_2 R_4}{(R_1+R_2)(R_3+R_4)} \qquad (D.2)$$

Note that Equation D.2 is valid regardless of whether the bridge is balanced or not.

If the bridge is balanced $\frac{V_o}{V_i} = 0$ that is $V_o = 0$

Therefore we have $R_1 = R_2 = R_3 = R_4$

$$\text{or} \quad \frac{R_1}{R_2} = \frac{R_4}{R_3}$$

If the resistance of the gauges now vary (due to an imposed load), the value of V_o will no longer be zero. Making the assumption that ΔR_i is much smaller than R_i (which is generally true) allows us to disregard second order factors, therefore we have

$$\frac{V_o}{V_i} = \frac{1}{4}\left(\frac{\Delta R_1}{R_1} - \frac{\Delta R_2}{R_2} + \frac{\Delta R_3}{R_3} - \frac{\Delta R_4}{R_4}\right) \qquad (D.3)$$

substituting Equation D.1 into the above equation

$$\frac{V_o}{V_i} = \frac{K}{4}\left(\varepsilon_1 - \varepsilon_2 + \varepsilon_3 - \varepsilon_4\right) \qquad (D.4)$$

Measurement of bending strain

Consider the example of the cantilever shown below.

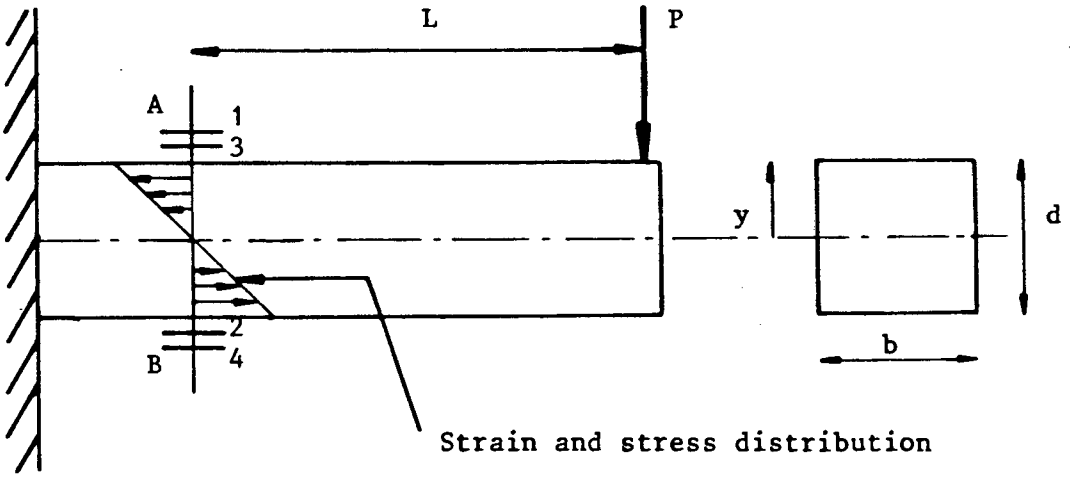

When load P is applied at the end on the cantilever, bending stresses are induced at section AB - tensile stresses on face A and compressive stresses on face B. These stresses may be calculated using the following equation

$$f = \frac{M.y}{I} \qquad (D.5)$$

where M = applied moment = $P.L$

y = distance from neutral axis to gauge = $\frac{1}{2}\,d$

I = second moment of area of the section = $\frac{bd^3}{12}$

These stresses may be related to the strains using the following equation

$$\varepsilon = \frac{f}{E} \qquad (D.6)$$

where E = Young's modulus.

The strains at the top and bottom of the section may be assumed to be equal and, therefore, we can write Equation D.4 as follows

$$\frac{V_o}{V_i} = \frac{K}{4}\,[\,\varepsilon_1 - (-\varepsilon_2) + \varepsilon_3 - (-\varepsilon_4)\,]$$

since $|\varepsilon_1| = |\varepsilon_2| = |\varepsilon_3| = |\varepsilon_4| = |\varepsilon|$ we have

$$\frac{V_o}{V_i} = K.|\varepsilon| \qquad (D.7)$$

and substituting Equation D.6 into the above equation we get:

$$\boxed{\frac{V_o}{V_i} = \frac{K.f}{E}} \qquad (D.8)$$

Therefore, the above expression gives the output voltage of the bridge in terms of the gauge factor, stress at the section, Young's modulus and the input voltage. This equation is used for design purposes only and each bridge must be calibrated before experimental measurements are made. Note that it is important that the strain gauges 1 and 3 and gauges 2 and 4 are on opposite sides of the beam to ensure that Equation D.7 is valid.

18 JUN 1987